UNIVERSITY OF THE
WITWATERSRAND,
JOHANNESBURG

A Review of Mineral Exploration at the Karingarab Carbonatite, Southern Namibia.

Jennifer Ndapanda Nehoya

Student Number: 833888

This document serves as a research report submitted to the Faculty of Science, University of the Witwatersrand, in partial fulfilment of the requirements for the degree of Master of Science in Economic Geology by coursework and research. This thesis was completed under the supervision of Professor Paul Nex.

Signature of Candidate

12th March 2023

Date

Declaration

I declare that this report is my own, unaided work. I have read the University Policy on Plagiarism and hereby confirm that no plagiarism exists in this report. I also confirm that there is no copying nor is there any copyright infringement. I willingly submit to any investigation in this regard by the School of Geosciences and I undertake to abide by the decision of any such investigation.

Acknowledgement

Thank you to my family, Professor Paul Nex, Professor Judith Kinnaird, Professor Richard Minnitt, the twittersphere and my colleagues at Namdeb and Anglo American for the support.

Abstract

This research report reviews the Karingarab Carbonatite, which is one of several alkaline and carbonatite occurrences in Namibia targeted for rare earth element (REE) potential which are used in medical, renewable energy, technology and military applications. Several exploration campaigns have occurred at the Karingarab Carbonatite since 1977 and all indicate positive concentrations of REEs at the deposit.

The Karingarab Carbonatite (68 Ma) is one of 41 alkaline and carbonatite occurrences in Namibia which is documented in this report and is very similar in terms of composition, age and emplacement to the Dicker Willem (49 Ma) and the Gross Brukkaros carbonatites (77 Ma) all located along south-west to north-east trending structures on the west coast of southern Namibia.

The Karingarab Carbonatite lies in the center of a 2.5 km diameter circular vent raised 300 m above sea level, the edges of the vent are brecciated extrusive phonolites and other alkali silicate rocks with country rock fragments of phyllites and schists of the Oranjemund group, crosscut with late stage dykes of varying compositions in the alkaline and carbonatite series. Four main lithology types are identified through their distinct geochemical signatures with varying degrees of weathering and alteration. The target and main lithology is a layered extrusive carbonatite with lapilli of various shapes and sizes diluted in parts with mostly phonolites, schists and phyllites. The second more common lithology is extrusive phonolites which are mostly brecciated with cross cutting carbonatite dykes. The third lithology type is formed by clay rich autoclastic volcanic breccias which are a mixture of all the proximal and local rock types of the Oranjemund group, lastly the fourth lithology is formed by overburden which includes wind-blown dune sands and calcrete. The extrusive carbonatite lapilli is the dominant ore type, with deeper, fresh and unaltered carbonatites still mineralized and carrying lower grades while the shallower, weathered and altered carbonatite shows supergene enrichment and extremely high grades. This enrichment was upgraded by events in the early Paleogene which included deep erosion and surface weathering events along with a regional surface silcretization event capping and trapping mineralization.

Preliminary findings following the first two drilling campaigns indicate a potential to produce from the carbonatite, 181 million tonnes of ore with 3.5 million tonnes of total rare earth oxides (REOs) at an average grade of 1.9% total REEs. The deposit remains partly open at depth, with satellite concealed volcanic occurrences still to be explored. Should the target become an operational mine, responsible sourcing will need to be considered particularly how to extract, refine, transport and process REEs in a manner which satisfies environmental, social and governance requirements (ESG) while ensuring the mineral value chain and potential industry spill-over is managed sustainably.

Major risks to the target involve the criticality of supply which may be managed through monitoring geopolitics in supply, and technology improvements in substitution and recycling for the REEs and their products. Apart from these economic interests, the observations and studies on the subsurface lithologies at Karingarab will be invaluable to academia through improved literature on carbonatites, REE deposit genesis and the regional geology where much is covered by sand.

Table of Contents

List of Figures

List of Tables

1. Introduction

This research report focuses on exploration of the Karingarab Carbonatite, which is one of several alkaline and carbonatite occurrences in Namibia targeted for their rare earth element (REE) potential. This report will investigate the economic importance of the target commodity, provide a review of occurrences and general emplacement of carbonatites, the geology of the Karingarab Carbonatite, and a review of exploration at the target since discovery in 1977 highlighting the potential of the deposit.

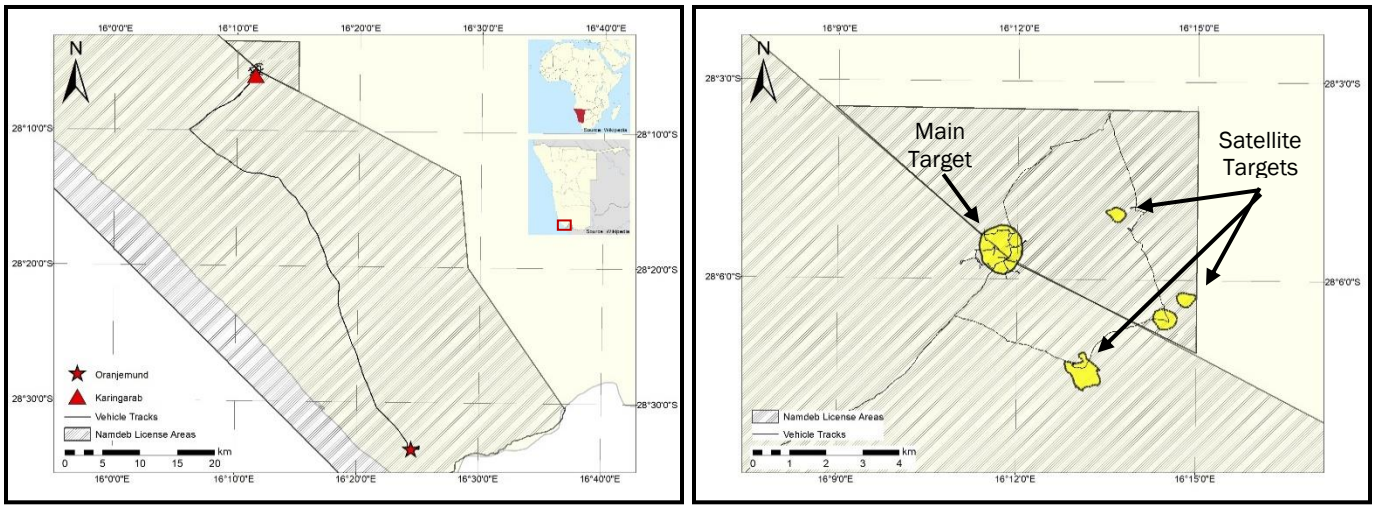

Figure 1: Locality map of the Karingarab Carbonatite, in southwest Namibia highlighting the main target and smaller satellites.

Karingarab (Figure 1) is located in southern Namibia and is 55 km north of the placer diamond mining town of Oranjemund. The main and largest target is named the Karingarab Carbonatite and together with the adjacent unnamed and unexplored satellites form the Karingarab Complex. The complex is in the restricted Tsau-//Khaeb National Park formerly known as the Sperrgebiet National Park.

Limited public data is available on the Karingarab Carbonatite as it is located within a restricted diamond area. In Miller, (2008) reference is made to work by Stocken, (1978) who describes the surface outcrop at the center of the Karingarab Carbonatite as interlayers of ferrous brown and dolomitic grey carbonatite with magnetite and manganese oxide banding while the outer zone is described as a brecciated, manganese-rich, brown silicified

carbonatite. His observations of outcrop noted that the area proximal to the main carbonatite hosts porphyritic phonolite plugs and dykes.

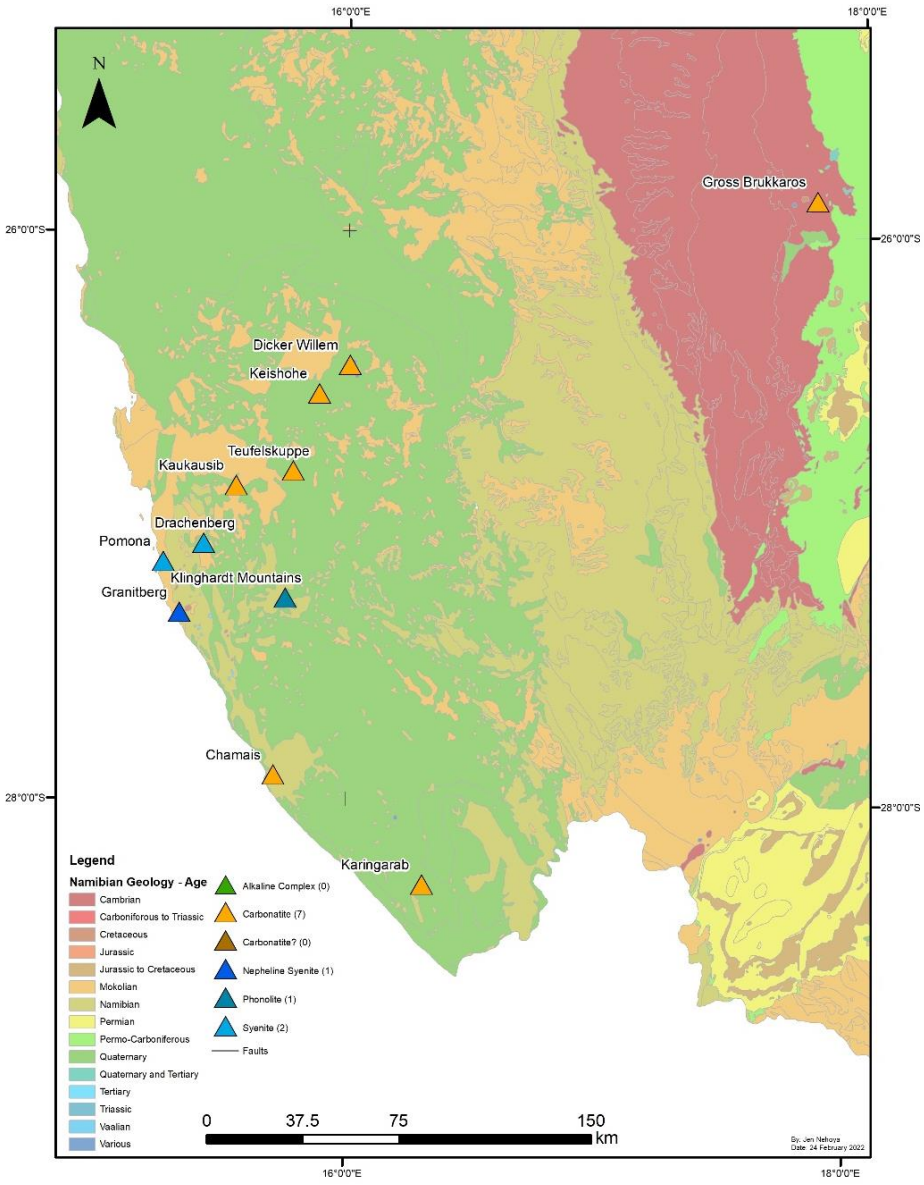

Figure 2: Alkaline and carbonatite magmatic and volcanic occurrences in South-West Namibia.

Several volcanic and magmatic events have taken place in southern Namibia (Figure 2) including those of the Lüderitz Alkaline Province which is a swarm of alkaline and carbonatite intrusions emplaced in the early Cretaceous (Verwoerd, 1993) named the Drachenberg, Pomona and Granitberg which are approximately 150 kilometres north of Karingarab.

Verwoerd (1993), states that Karingarab might not form part of this igneous province due to the distance between them. Geochronological studies are ongoing and preliminary dates indicate that the Karingarab Carbonatite may be younger than the events that formed the Lüderitz Alkaline Province. Other volcanic and magmatic occurrences include the Klinghardt Phonolite suite from the Eocene (Verwoerd, 1993) and the early Tertiary igneous events that formed the Dicker Willem, Keishöhe, Teufelskuppe and Kaukausib carbonatites (Verwoerd, 1993).

Records of various exploration campaigns at the Karingarab Carbonatite are documented from 1977 where early mapping and surface sampling campaigns took place by De Beers geologists (formerly Consolidated Diamond Mines (CDM)) to the present day multi-disciplinary exploration campaign by Namdeb (Namibia De Beers) Diamond Corporation geologists. A summary of the exploration techniques and results will be presented highlighting the evolution of exploration methodology due to advances in technology triggered by the demand for REEs at the start of the 21st century.

To date, all exploration activity continues to indicate positive concentrations of REEs at the Karingarab Carbonatite and it is only through further exploration and detailed analysis of the available core and data that can determine the potential limitations of economic extraction, the emplacement system, mineralization types and overall scale of the deposit.

The REEs are a group of critical metals consisting of the 14-lanthanide series of elements (Figure 3), excluding promethium (Pm) which is unstable naturally and including scandium (Sc) and yttrium (Y). The highest demand for these critical metals are for use in medical, renewable energy, military and new technology applications which include the permanent magnets used in hybrid or electrical motor vehicles, wind turbines and modern weapons systems as well as fibre optics, lasers, phosphors, speciality metal alloys, rechargeable batteries and catalysts in petroleum refining. The REEs have also played a crucial role in the slimming down and portability of hard drives and consumer electronics (Harmer & Nex, 2016).

The critical metals are a group of evolving metals that are reviewed and grouped as critical due to economic importance and insecurity of supply. Even though the REEs and other critical metals are naturally abundant throughout the earth's crust, the occurrence of economic prospects remains scarce (Jowitt et al., 2018).

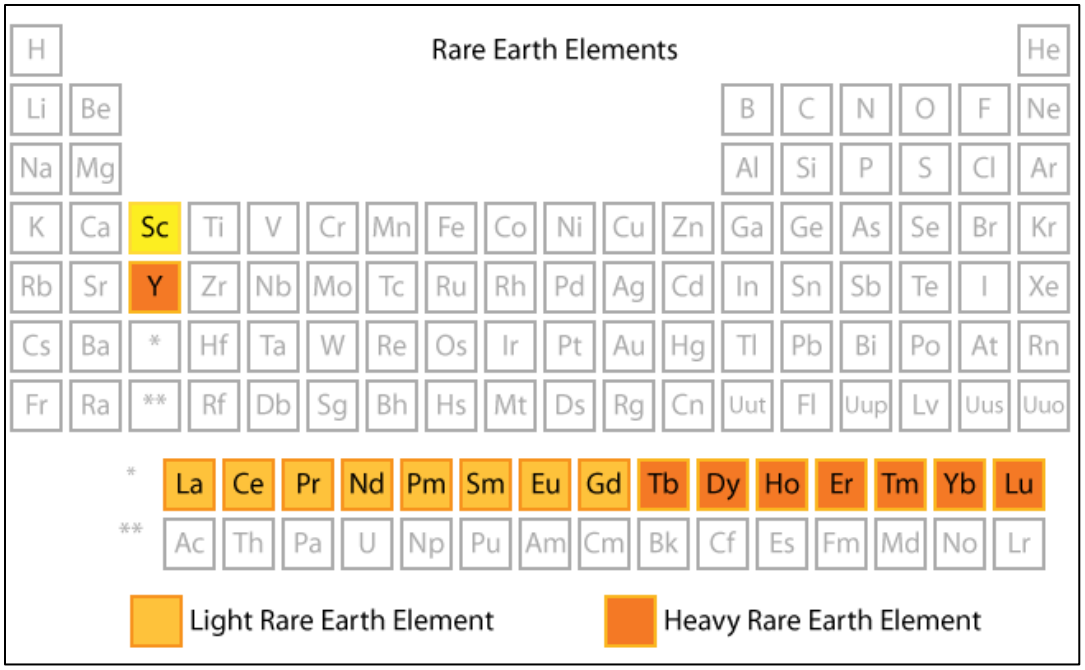

Figure 3: Periodic table of elements highlighting REEs with Sc and Y (Coint & Dahlgren, 2019)

Economic REE deposits can be hosted in various deposit styles but are more common as a result of magmatic activity which produces carbonate, phosphate, or silicate host minerals, which is most common in carbonatite-alkaline-silicate systems. Mineralized carbonatites have the potential for multiple commodity deposits and are also a significant source for niobium, apatite, vermiculite, copper, titanium, fluorite, thorium, uranium, natural zircon and iron (Simandl & Paradis, 2018). In addition to economic interest, the emplacement setting of carbonatites when deformed may also mark sutures where oceans have existed and can contribute to better understanding of the earth's mantle and plate tectonic cycles (Burke et al., 2003).

1.1. Aim

This research report will cover the economic importance of REEs as a commodity, review the occurrence and general emplacement models of carbonatites, the geological setting of the Karingarab Carbonatite deposit, and provide a review of exploration at this deposit since the late 1970s and summarize the economic potential of the deposit.

1.2. Objectives

As the author of this exploration review, I, Jennifer Nehoya, am an employee of Namdeb and currently responsible for exploration at Karingarab from 2016 to the present. I have been responsible for overseeing drilling and logging of the 2016 reverse circulation campaign, initial modelling, subsequent studies involving 2014 drill core for XRD and petrographic analysis, hand selecting phlogopite from the carbonatite for dating the carbonatite, analysing the geochemical results as well as licensing and reporting. Since 2019, I have been the technical and operations senior geologist managing and executing multi-disciplinary exploration project management which includes ground geophysics, mapping, aerial photography and a drilling campaign delivering 11,000 m of diamond core for processing. The objective for this review is to compile and present information on project activity prior to recent rolling exploration campaigns in 2019 and the following topics:

- The economic importance of REEs
- Global occurrence of carbonatites
- Alkaline and carbonatite occurrences in Namibia
- Geologic setting of the Karingarab Carbonatite
- Details of exploration activity at the Karingarab Carbonatite which includes:
    - Ground mapping
    - Grab samples for petrology and geochemistry
    - Reverse circulation drilling
    - Diamond core drilling
    - Downhole geophysics (wireline surveys)
    - Petrography
    - Geochronological studies
    - Internal research
- Potential of the Karingarab Carbonatite deposit

2. The Criticality of Rare Earth Elements

Rare earth elements (REE) are vital for components and advancements in technology, medical, renewable energy and military applications. The occurrence of REE deposits worldwide is hosted in various deposit types and the exploitable reserves are dominated by China, Vietnam, Brazil, Russia, India, Australia and the United States of America (Figure 4).

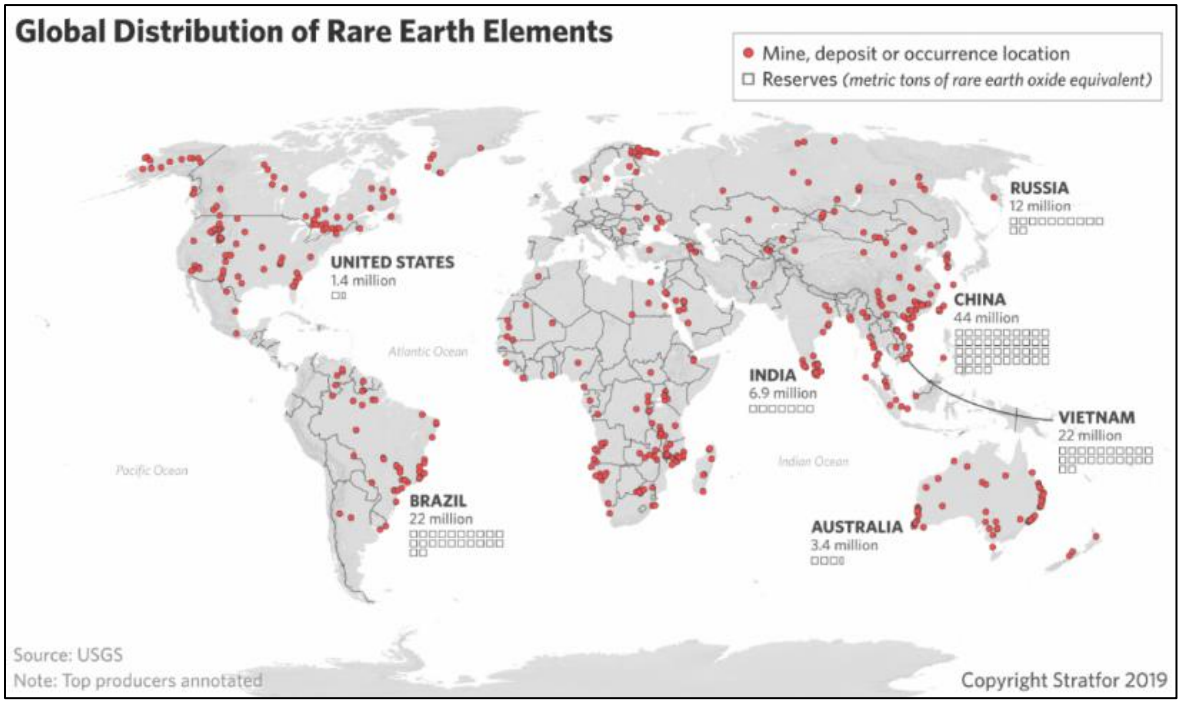

Figure 4: Global distribution of rare earth element deposits (Stratfor, 2019).

Commodities such as the REEs are classified as critical when there is a high economic importance combined with a high chance of supply disruption. Defined by the European Commission (EU, 2010) and National Academy of Sciences (USNAS, 2008), the supply risks are broad and include the scarcity of a commodity due to a lack of natural geological occurrences, the available extraction technology and whether the commodity may be substituted or recycled. Other factors that affect criticality are the diversity and stability of supply locations or companies and whether production of the metal is as a by-product of other commodities. The dominant supplier of critical raw materials globally is currently China which has resulted in the perception that supply risks may be high (Figure 5).

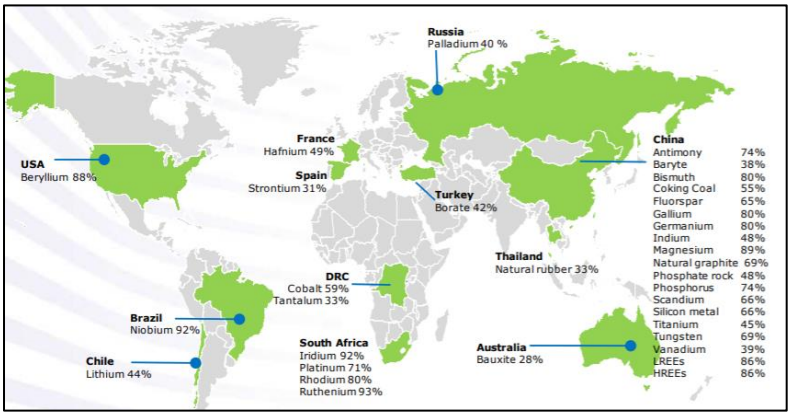

Figure 5: Global supply of critical raw materials by largest share per country (European Commission, 2020).

The criticality rating for commodities evolves over time as the need for the metals vary by region accompanied with the evolution of technology and application (Skirrow et al., 2013). The REEs have the highest risk of supply however, the criticality can be reduced by increasing security of supply Figure 6. Security of supply may also be improved by diversifying global sources or applying principles of responsible sourcing through increased knowledge of the resources geology to classify economic deposits, and studying current mining, processing and marketing operations to extract data on the mineral resource accounting, mineral economics, material flow analysis and mineral processes applied (Arribas et al., 2018).

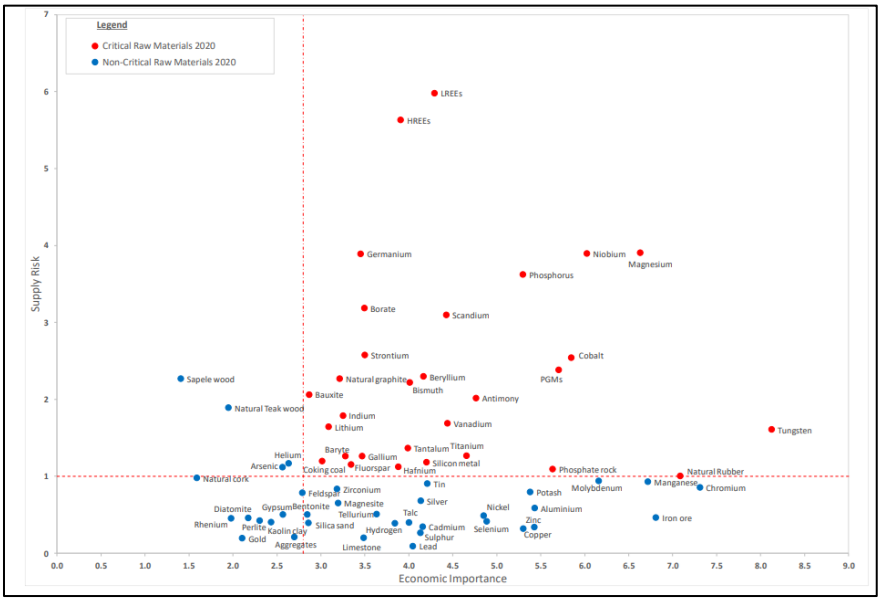

Figure 6: 2020 European Union Criticality Matrix (European Commission, 2020)

3. Global Occurrence of carbonatite hosted rare earth deposits.

Rare earth elements (REEs) or lanthanoids occur naturally as trace elements in many minerals in the earth's crust. Most enrichment occurs because of magmatic activity producing carbonate, phosphate or silicate minerals in rhyolites, carbonatites or apatite veins along sutures in margin settings during rift events (Figure 7) (Skirrow et al., 2013). For carbonatites, the total amount of REEs in the melts is fixed following intrusion events and does not naturally increase or accumulate over time or from external sources, however, local redistribution and upgrading of the REE content in carbonatites can occur through metamorphic and hydrothermal events (Anenburg et al., 2021).

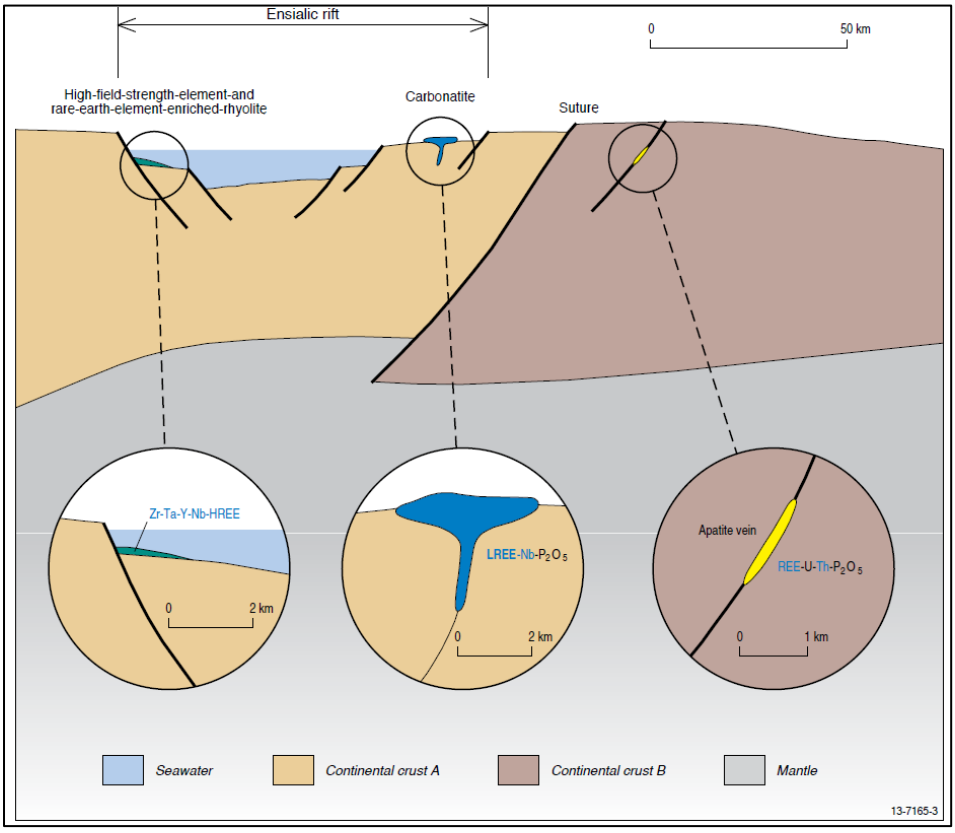

Figure 7: Illustration of various geological settings where rare earth element enrichment can occur (Skirrow et al., 2013).

Due to similarity in the size and shape of their atoms, the lanthanoid elements group together naturally and often substitute themselves in the ore minerals which are mined as either primary or secondary products and later refined to stable compounds such as oxides and salts

(Dobrescu, 2015). Considering the chemical affinity of each element, the lighter rare earth elements (LREE) are La, Ce, Pr, Nd, Sm, Eu and Gd and each have no paired 4f electrons in their atomic structure. The heavy rare earth elements (HREE) are Tb, Dy, Ho, Er, Tm, Yb, Lu (and Y) and have at least one paired 4f electron. Sm, Eu and Gd are sometimes referred to as medium rare earth elements (MREE) due to the gap in atomic number sequence created by Pm which does not occur naturally (Harmer & Nex, 2016).

A carbonatite is an igneous rock that forms from carbonate rich magma which originated in the earth's mantle. Illustrated in detail in Figure 8 carbonatite magmas form either from the melting of carbonate bearing lithospheric mantle which through metasomatism produces alkaline and calcite rich dolomitic melts or through fractional crystallization of carbonate rich and silica undersaturated magmas which also form nephelinites, melilitites or lamprophyres.

Yaxley et al., 2022 in Figure 8 describes the various stages of carbonatite formation. At stage 1, oceanic lithosphere is subducted and transports carbonate with the upper mafic oceanic crust. At stage 2, the surviving carbonate reaches the mantle transition zone. At stage 3, carbonatite melts are produced and through redox freezing form silicates, iron-nickel carbides and diamonds. At stage 4, if there is a presence of water, methane rich fluids are produced and through upwelling and plumes transports the carbon upwards. At stage 5, the melt decompresses, oxidizes and forms a carbonated silicate melt.

At stage 6, the melt starts to fractionate as it moves upwards evolving into carbonate bearing undersaturated mafic and ultramafic silicate melts. At stage 7, these melts reach the lithospheric mantle, causing metasomatism of surrounding mantle rock or ascend higher and form carbonatite melts. At stage 8, these carbonatite melts erupt onto the earth's surface Carbonatite emplacement is often accompanied by alkali metasomatism in the surrounding country rocks where fenitization occurs from fluids released during crystallization of the carbonatite (Anenburg et al., 2021).

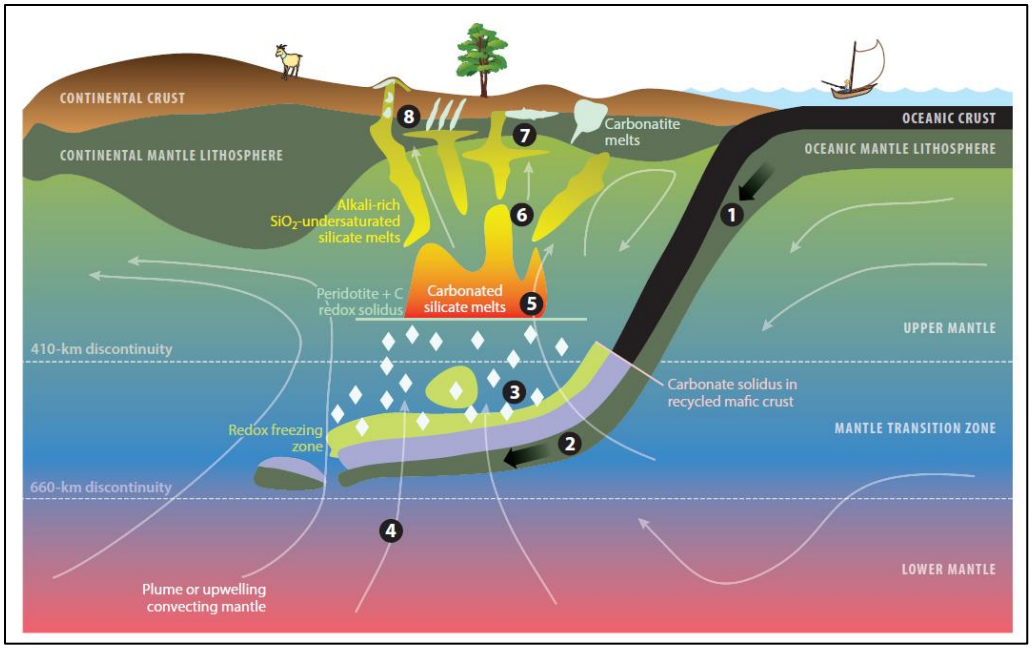

Figure 8: Schematic showing how carbonate and undersatured silicate melts are formed through deep recycling of carbon in the mantle. (Yaxley et al., 2022).

There are currently four main descriptive classifications for carbonatites used today which are based on chemical composition. These are calcite carbonatite, magnesium rich dolomitic carbonatite, siderite and calcite rich ferruginous carbonatite and iron rich ferrocarbonatite (Gittins & Harmer, 1997). A sodium rich natrocarbonatite is the fifth and uncommon occurrence of carbonatite observed at the only active carbonatite volcano in the world, the Ol'Doinyo Lengai volcano, located along the East African Rift, Tanzania (Anenburg et al., 2021).

Observed compositional changes of experimental carbonatite melts studied by Yaxley et al., (2022) looked at whether some carbonatites originated in the mantle or are the result of differentiation, immiscibility or fractionation. As alkaline silicate rocks are commonly associated with carbonatites, this may indicate either an origin from carbonated silicate melts (Tappe et al., 2017) or potential to have passed through the same crustal conduits without being petrogenetically related (Harmer & Gittins, 1998).

Once carbonatite melts from the mantle rise to surface, they encounter silicate and aluminium-rich crustal rocks as pressure decreases. This interaction between the two rock

types may consume the magnesium carbonate or dolomite component from the carbonatite and leave behind a calcite-rich carbonatite which requires higher fluxing components such as alkalis, fluorine or water for mobility after the departure of MgCO3. Once these carbonatites reach the cooler upper crust, calcite is the first to crystallize, leaving behind residual dolomite to crystallize in the uppermost crust and closer to the surface (Yaxley et al., 2022). Yaxley et al., (2022) further argues that calcite, dolomite and mafic silicate rich carbonatites observed on surface may all originate from the same parental magma depending on the complexity of the path taken from the mantle.

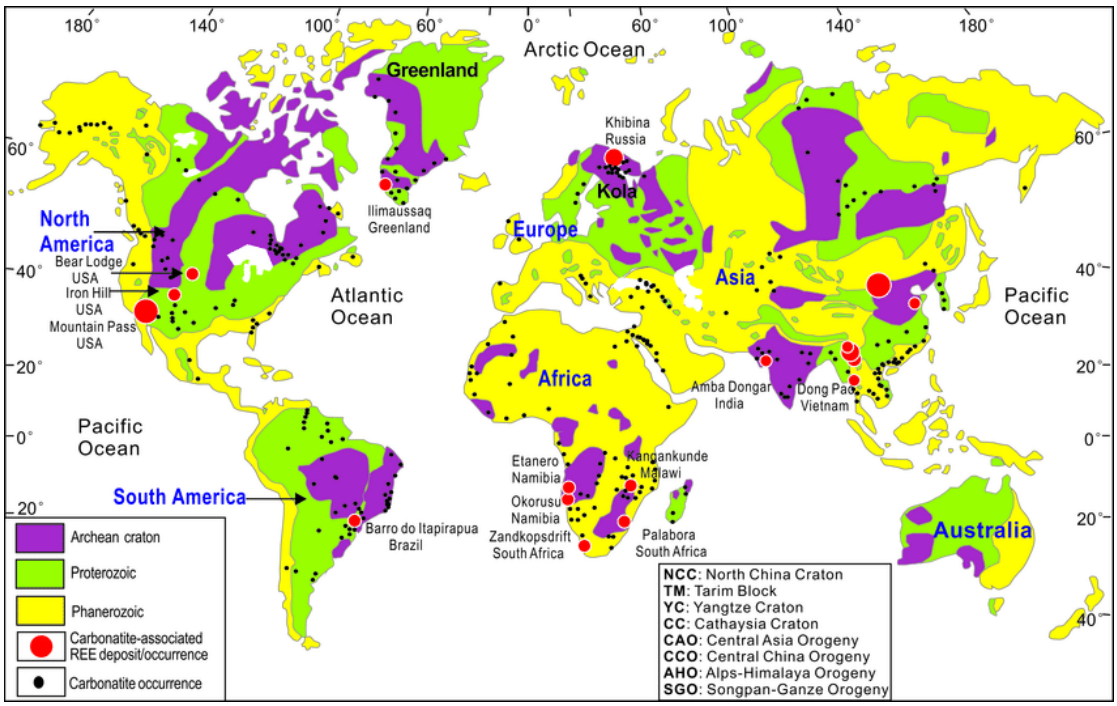

Figure 9: Map showing global carbonatite occurrences with carbonatite-associated REE deposits (CARD)s as red circles (Liu & Hou, 2017).

Carbonatites are not explicitly bound to specific geologic settings but are commonly found emplaced into Proterozoic and Phanerozoic continental crust and also in Archaean cratons. Of all carbonatites documented worldwide, only 10% are extrusive while the remainder are intrusive. Although carbonatites are the dominant source for REE deposits, of the 600 global carbonatite occurrences, only 10% are regarded as economic (Figure 9) (Simandl & Paradis 2018). Carbonatites that host REE deposits are commonly known as Carbonatite Associated REE Deposits (CARDs), (Liu & Hou, 2017).

A study by Hou et al., (2015) looked at the possible events and settings which potentially cause significant REE enrichment in the carbonatites of Southwest China. These carbonatites were located at the western margin of a craton and were subjected to accretion and strike slip faults caused by continental collision. The study suggested that cratonic edges, along divergent margins were the sources for super REE deposits with carbonatites forming from the melting of sub-continental lithospheric mantle (SCLM) further enriched by metasomatized REE and CO_2 rich fluids derived from subducted marine sediments. A comparison of barren carbonatites to known CARDs using fresh and unaltered carbonatite samples (Figure 10a & b) infers preferential enrichment being related to fluids instead of melts. High concentrations of barium suggests a derivation of CO_2 rich fluids from either marine sediments or subducted sediments and oceanic crust. These carbonatites, similar to Karingarab, Mountain Pass in North America and Lizhuang in China have 0.2% REE, 0.5% Sr and 0.1% Ba in their freshest samples' indicative of a combination of sources for enrichment such as crustal assimilation and an enriched heterogeneous parent source in the mantle combined (Hou et al., 2015).

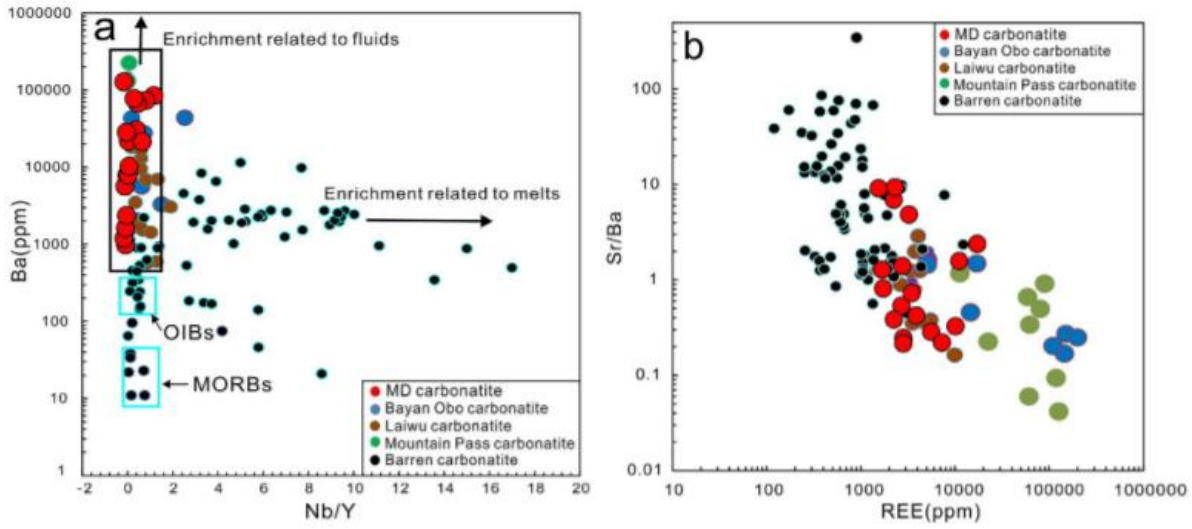

Figure 10: Comparison of barren carbonatites to known CARDs. 8a) Ba vs. Nb/Y: CARDs typically have low Nb/Y ratios (1:1) ±5% as fluid metasomatism does not easily fractionate chemically similar elements such as Nb and Y. This indicates enrichment due to fluid metasomatism which also produces sulphate minerals such as barite ($BaSO_4$) and celestine ($SrSO_4$). 8b) Sr/Ba vs. REEs: A weak and negative correlation exists between Sr/Ba ratios and REE concentrations as the metasomatism increases formation of celestine, barite and REE bearing minerals. (Hou et al., 2015).

4. Alkaline Rocks and Carbonatite occurrences of Namibia

Considering the various geological settings for carbonatites and the indicators of how carbonatites can be enriched with rare earth elements (REEs), Namibia has potential to host many economic deposits due to the complex geology which includes major tectonic events, mobile orogenic belts, accretion events, the presence of grabens and major erosion events. Namibia has over 50 carbonatite occurrences, frequently associated with alkaline rocks as shown in the geological map of Namibia in Figure 11.

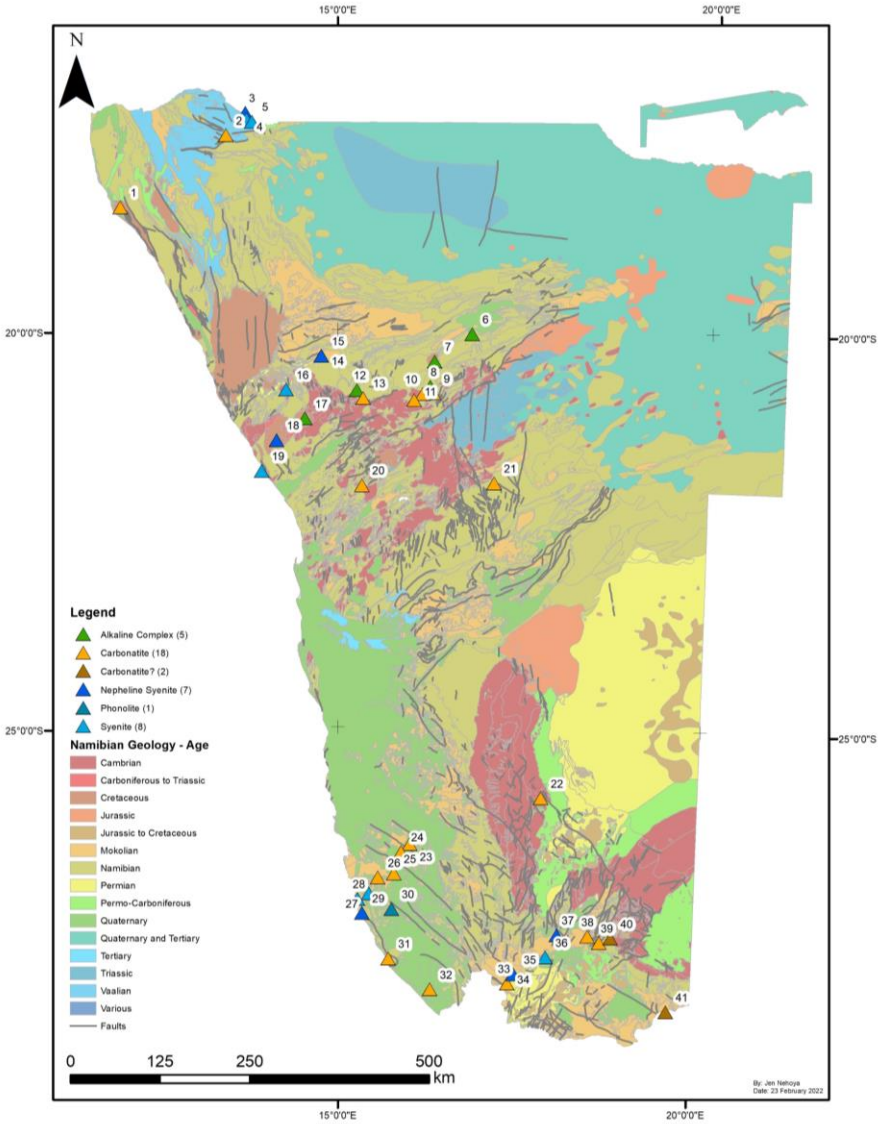

Figure 11: Carbonatite and Alkaline occurrences in Namibia, 1) Agate Mountain 2) Epembe 3) Kakumangua 4) Zebra Mountain Dykes 5) Swartbooisdrif 6) Okorusu 7) Paresis 8) Etaneno 9) Ondurakorume 10) Kalkfeld 11) Osongombe 12) Okenyenya 13) Kwaggaspan 14) Oas 15) Lofdal 16)

Doros 17) Brandberg 18) Messum 19) Cape Cross 20) Eureka 21) Otjisazu 22) Gross Brukkaros 23) Dicker Willem 24) Keishohe 25) Teufelskuppe 26) Kaukausib 27) Drachenberg 28) Pomona 29) Granitberg 30) Klinghardt Mountains 31) Chamais 32) Karingarab 33) Grootpenseiland 34) Marinkas Quelle 35) Kanabeam 36) Bremen 37) Haruchas 38) Mickberg 39) Weltevrede 40) Garub 41) Bokiesbank modified after Woolley, (2001).

Namibian carbonatites come in many forms from craters to dykes and are associated with various rock types including syenite, phonolite and other alkaline magmatism which all represents some similarity in either eruption style, intrusion and mineralogy and age of emplacement similar to what is observed at Karingarab. Of the over 50 occurrences of alkaline rocks and carbonatites in Namibia, 41 have been summarized and the data presented in Table 7 of the Appendix. This has been summarized mainly from Stocken (1978), Verwoerd (1993), and Woolley (2001).

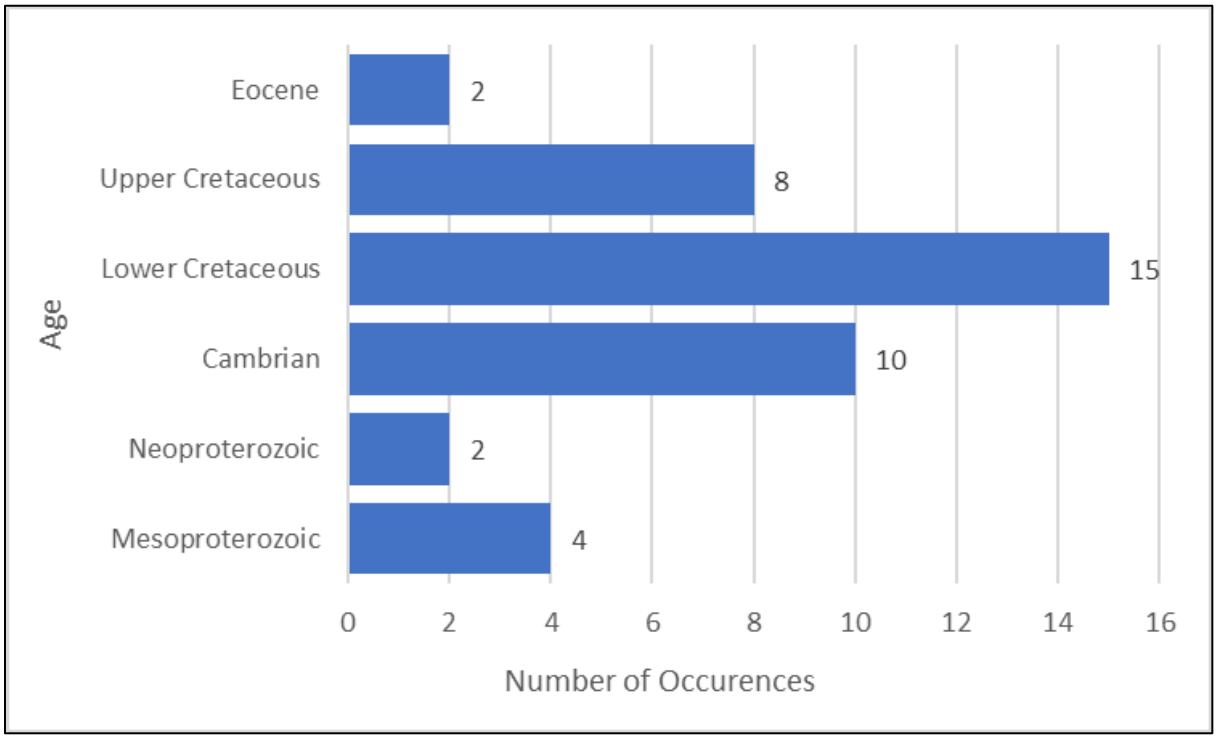

Figure 12: Age of Namibian carbonatites indicating major activity from the Cambrian and Cretaceous periods.

The oldest of the Namibian occurrences summarized by age in Figure 12, are the Epembe carbonatite dyke, Swartbooisdrif, Kakumangua and Zebra Mountain syenite dykes which were emplaced along north-west trending faults in northern Namibia during the Mesoproterozoic,

while the youngest Dicker Willem carbonatite along with the Klinghardt phonolite suites was emplaced into the Gariep belt, in the south of Namibia during the Eocene. The majority of occurrences were emplaced in the Cambrian and Cretaceous.

Most carbonatites in Namibia are characterized by concentric shapes and structures and from field observations have high relief and steep sides compared to their surrounding plains. Country rocks surrounding these occurrences are often fenitized and show brecciation as proximity to the complex increases with outer rings composed of syenite and phonolite. Examples of these include Agate Mountain, Ondurakorume, Kalkfeld, Osongombe, Otjisazu, Gross Brukkaros, Dicker Willem, Teufelskuppe and Karingarab which are younger and emplaced between the lower Cretaceous and the Eocene. Of these occurrences only Agate Mountain, Gross Brukkaros and Karingarab show evidence of eruptive activity while the rest are predominantly intrusive.

Of all the carbonatite hosted REE exploration targets in Namibia, Lofdal is the most advanced project and recently completed a preliminary economic assessment in October 2022 after declaring an earlier resource estimate of 42.57 million tonnes at 0.17 % TREO above a 0.1 % cut off grade as measured and indicated resources (Witley et al., 2021). The Lofdal carbonatite consists of multiple intrusions of nepheline syenite cross-cut by two plugs of carbonatite bodies known as the Main Intrusion and the Emanya Intrusions along with a swarm of phonolitic and carbonatitic dykes. Lofdal is unique as it is enriched in HREE prevalent in dykes (Harmer and Nex, 2016).

5. Location of the study area

5.1. Regional Geology

Namibia, located on the southwestern coast of Africa, geomorphologically evolved with southern Africa and has undergone multiple phases of intracontinental rifting, spreading, subduction and collision for the past 3,500 Ma where some of the oldest parts of Namibian continental crust formed through accretion onto the Kaapval craton at 2 Ga (Miller, 2008). Although surviving many supercontinent cycles, of note for the development of southern Africa, shown in Figure 13, are the movements of the Kalahari craton which was part of Rodinia and assembled in the later Proterozoic from 1,000 Ma. With the split of Rodinia, Gondwana formed along with the Damara Orogen in the Neoproterozoic from 550 Ma, eventually breaking up to form the South American and African continents in the Cretaceous from 115 million years ago (Schneider, 2008).

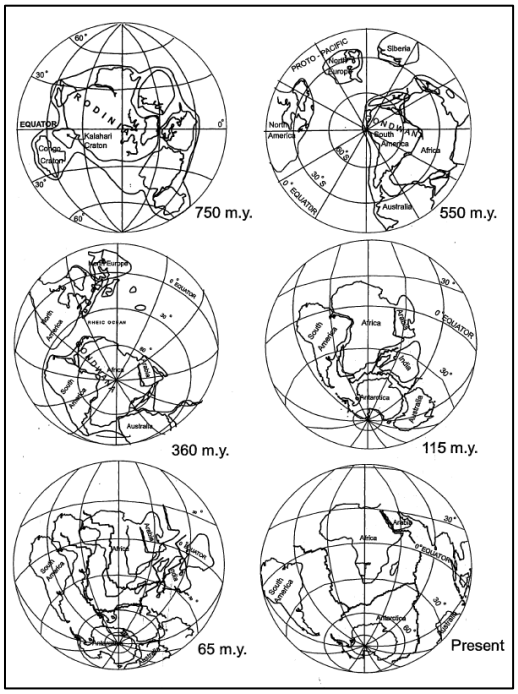

Figure 13: Evolution of Southern Africa from the Neoproterozoic to the present (Schneider, 2008).

The events that occurred during the Damara Orogen in the Neoproterozoic resulted in three distinct tectonic mobile belts (Kaoko, Damara and Gariep) which separated the Congo and Kalahari cratons and whose rocks cover a large portion of Namibia. These 3 orogenic belts meet at a triple junction near the coastal town of Swakopmund at the center of Namibia's

coastline. The northern most is the Kaoko Belt which trends north-north-west along the coast into Angola while the Damara belt trends north-east and crosses the country into Zambia (Figure 14). The Gariep Belt extends southwards along the coast joining the Saldania Mobile belt in South Africa (Miller, 1983).

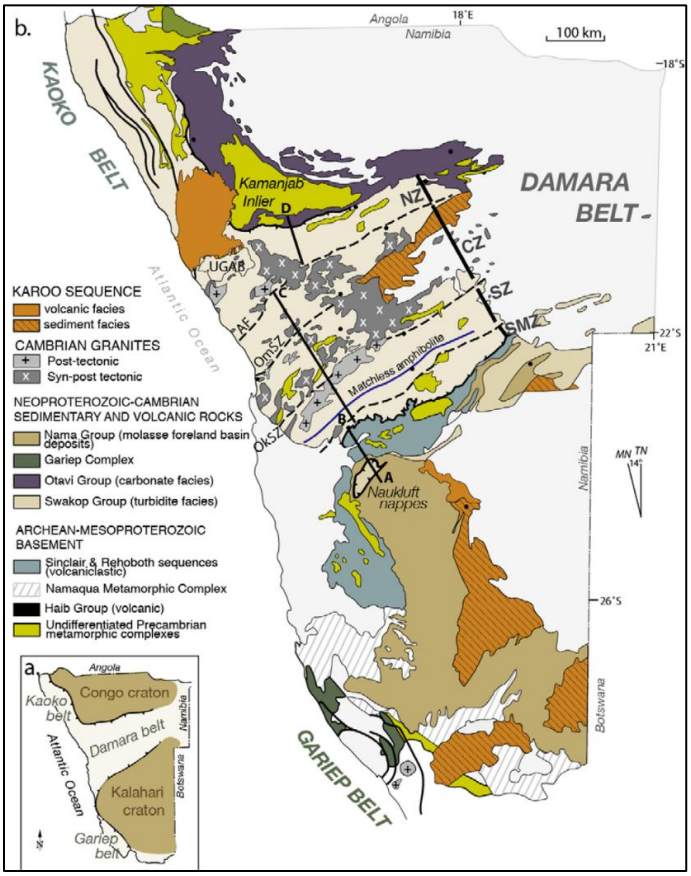

Figure 14: Simplified Geological Map of Namibia indicating the 3 mobile belts of the Damara Orogen (Foster & Goscombe, 2013).

The Gariep Belt has been studied in detail by Frimmel, (1995) who observed preservation and records of multiple tectonic events such as crustal thinning from the breakup of a super continent in the Mesoproterozoic, to continental rifting, basin formation, basin closure and continent collision for the formation of Gondwana in the Neoproterozoic. Frimmel, (1995) first observed that the original extent of the Gariep basin had been obliterated due to intense folding, thrusting and wrench faulting with only the eastern margin of the basin still preserved. The remaining preserved area comprises of two major tectonostratigraphic units, the Port

Nolloth Zone in the east and the Marmora Terrane in the west separated by a structural and lithological discontinuity, the Schakalsberge Thrust (Frimmel, 2000).

The stratigraphy and evolution of the Gariep Belt in Figure 15 starts with the continental thinning of the pre-Gariep basement rocks of the Namaqua Metamorphic Complex which produced felsic magmatism of the Richtersveld Suite from 837 Ma to 750 Ma, during this time rift deposits of the Stinkfontein subgroup were deposited as coarse-grained siliclastics with minor volcanic and pyroclastic deposits as well as other depositional material consistent with alluvial and delta settings (Frimmel, 2000). These deposits formed in grabens resulting from the continental rifting which were subparallel, north-east trending and deepening towards the south (Frimmel, 2000). This event was followed by a swarm of mafic dykes of the Gannakouriep Suite during continental splitting which occurred at 750 Ma (Frimmel, 2008).

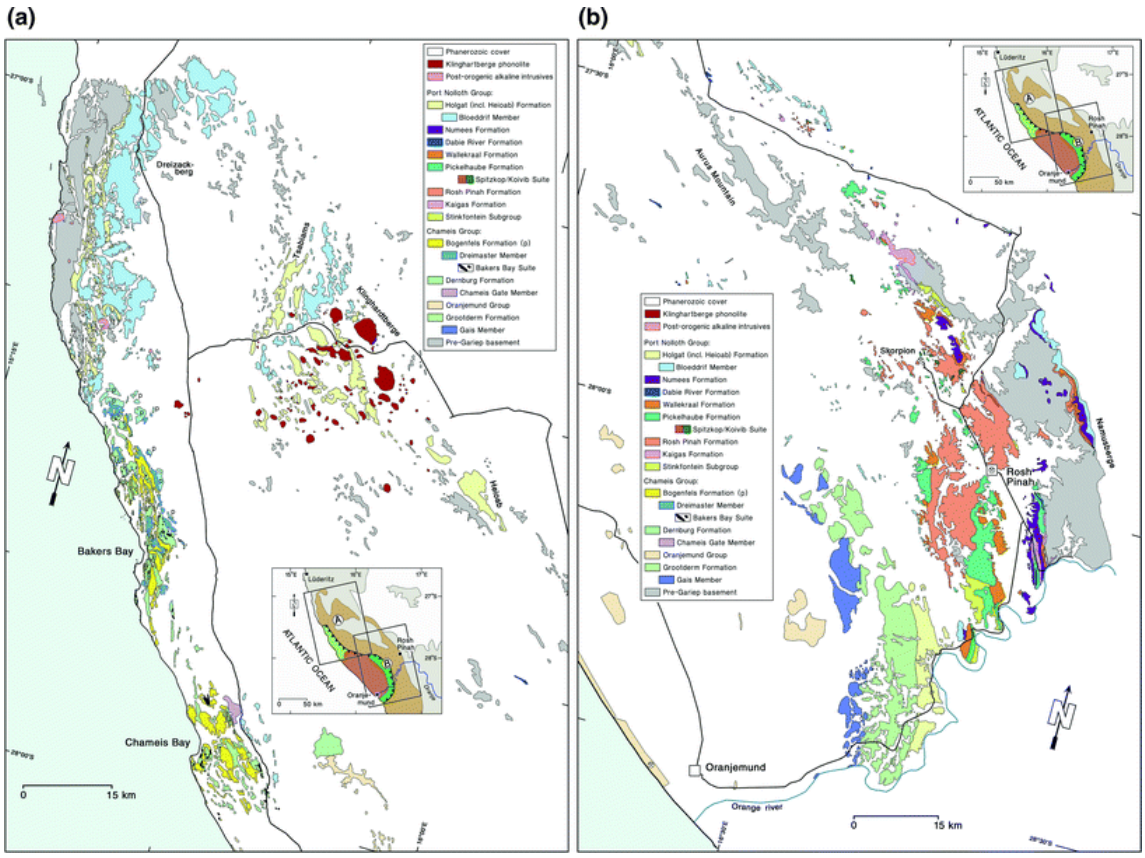

Figure 15: Lithostratigraphic Map of the Gariep Belt showing a) the northwestern block where Chameis and Port Nolloth subterranes dominate b) the southeastern block where the Schakalsberge separates the Oranjemund subterrane from the Port Nolloth zone (Frimmel, 2008).

At 750 Ma a global glaciation older than both the Sturtian and Marinoan events also occurred which deposited diamictites of the Kaigas formation above the Stinkfontein Subgroup (Frimmel, 2000). Around this period the sedimentary exhalative sulphide deposits of the Rosh Pinah Formation formed in these sub basins associated with late-rift, felsic extrusive igneous activity (Frimmel, 1995). Later, at about 640 Ma, another global glaciation event, the Marinoan, occurred creating a major erosional unconformity event which cut down into the basement rocks in some places as no record of the glaciation event is present in the Gariep Belt, Frimmel, (2000) speculates that this portion of the Gariep Belt may have been elevated and exposed during this time. This event was followed by a depositional event on the erosional unconformity which consisted of coarse-grained, siliclastic sediment and dolomitic mega-breccias of the Wallekraal Formation, followed by shallow marine stromatolite reef mounds of the Dabie River Formation as the western most graben opened into a narrow marine basin with oceanic crust for a base. In the marine basin, at about 600 Ma, mafic and ultramafic rocks of the Dernburg and Grootderm Formations accumulated which Frimmel, (2000) determined to have similar geochemical affinity to mid-ocean ridge and ocean island arc signatures with observations of island mounts covered in algal reef and marine evaporites.

A third glaciation event, known as the Gaskiers or Moelv event, occurred between 590 and 565 Ma which is correlated with the Numees Formation diamictites of the Port Nolloth Group (Frimmel, 2000). These diamictites are covered by cap carbonates and thick, turbiditic siliclastic successions of the Holgat and Bogenfels Formations as well as the Oranjemund Group during the closure of the Gariep Basin. As the basin closed, Frimmel (2000), observed that these deposits formed on top of advancing thrust sheets of the Marmora terrane prior to continental collision between 550 and 545 Ma. During the collisional event, contractional deformation occurred accompanied by the formation of a fold and thrust belt and low- to medium- grade metamorphism. As rocks were exhumed, erosion occurred depositing sediments into the Nama foreland basin north-east and inland of the Gariep (Frimmel, 1995).

The last major events occurred in 507 Ma, when Nama molasse sediments of sandstones, shales and conglomerates were deposited in the basin while post-orogenic alkaline magmatism occurred along the Kuboos-Bremen Line in the south (Frimmel, 2000). From the Cambrian to the Cretaceous periods, the uneroded remains of the Gariep Belt formed a landmass now bordered on the south-east by the Karoo basin, and only in 130 Ma when South

America split from Southern Africa, was the remaining landmass of the Gariep Belt down faulted to the west, partly submerged into the Atlantic Ocean with the South America equivalent preserved in the Rocha Formation of Uruguay (Frimmel, 1995).

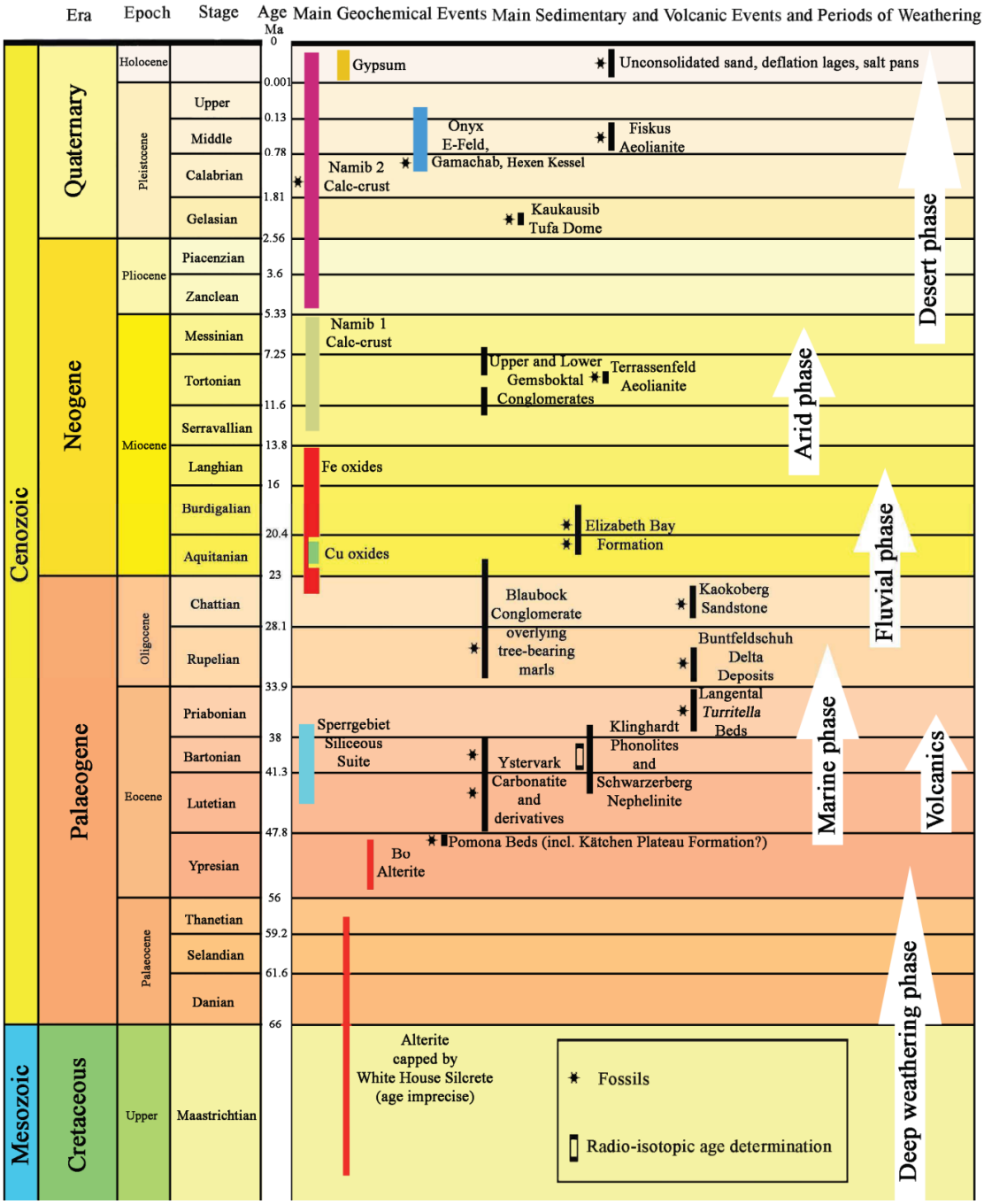

Figure 16: Summary of the main geological events since the Mesozoic in the Northern Tsau-//Khaeb, Namibia, Pickford, (2015).

Pickford et al, (2014) considers the northern Tsau-//Khaeb National Park which hosts most of the Gariep Belt as holding record of many geological events since the break-up of Gondwana. Pickford et al, (2014) through many expeditions, has collected and documented fossils and evidence of weathering, erosion, transportation, deposition, volcanism, diagenesis, pedogenesis, tectonic activity and eustatic sea level changes (Figure 16) with dates of events controlled by fossils and radio-isotopic dating methods. For an area that has been undergoing weathering and erosion since the split from Gondwana, Pickford et al., (2014) notes that the Ystervark, Schwarzerberg and Klinghardt volcanism in the Eocene disrupted this erosion, with still preserved carbonatite ash forming up to 25 m thick deposits in depressions.

These events were followed by volcano related hydrothermal activity which caused the surficial rocks to harden and become resistant to erosion through silicification. In Figure 16, the Ypresian Bo Alterite event pre-dates the Sperrgebiet Siliceous Suite, a suite which occurred during the Eocene when most carbonatite and phonolite volcanic activity took place in the Sperrgebiet. The identification of fossils in the Sperrgebiet Siliceous Suite has determined that this suite does not form part of the African Surface Silcretes, however, Pickford, et al, (2015), states that the preceding White House Silcrete event is of Cretaceous age and may correlate to other African Surface Silcretes mapped elsewhere in the continent.

5.2. Local Geology

The Karingarab Carbonatite, at depth, intrudes into the Marmora Terrane which is subdivided into three distinct subterranes namely the Schakalsberge, Oranjemund and Chameis as shown in Figure 17 from Frimmel (2008). The Schakalsberge represents an unconformity between the Marmora Terrane and Port Nolloth Zone and consists of the Grootderm mafic volcanics overlain by the Gais carbonates very similar to the stratigraphic units of the Chameis subterrane. Frimmel, (2008), suggested grouping both within the Chameis Group as the Chameis Group is dominated by mafic metabasalts, oolitic dolomites, volcanic tuffs and siliclastics over a basement of phyllites, chlorite schists, and quartzites with diamictites also present.

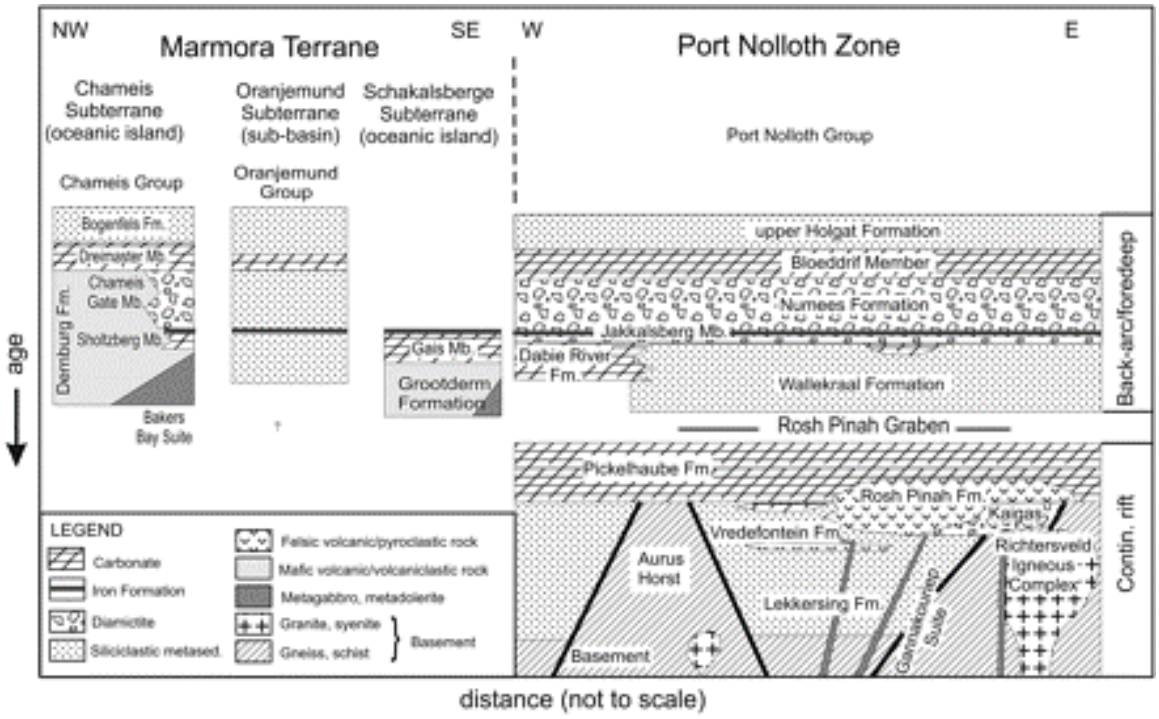

Figure 17: Lithostratigraphy comparing the Marmora Terrane and Port Nolloth Zone (Frimmel *et al*., 2008)

From field observations, rocks of the Oranjemund Group within the Marmora Terrane dominate within the area surrounding the Karingarab Carbonatite and unlike the Chameis Group that contains abundant mafic volcanic rocks, the Oranjemund Group described by Basei et al., (2005) is dominated by chlorite schists with a base of laminated chlorite phyllites followed by dolomites, ferruginous thin chert bands and low metamorphic grade quartz arenites, feldspathic arenites and argillites and remains mostly covered by aeolian sand.

5.3. Area Geology

The Karingarab Carbonatite is observed as a low circular hill rising above the surrounding plains which are covered in aeolian sands (Figure 18). The main target has a diameter of 2.5 km and smaller concealed intrusives with similar geophysical magnetic signatures are observed towards the south and southeast. The area geology was mapped by Wilson in 1978, Siegfried in 2014 and Nehoya et al. in 2020. As of 2022, four broad categories of outcrop lithologies remain which are; 1) phonolite and lamprophyre dykes, 2) carbonatites of various

compositions; 3) surficial sediments such as a lag of manganese and iron oxides occasionally hosted in calcrete and lastly 4) thick windblown sand overburden which correlate to what was first observed and defined by Wilson in 1978.

Figure 18: View of the Karingarab Carbonatite from the western access road facing east, at a distance of 7 km.

Confirming previously mapped outcrop, this author observed that references to country rock includes schists and phyllites in outcrop on the access road 15 km west of the carbonatite hill. On the carbonatite hill, various silicified and wind etched carbonatite is observed, finer-grained towards the north and often coarser and re-crystalized towards the east and centre and again gradually becoming more aphanitic towards the west and south. Abundant magnetite, pyrite and often dendritic manganese oxides are visible and disseminated throughout the complex in the disseminated lag and observed in outcrop. Flow banded siliceous lamprophyres outcrop on the western slopes of the hill with brecciation increasing towards the central carbonatite. On the south-west of the carbonatite, a porphyritic phonolite dyke trends north-west to south-east for 500 m and has visible feldspars, pyroxenes and clasts of country rock schists. Throughout the complex, many clasts of various lithologies are observed, including highly jointed and fine-grained blue calcite-rich limestones which are found as flat pavement 500 m north of the complex.

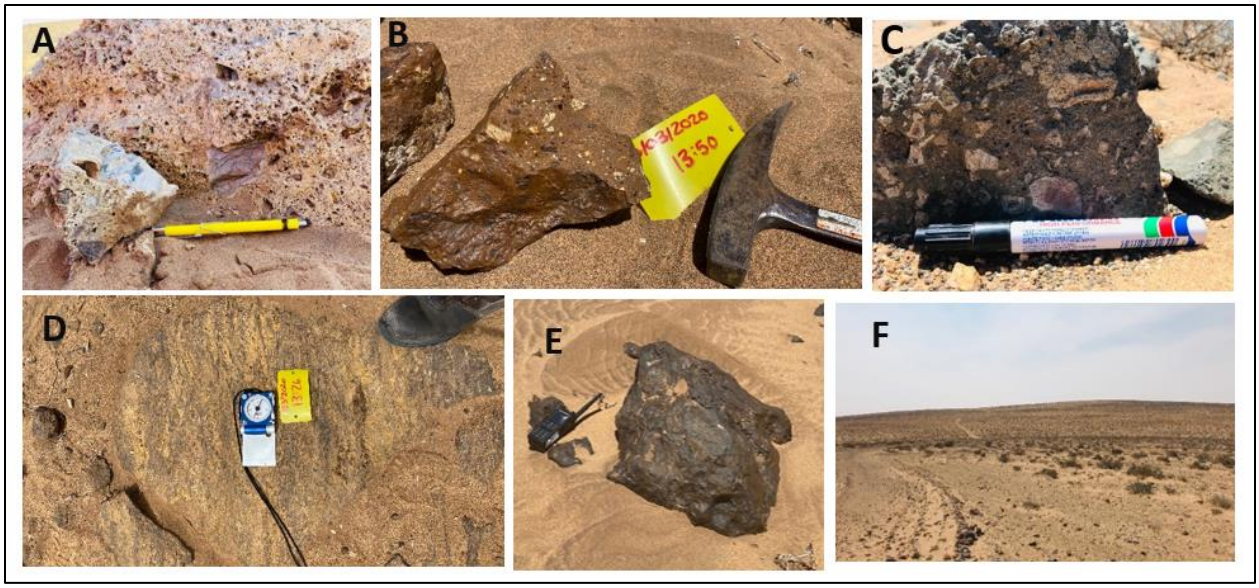

Figure 19: Common rock types observed in outcrop at Karingarab. A) Siliceous and vesicular lamprophyres, B) Oxidized and silicified clastic phonolite C) Porphyritic phonolite D) Granular banded carbonatite E) Fine grained silicified carbonatite F) Surficial Fe-Mn rich lag on aeolian dune sand.

Three separate outcrops of nepheline-bearing porphyritic phonolite were observed with large phenocrysts of feldspars, pyroxenes and lithic clasts (Figure 19 B&C). Only one outcrop of lamprophyre dyke (Figure 19 A) was observed and together these units appear to form two separate smaller hills and a dyke on the north-west and west of the main complex.

On surface two main facies are present, the first, being a coarse grained, banded, lighter coloured carbonatite with specks of calcite, intergrown barite and inward dipping magnetite present (Figure 19 D). Other minerals identified in this carbonatite are micas (phlogopite), dolomite, iron and dendritic manganese oxides, clays such as goethite and preserved yellow and green powdery REE ore minerals (monazite and bastnäsite).

The second carbonatite in outcrop, which appears as a gossan, is harder, darker in colour and finer-grained (Figure 19 E) which due to crosscutting relationships appears younger than the banded lighter coloured carbonatite. On surface it appears hard and silicified, however, upon breaking a fresher specimen, it is more weathered and granular, chocolate brown in color with a matrix richer in clays, pyrites, micas and manganese and iron oxides. This carbonatite type

appears as dykes and veins transgressing the banded lighter carbonatite as well as forming several plugs up to 300 m in diameter on the main carbonatite hill where exposed.

Apart from where outcrop is observed, the area is covered by superficial material (Figure 19 F) interspersed with calcretes and silcretes. The superficial deposits are dominated by windblown aeolian sands and alluvial fan deposits. The alluvial fan deposits which form an iron and manganese oxide rich lag off the main target, flows seaward towards the north, north-west and west. The events that lead to the silicification of surficial carbonatite and formation of calcretes over the carbonatite are responsible for the preservation of the carbonatite and for trapping its enriched REE mineralization even after the subsequent multiple erosion events that transported diamonds offshore and potentially produced the lag. The Karingarab carbonatite was preserved potentially by the same regional silicification event evident in other parts of the Sperrgebiet such as the White House Silcrete event in the late Cretaceous or the Bo Alterite event in the Eocene (Pickford, 2015).

6. Exploration at Karingarab

Multiple exploration projects have occurred at Karingarab for which the earliest documented records are from 1977, exploration is active and ongoing in 2022.

6.1. 1977 – 1978: General Mapping and Sampling

The first sampling campaign on the prospect took place in 1977, with mapping and the collection of 16 rock chip and soil samples. These samples were analyzed and returned anomalous Pb, Zn, Ba, Mo, Th, La, Nb and Y values. As the high values drew interest to the prospect, a second more comprehensive geochemical sampling and mapping campaign was scheduled for the same year. For the second sampling campaign, 256 representative samples were collected on a grid of 3x3 km, with samples collected every 200 m on N-S lines.

These samples were composed of Fe - Mn gossan carbonatite fragments, phonolite, fenitized country rock outcrop and cemented calcrete conglomerate. They were submitted for geochemical analysis by XRF. Additional exploration activity included a theodolite survey at 200 m spacing to produce a topographic map of the complex and a scintillometer survey to detect radiation was also conducted at 50 m intervals on the 200 m lines.

Exploration continued in 1978, with a sampling campaign on narrower 6 x 50 m square grids. 173 samples in total were collected and assay results confirmed the existing chemical anomalies, however a conclusion was reached not to prospect the carbonatite further (Figure 20).

> These results effectively downgrade the carbonatite as a possible porphyry molybdenum deposit.
>
> From the commercial view point, P_2O_5 remains the most likely economic constituent of the carbonatite. However analytical results are still awaited.

Figure 20: Extraction of conclusion of initial prospecting over the Karingarab Carbonatite in 1978, Wilson (1978).

6.2. 2005 – 2010: Regional Magnetic Survey and Grab Samples for REE Analysis

Following a 27 year hiatus, in 2005 the target was revisited by Anglo American Prospecting Services (Ambase) to explore the rare earth element (REE) potential and 7 grab samples were collected and analyzed for major oxides (Table 1). Of the 7 samples, 6 out of 7 contained more than 1% total rare earth elements including Sc and Y (TREE) and one of the 6 grab samples exceeded 8% TREE (Table 2). The lighter shaded tiles indicate the common banded carbonatite units whilst the darker shaded units indicating gossan and brecciated units.

Table 1: Major oxide element analyses (in %) with selected trace elements of 7 grab samples from Karingarab, Schaefer, (2005).

Sample	Rock Type	SiO2	Al203	Fe203	MgO	CaO	Na20	K20	TiO2	P205	MnO	Cr203	Ba (ppm)	Ni
OB7987	CARB	0.78	0.14	8.65	16.65	27.43	0.08	0.05	0.04	1.51	1.6	0.001	15663	5
OB7988	CARB	1.14	0.26	27.96	6.45	27.39	0.12	0.05	0.39	1.35	1.49	0.001	23391	5
OB7995	CARB	0.63	0.16	4.61	14.8	34.09	0.1	0.07	0.01	0.68	1.41	0.001	9192	11
OB7989	GOS	1.65	1.33	28.91	0.11	1.07	0.33	1.38	0.18	0.62	44.13	0.001	50492	5
OB7990	GOS	3.21	4.08	35.58	0.01	0.91	0.09	0.13	0.18	1.15	18.43	0.018	39701	5
OB7991	GOS	2.22	2.81	21.86	0.09	0.35	0.2	1.25	0.32	0.46	48.37	0.001	62332	14
OB7992	GOS	4.74	2.28	38.73	0.16	1.31	0.15	0.58	0.2	0.76	30.08	0.001	51418	22

Table 2: REE analytical data (in ppm) of 7 grab samples from Karingarab, Schaefer, (2005).

Sample	Rock Type	Sc	Y	La	Ce	Pr	Nd	Sm	Eu	Gd	Tb	Dy	Ho	Er	Tm	Yb	Lu	REE_sum
OB7987	CARB	11	92	10500	16035	1238	3068	202	36	113	9	28	3	7	1	4	1	3.12%
OB7988	CARB	23	199	3253	7011	609	1556	138	31	84	10	44	7	18	2	13	2	1.28%
OB7995	CARB	61	268	7897	10876	863	2422	283	68	179	17	68	9	20	2	12	1	2.27%
OB7989	GOS	60	348	1110	4261	591	2644	571	143	309	32	129	16	36	5	29	3	0.99%
OB7990	GOS	100	6424	29934	12761	>10000	>10000	9704	2366	4585	554	2062	237	524	68	360	38	**8.32%**
OB7991	GOS	64	995	2632	1642	804	3874	1006	284	666	87	361	56	134	19	111	14	1.17%
OB7992	GOS	164	910	9901	14612	2245	7649	1211	317	804	93	344	44	94	12	70	8	3.74%

From the regional magnetic surveys conducted by Branko Corner, AMBASE detected potential satellite intrusions east of the main target (Figure 21) however, ground truthing could not confirm visible outcrop synonymous with Karingarab due to sand cover.

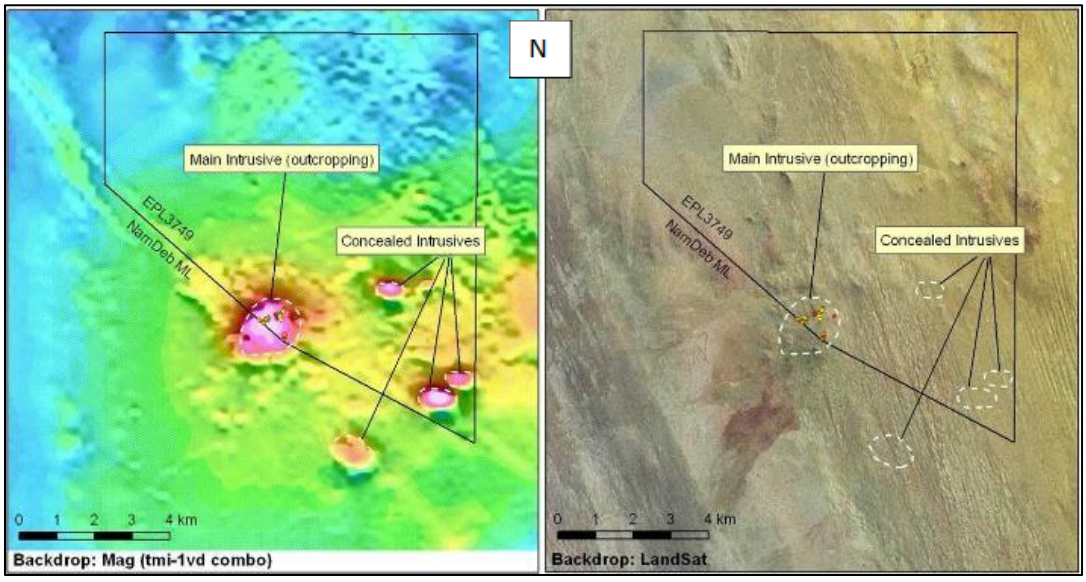

Figure 21: Main and concealed intrusions on EPL 3749 and ML 43, Schaefer (2005).

In 2010, a reconnaissance grab sampling campaign was initiated over the main carbonatite to confirm previous assays (Table 3). From the analysis, Schaefer (2010) noted that in banded lighter coloured and less weathered carbonatites total REE averaged at 2.2%, ranging between 0.78% and 5.47%, while for detrital and brecciated carbonatites an average of 0.58% TREE was encountered. The Fe-Si rich carbonatites (fine grained, dark, hard, gossan-like) recorded the highest grade of TREE of 2.79% (Figure 22).

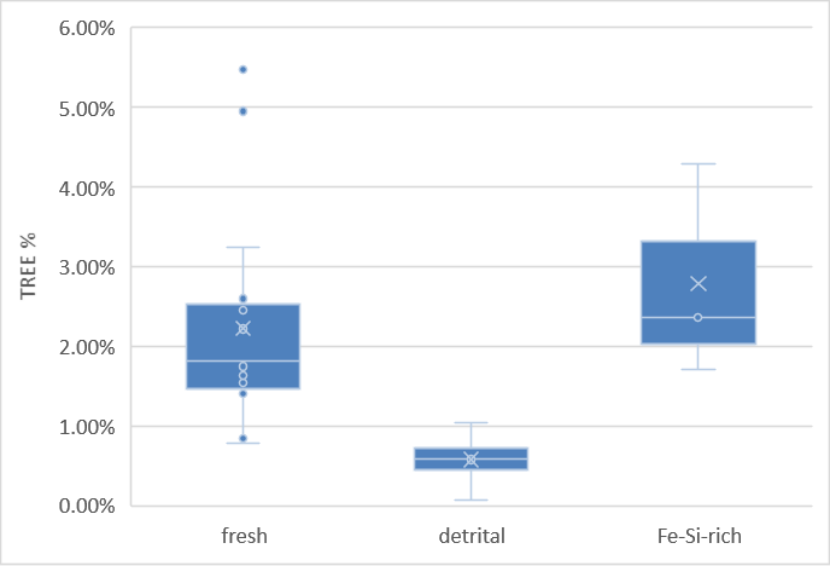

Figure 22: Box plots of average total rare earth element percentage of grab samples from Karingarab.

Table 3: REE assay results (in ppm) of 22 grab samples from Karingarab. Fresh and pure carbonatites are highlighted in very light blue, detrital and brecciated carbonatites in light blue and silicified with high Fe-Si content in a darker shade of blue. Schaefer, (2010).

Sample	Type	Ce	La	Pr	Nd	Sm	Eu	Gd	Tb	Dy	Ho	Er	Tm	Yb	Lu	Total	TREE-Sum	Y
1	fresh	23,600	19,500	1,710	4,190	273	45	130	8	28	4	7	1	4	0	49,498	4.95%	109
2	fresh	9,110	6,020	729	2,060	194	38	92	9	37	6	14	2	8	1	18,319	1.83%	161
3	fresh	8,330	5,130	777	2,550	334	70	164	17	72	11	22	2	12	1	17,492	1.75%	262
4	fresh	3,990	1,850	472	1,650	230	54	115	14	62	10	23	3	14	2	8,486	0.85%	274
5	fresh	7,070	4,800	696	2,200	299	67	149	17	75	12	27	3	16	2	15,433	1.54%	355
6	fresh	15,200	11,600	1,210	3,400	371	84	219	24	123	23	60	7	33	4	32,357	3.24%	706
7	fresh	8,310	4,820	729	2,140	177	32	75	7	30	5	15	2	10	1	16,353	1.64%	151
8	fresh	10,800	7,330	979	2,710	234	48	82	8	35	5	9	1	4	1	22,247	2.22%	120
9	fresh	3,630	1,900	414	1,430	186	42	84	9	40	6	11	1	5	1	7,758	0.78%	144
10	fresh	8,750	5,730	809	2,320	226	48	90	10	49	9	25	4	22	3	18,094	1.81%	286
11	fresh	7,140	3,470	703	2,260	244	47	110	11	44	7	15	2	9	1	14,062	1.41%	168
12	fresh	11,500	9,660	901	2,260	166	33	64	6	27	4	9	1	5	1	24,636	2.46%	104
15	fresh	3,870	2,250	439	1,820	298	59	118	11	44	7	15	2	10	1	8,943	0.89%	178
16	fresh	26,200	20,000	2,010	5,340	521	115	311	31	130	19	37	4	16	2	54,735	**5.47%**	469
17	fresh	12,400	9,500	956	2,590	253	50	125	12	48	7	15	2	9	1	25,968	2.60%	179
AVE. FRESH		**10,660**	**7,571**	**902**	**2,595**	**267**	**55**	**128**	**13**	**56**	**9**	**20**	**2**	**12**	**1**	**22,292**	**2.23%**	**251**
18	detrital	3,210	1,090	283	1,100	166	36	90	11	51	8	21	3	17	2	6,090	0.61%	210
18b	detrital	6,190	1,790	379	1,410	208	48	144	19	98	17	43	6	33	4	10,389	1.04%	352
18c	detrital	330	159	38	142	27	7	20	3	21	4	13	2	13	2	780	0.08%	157
19	detrital	1,750	1,630	382	1,530	218	47	110	13	61	11	29	4	22	3	5,809	0.58%	339
AVE. DETRITAL		**2,870**	**1,167**	**271**	**1,046**	**155**	**34**	**91**	**11**	**58**	**10**	**26**	**4**	**21**	**3**	**5,767**	**0.58%**	**265**
20	Fe-Si-rich	9,130	2,330	791	3,250	551	140	414	52	242	38	93	12	73	10	17,126	1.71%	869
21	Fe-Si-rich	17,900	10,100	2,310	8,870	1,500	372	965	114	461	64	139	17	100	14	42,926	4.29%	1,464
22	Fe-Si-rich	1,380	6,230	2,050	9,570	1,910	452	966	119	499	73	160	20	117	17	23,563	2.36%	1,199
AVE. Fe-Si-RICH		**9,470**	**6,220**	**1,717**	**7,230**	**1,320**	**321**	**782**	**95**	**401**	**58**	**131**	**16**	**97**	**14**	**27,872**	**2.79%**	**1,177**

Following the campaigns in 2010, a 4-year hiatus ensued, and very little activity took place at Karingarab. Regional work in the Sperrgebiet took place including detailed geophysical magnetic and radiometric surveys and a reconnaissance mapping exercise of outcrop (Figure 23) over the main target by Siegfried, (2014) confirming and building on the earlier observations while also mapping new outcrop exposures uncovered by prevalent winds.

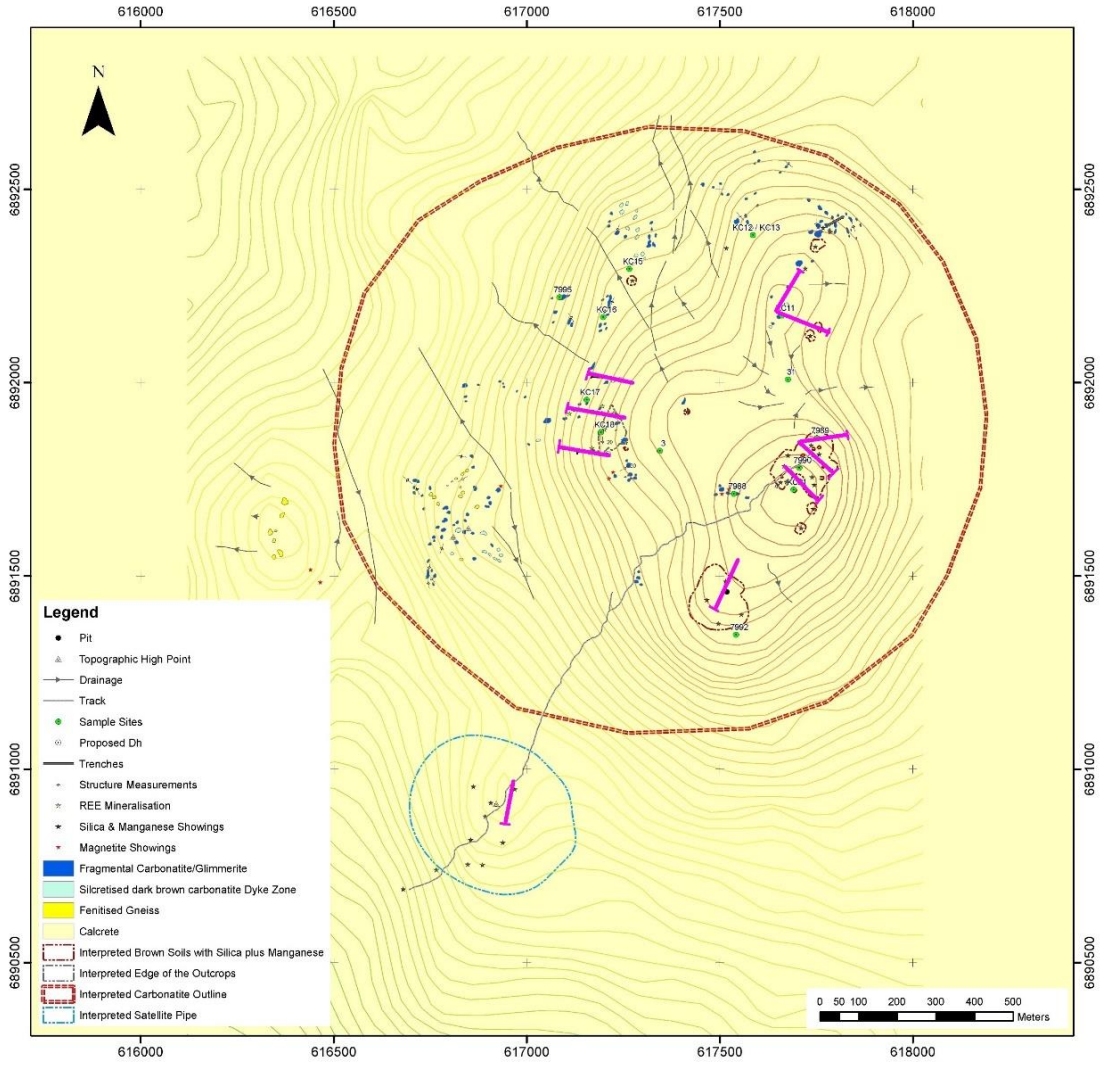

Figure 23: 2014 Reconnaissance mapping and proposed drilling locations, Siegfried (2014).

6.3. 2014 Diamond Drilling Campaign

Following a renewed interest to explore the target supported by the geophysics and mapping, the first drilling program at Karingarab took place from 2014 - 2015 (Figure 24). 10 HQ sized, 65◦ inclined drillholes of 100 m depth each were proposed using diamond drilling for a total of 1,000 m. Diamond drilling was aimed at high magnetic geophysical targets and outcrops of interest from the mapping (Figure 23) to gather more geological information on the subsurface through detailed lithological logging, collecting of samples for chemical and mineralogical studies and complete downhole geophysics with optical televiewer (OPTV) images.

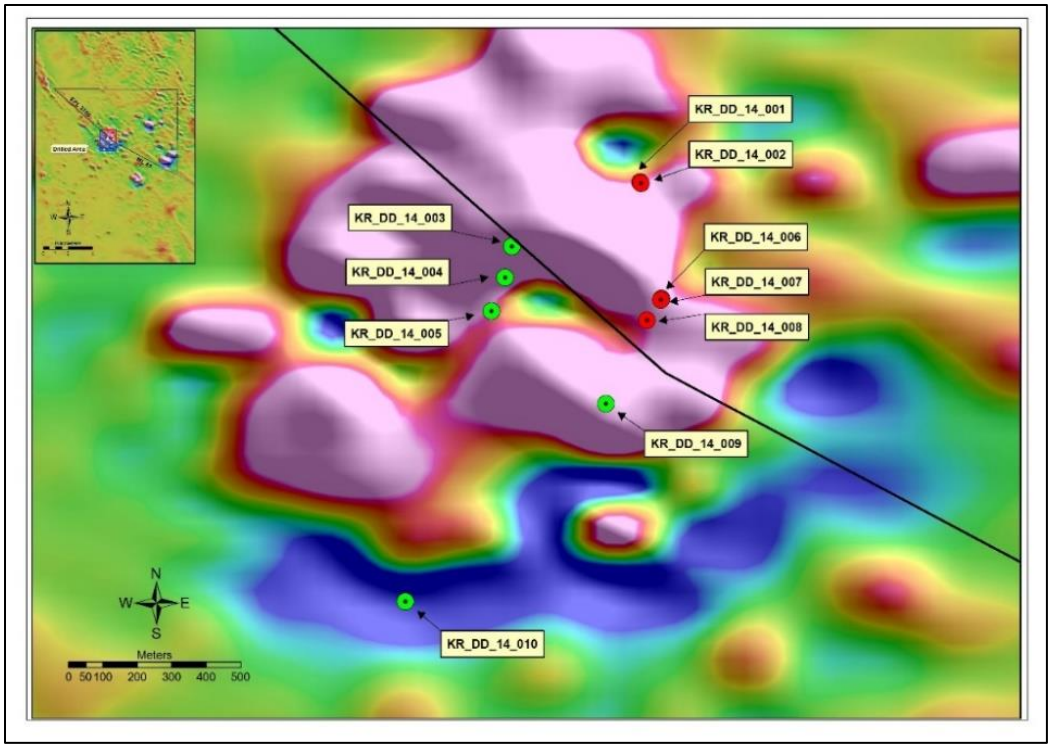

Figure 24: Map showing diamond drilling borehole positions superimposed on Total Magnetic Intensity (TMI) data for the Karingarab Carbonatite, Grobbelaar (2014).

Following the success of the drilling campaign, and the first time that subsurface lithologies were observed, 6 types of carbonatites, 4 types of phonolites and other minor rock types were identified below surface (Figure 25). These ranged from fresh to deeply weathered, fine- to medium- grained, with varying amounts of minerals, layering and banding, volcanic clast enrichment and dilution with phonolites, country rock and other alkali igneous rocks. All boreholes showed weathering in carbonatites at depth and no fresh carbonatites were intercepted.

In comparison to mapped outcrop, the sub-surface lithologies confirmed that although some textures and mineralization were preserved, the outcrop was highly altered through silicification and not a true indication for the subsurface lithologies and their degrees of weathering.

Carbonatite Types
CRBNT1: Banded Carbonatite, non-magnetic. Fine-medium grained.
CRBNT2: Banded Carbonatite; magnetic. Fine-medium grained
CRBNT3: Mottled Carbonatite with less pronounced banding. Medium grained.
CRBNT4: Very fine grained Carbonatite, magnetic, Mn dendrites prominent
CRBNT5: Clast rich Carbonatite. Has a high percentage of Phonolite clasts and other clasts.
CRBNTV: Volcanic Clast rich Carbonatite.
Phonolite Types
PHNT1: Unfractured Phonolite/massive; more weathered.
PHNT2: Fractured Phonolite with minor Carbonatite infill in fractures (vein-like structures).
PHNT3: Clast rich Phonolite comprised of pebble sized clasts.
PHNTc: Phonolite clasts
Calcrete Types
CNGL1: Matrix supported Calcrete conglomerate with abundant Fe oxide and manganese (Mn) clasts.
CLCRT2: Calcrete, minimal manganese (Mn) clasts.
Barite Rock
BRTR: Barite rock characterized by white powdery mineral. High relative density
Clasts
CLSTv: Various clasts
Other
RBINF: Red brown infill
RBS: Red brown sand
CL: Core Loss

Figure 25: Initial log codes for first subsurface lithology identified at Karingarab (Grobbelaar, Itengula and Siegfried, 2014)

Preliminary portable Niton XRF data was collected at points every 0.5 m intervals on the core and used to optimise logging and sample selections. Apart from one hole which consisted mostly of clastic alkali silicates, all samples were dispatched for wet chemistry analysis with samples bound to lithologies and ranging between 0.8 m and 1.2 m intervals.

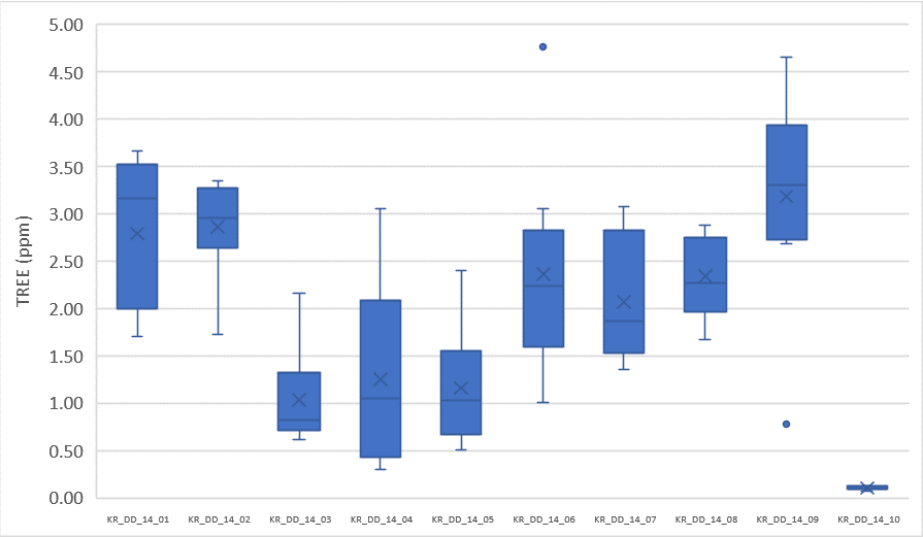

Figure 26: Average TREE per hole for the diamond drilling campaign from wet chemistry.

Results from geochemical analysis of samples from the first drilling campaign (Figure 26) were positive for enrichment below surface. High grade and continuity due to weathering were

observed on the east of the complex. Although grades varied laterally and downhole, the average for the 10 holes assayed was 1.9% TREE with varying lithologies encountered and no clear relationship between depth and grade (Figure 27).

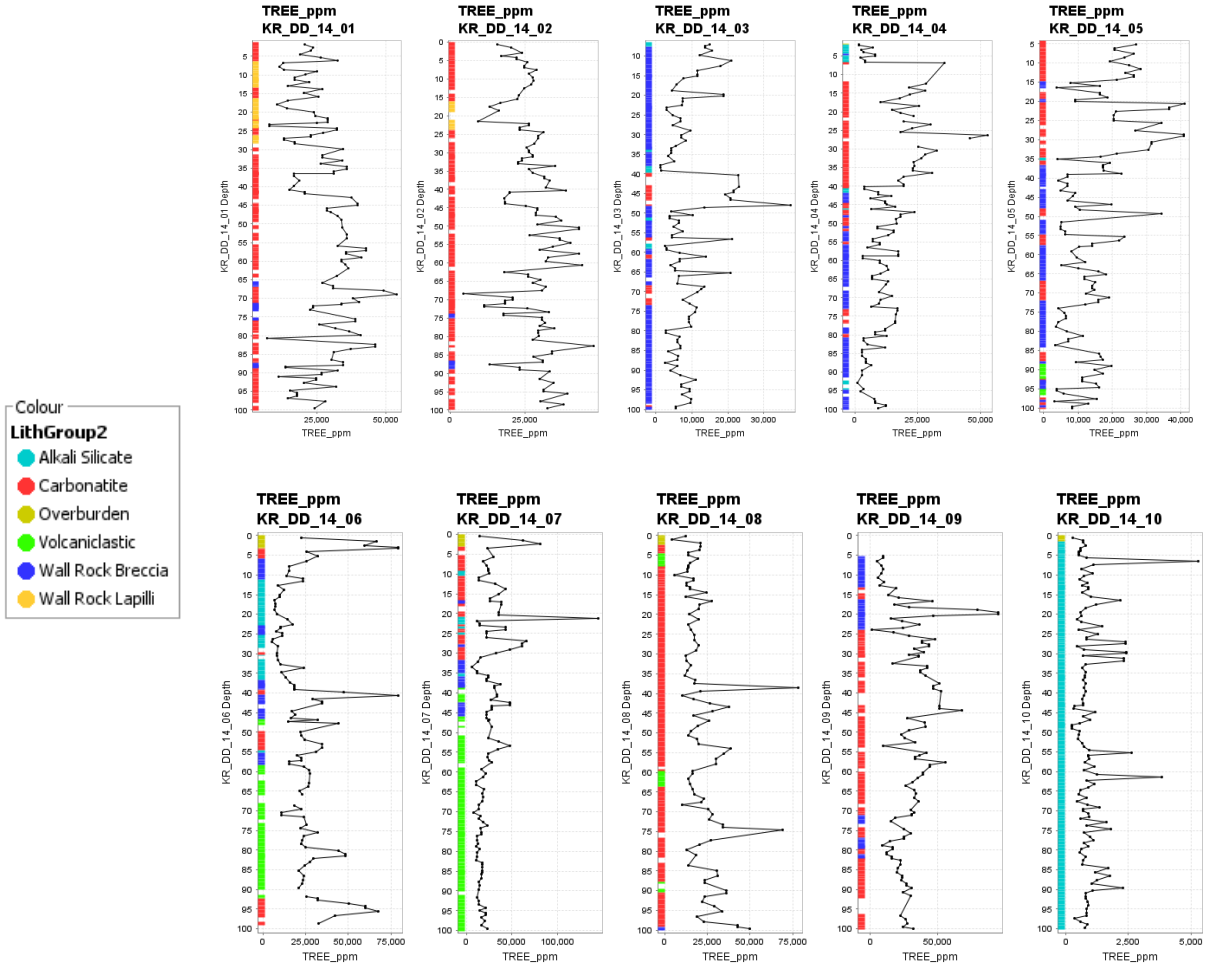

Figure 27: Downhole plots of grade and lithology from the 2014 Diamond drilling (DD) campaign.

Of interest to note is the variability in lithology between holes which shared a collar such as the pair of holes 1 and 2 and the pair of 6 and 7. These holes were drilled at 65 degrees dip and opposing azimuths.

In addition to geochemical assays, further analysis was conducted on the core to identify and quantify the REE ore-bearing and gangue minerals as well as the mineralogical relationships of the carbonatite. Four core samples were sent to Mintek in South Africa for X-Ray Diffraction (XRD), Scanning Electron Microscopy (SEM) and bulk modal mineralogy investigations. These four samples were chosen based on the lithology, alteration profile and preliminary TREE

content with the findings of Carelse, (2017) summarized in Figure 28, Figure 29, Figure 30 and Figure 31.

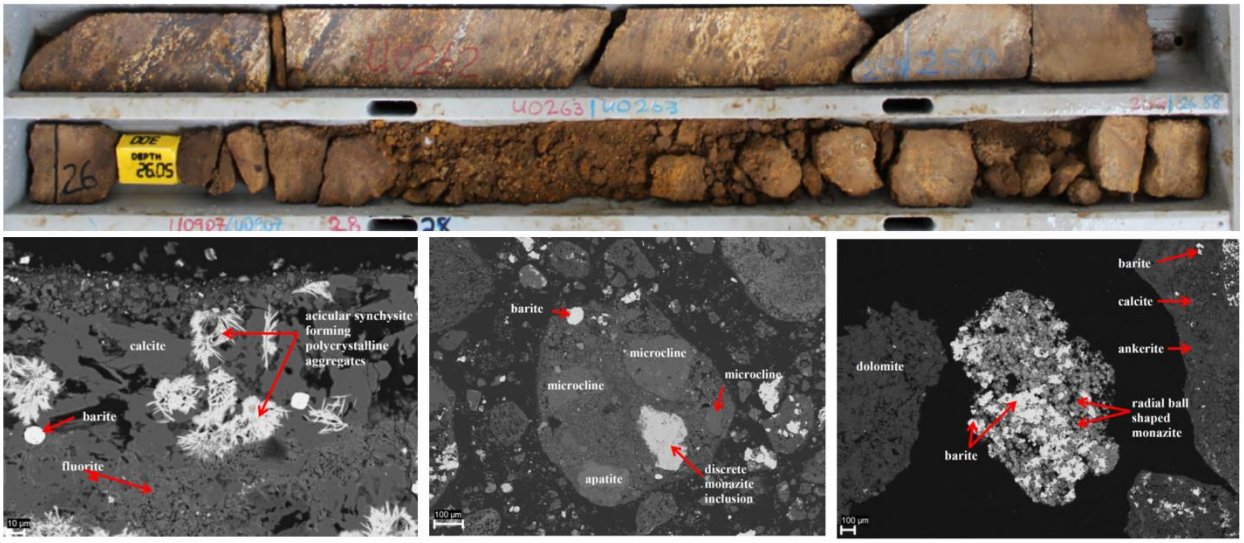

Figure 28: KR_MIN_16_001, this sample was collected from a banded and weathered carbonatite in hole KR_DD_14_04 at a depth of 25.88 – 26.88 m, with a TREE content of 6.95%. Results determined that the matrix comprised of carbonates such as ankerite, dolomite and calcite with a highly porous texture. The pore spaces were intergrown with light REE bearing polycrystalline aggregates of acicular synchesites and ball shaped radial growth Ca-monazite (cheralite). These REE bearing minerals are more associated to barite than the Fe (goethite) and Mn (hollandite and romanechite) oxyhydroxides.

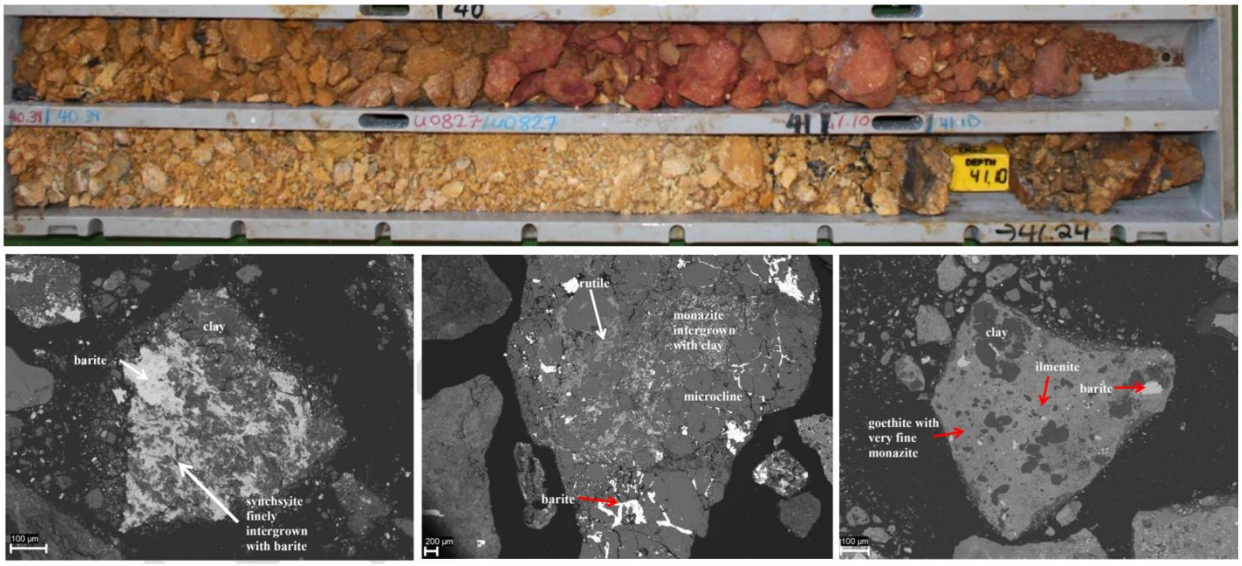

Figure 29: KR_MIN_16_002, this sample was collected from an extremely weathered textureless, fine grained unit within a kaolinized and oxidized unit in hole KR_DD_14_06 at a depth of 40.39 – 41.10 m, with a TREE content of 9.93%. This sample is dominated by barite, microcline, fluorite and clay minerals with the REE minerals of monazite and synchesite either finely intergrown as clusters of

acicular crystals or filling the matrix as anhedral discrete crystals.

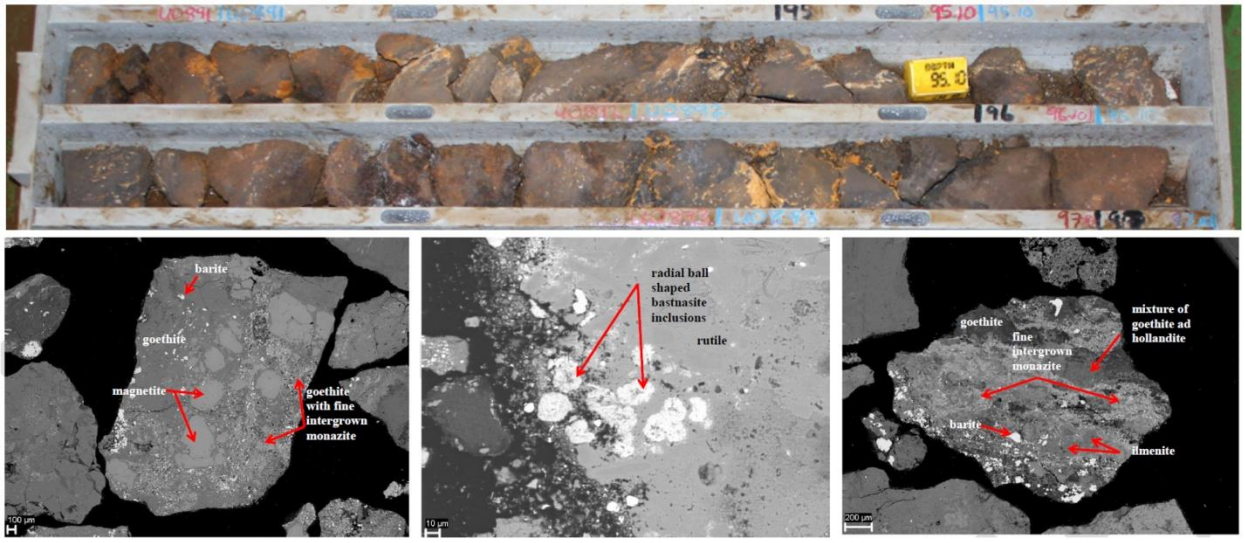

Figure 30: KR_MIN_16_003, this sample was collected from a highly weathered barite rich unit with a high felt density further down in hole KR_DD_14_06 at a depth of 95.10 – 96.10 m, with a TREE content of 8.08%. This specimen was dominated by barite and the oxyhydroxides goethite, romanechite and hollandite often forming concentric zoning or banding. The REE minerals in this unit were diverse and identified as monazite, florencite, synchesite, bastnäsite and cerianite finely intergrown or forming ball shaped radial features.

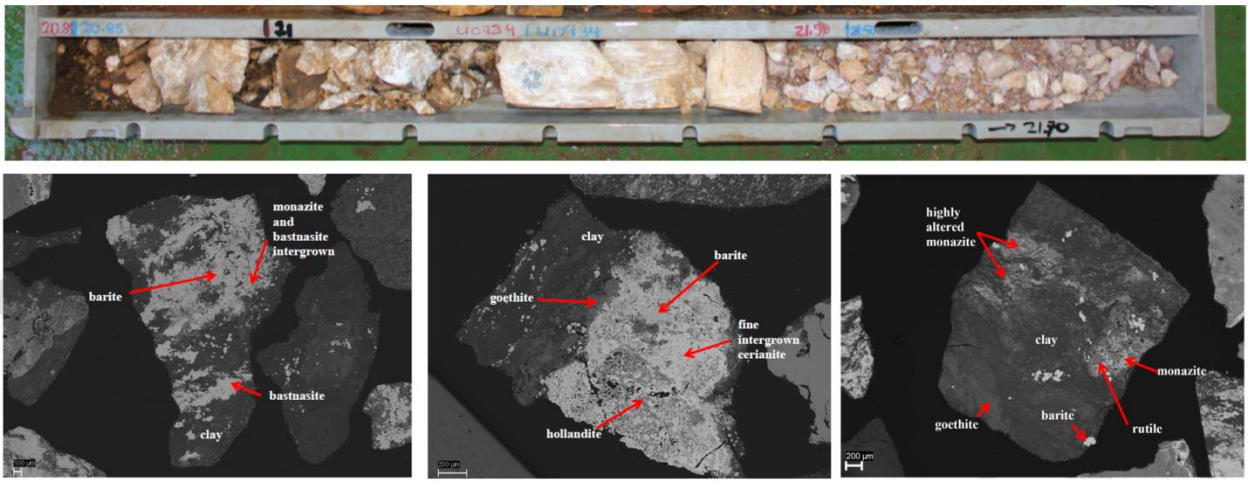

Figure 31: KR_MIN_16_004, this sample similar to that of Figure 29, was collected from an extremely weathered, textureless, fine grained barite rich unit with a high felt density and a soapy feel in hole KR_DD_14_07 at a depth of 20.85 – 21.50 m, this sample interval had the highest TREE content of the campaign of 17.40%. This specimen was dominated by barite and clay minerals. In these specimens, the REE mineralogy was intergrown with the clay forming banding and zonations and appeared much larger in size than the other specimens with monazite highly altered with its structure depleted in phosphorous and enriched in Fe.

Samples were characterized in terms of gangue and ore mineralogy, textures and associations. The mineralogical tests indicated that bastnäsite and monazite are the dominant REE ore minerals with minor synchesite and florencite with all occurring as inclusions or interstitial growths filling pore spaces, zones and bands. Dolomite and microcline were identified in substantial quantities with minor barite and fluorite. Clay minerals which characterize the more weathered, higher grade and shallower lithologies were identified as goethite, hollandite and romanechite.

In addition to this drilling program, each diamond drillhole was accompanied by a downhole geophysics survey which took place shortly after drilling (Figure 32). These downhole traces also included optical televiewer photographs as the probing tools moved down the holes to detect in-situ structural features of the various rock types. Additional survey methods including resistivity, density and magnetic susceptibility which were used to determine the passive signatures of the lithology encountered. Caliper readings were also studied to identify potential fractures and cavities.

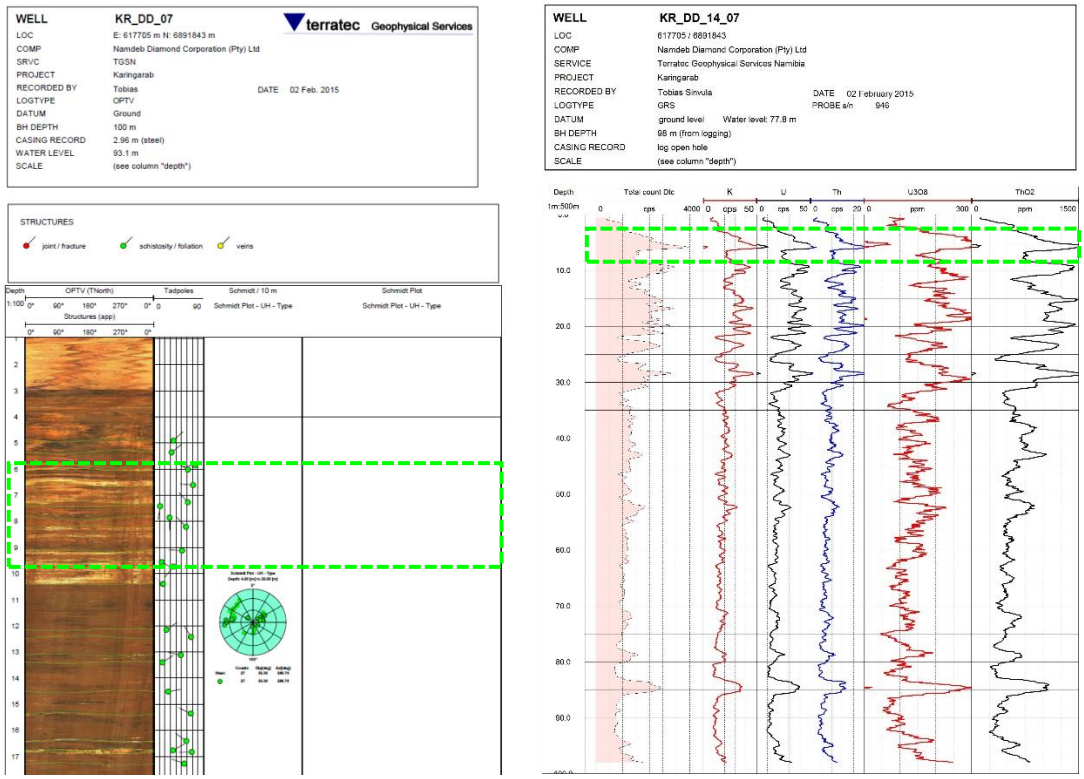

Figure 32: Downhole geophysical logs of DD borehole KR_DD_14_07 indicating structures detected in OPTV (left) and downhole surveys with positive response in radioactive elements U, K and Th at 6-9

m (right). This section was logged as a light-yellow and brown, clastic and banded carbonatite with a presence of clays and TREE at 2.5%

6.4. 2016 RC Drilling Campaign

The second drilling program at Karingarab took place in 2016 with 21 inclined drillholes mostly of 150 m depth using reverse circulation (RC) drilling for a total of 3,000 m (Figure 33). This drilling was proposed to test outcrop and build on the growing library of subsurface information by drilling deeper than the previous campaign and particularly on the edges of the carbonatite to determine the extent of the target below surface both laterally and vertically.

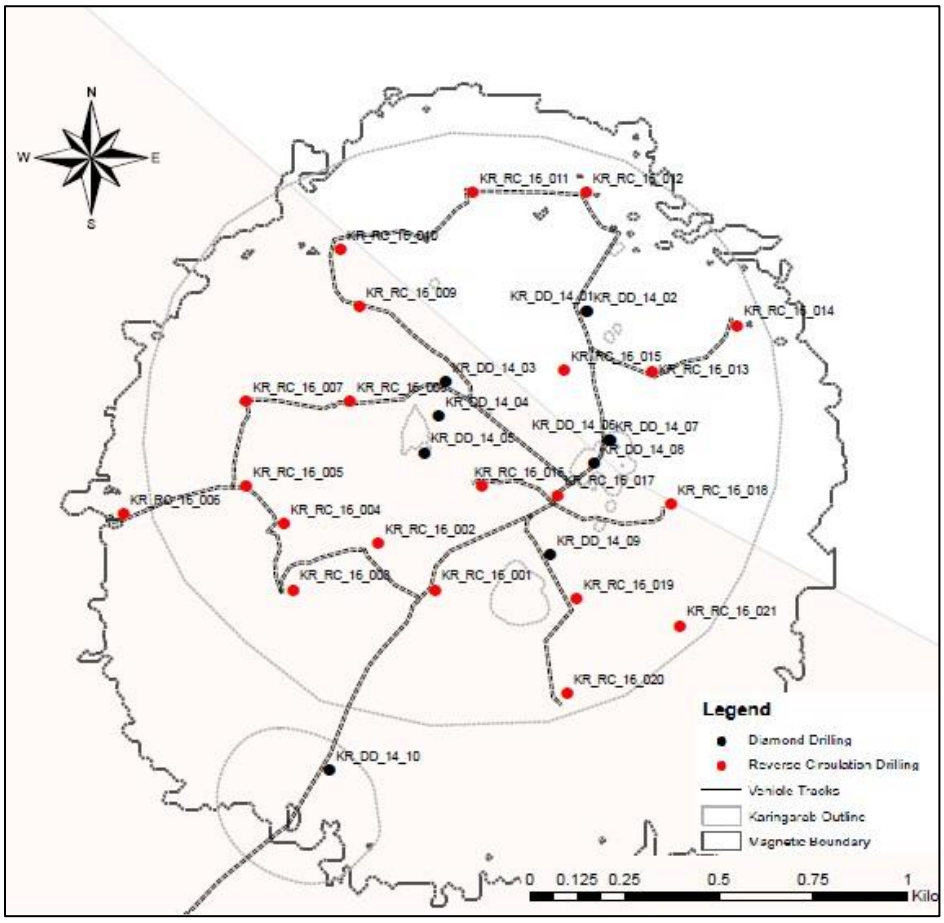

Figure 33: Overview map of the Karingarab Carbonatite showing 2016 RC Drilling in red, prior DD drilling in black.

Drill chips generated were logged and sampled on 1 m intervals, which provided a total of 3,000 samples. The trend for anomalous REE content at Karingarab continued with the assay

results (Figure 34). Mineralization and weathering were confirmed at depths of up to 180 m. Most interestingly from these results, it was determined that anomalous REE (including Sc and Y) was present in various lithology types and not constrained to the weathered carbonatites.

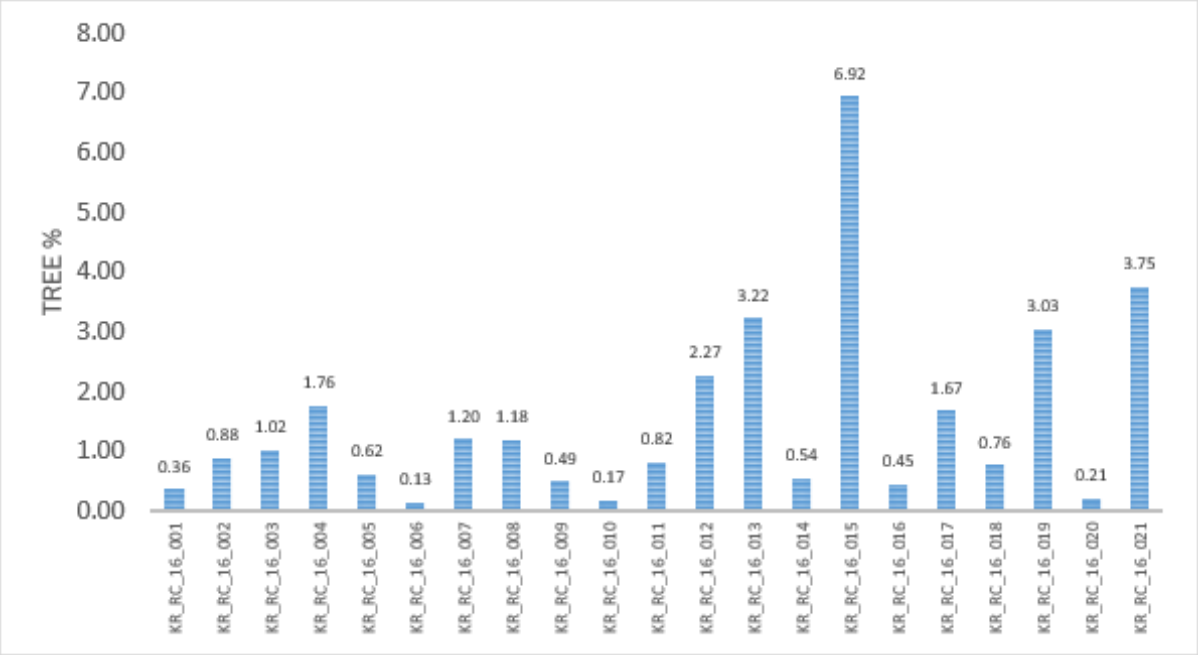

Figure 34: Average total rare earth element results (including Sc and Y) of RC samples per drillhole.

Although grades varied laterally and downhole, the average for the 21 holes assayed was 13,000 ppm TREE including Sc and Y. Higher grades where holes had an average of more than 30, 000 ppm TREE, positively correlated to higher degrees of weathering occurring on the north to southeastern half of the carbonatite hill. Lower grades and more dilution were observed on the western half of the carbonatite where fresher unweathered intersections were encountered, however, grades were moderate and averaging between 10,000 – 30,000 ppm TREE and could not be constrained to any lithological boundary due to the high dilution with reverse circulation drilling.

The campaign confirmed positive results and indicated in some areas that the deposit was still open at depth and in other areas that mineralization may be deeper than anticipated

below lower grade or barren material in the fresher carbonatites such as in holes 2, 4, 5, 9 and 18 (Figure 35).

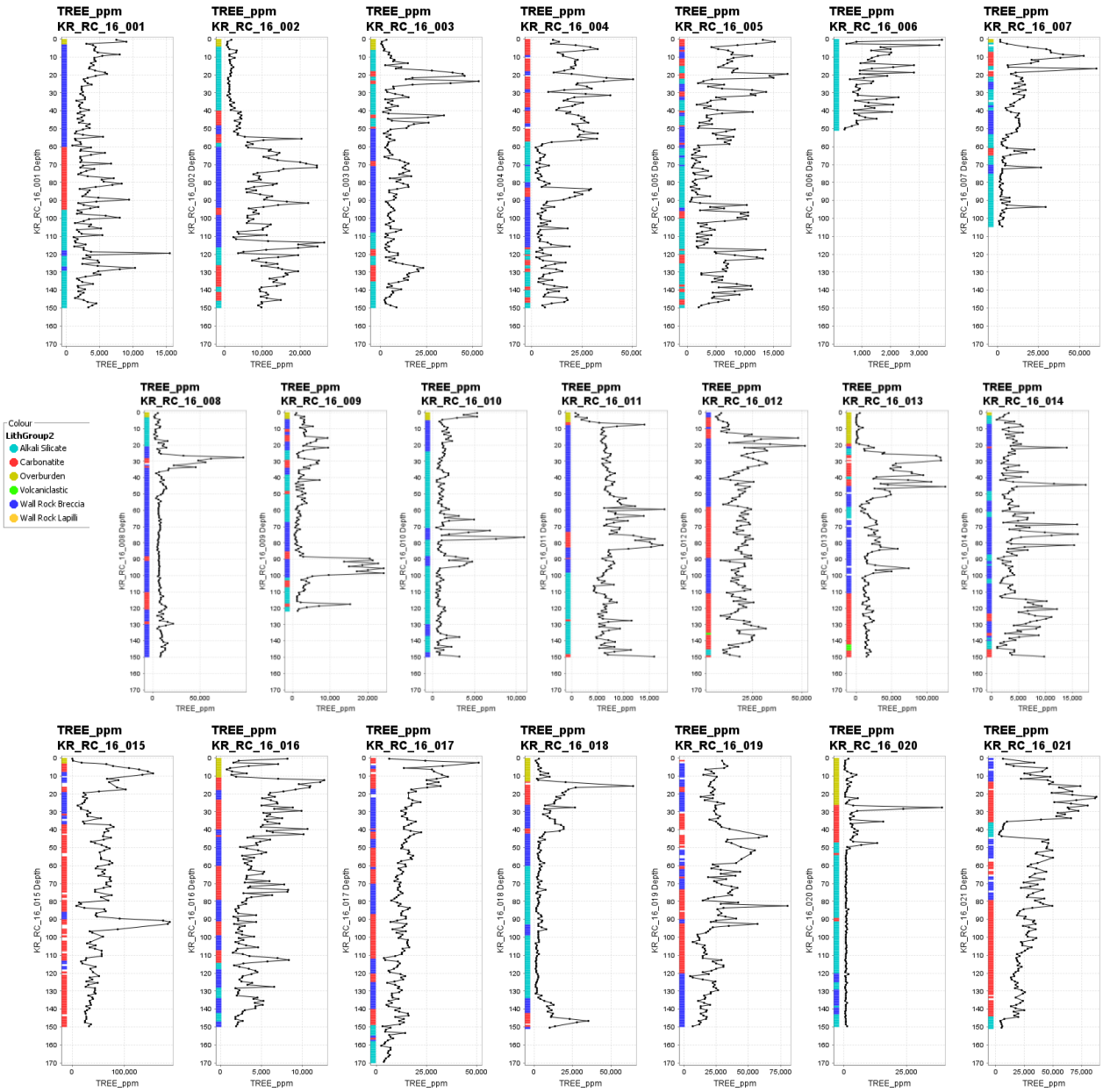

Figure 35: Downhole plots of grade and lithology from the 2016 Reverse Circulation (RC) drilling campaign

6.5. Isotopic Dating and Geochronological Studies

Given the known ages of other similar intrusives in the Tsau-//Khaeb National Park namely the Drachenberg, Pomona and Granitberg with lower Cretaceous ages (132-130 Ma) and those outside such as Dicker Willem (49 Ma) Reid & Cooper (1998) and Gross Brukkaros (77 Ma) (Verwoerd, 1993) the Karingarab Carbonatite was initially inferred to be mid-Eocene in age. Two studies were undertaken to determine the age of the deposit.

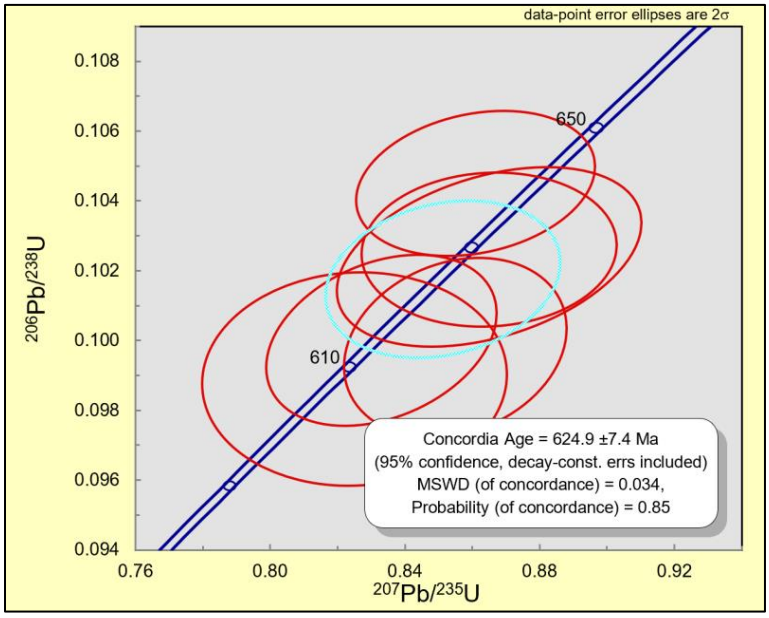

Figure 36: Graph depicting Concordia age determined from 15 zircons of an outcrop sample at Karingarab (Siegfried, 2016)

In the first study, a surface sample from an undetermined lithology outcrop at Karingarab was selected (pers. comms Siegfried, 2017). From this sample only 15 detrital Zircons in the size range of 75-200 microns were detected by Actlabs using the U-Pb dating method. An age of 624.9 Ma (Figure 36) was determined coincident with the Marinoan glaciation event in the Cryogenian period of the Neoproterozoic Era, a period for which there is no geological record available in the Tsau-//Khaeb National Park due to a major erosional unconformity created during a time when the Gariep Belt is believed to have been uplifted (Frimmel, 2000). As this age is within the same range and even pre-dating some of the country rock around the complex, these zircons may have been brought to surface through contamination during emplacement.

A follow up study was conducted using a different mineral and a different dating method. In this study, mica (phlogopite) was hand selected from RC drillhole chips at a contact between fresh carbonatite and phonolite at 149-150 m depth from RC hole 16 at the centre of the complex.

Figure 37: Phlogopite mica from 2016 RC hole 16, collected at a depth of 149m in contact between fresh carbonatite and phonolite in the centre of the Karingarab Carbonatite.

For these mineral specimens (Figure 37), the method of K/Ar isotopic dating was used by Actlabs in Canada and determined an age of 68 Ma as a date for the carbonatite intrusion. This age would suggest broader upper Cretaceous volcanism in the Tsau-//Khaeb potentially linking Karingarab to the Cenozoic eruptive events of the Keishohe, Teufelskuppe and Kaukausib carbonatites (Dauteuil et al., 2018).

6.6. Geochemical Relationships and Lithology

Although multiple lithologies and subunits of lithology have been observed, the subsurface lithology at Karingarab can be grouped into 6 main representative rock types which each present a unique geochemical signature for which data used in analysis is in Table 8 of the appendix and shown graphically in Figure 38. These comprise mainly of:

i. Carbonatites in varying degrees of weathering, crystallinity and texture.
ii. Alkali silicates which consist of phonolites and nepheline syenites.
iii. Overburden which consists of aeolian sand, surficial lag, calcretes and silcretes.
iv. Volcaniclastics which are autoclastic volcanic breccias with varying clasts of country rock and proximal intrusives mixed, sometimes clay rich or appearing as bedded formations.
v. Country or wall rock breccia which consists of brecciated schists and alkali silicates with varying matrices.
vi. Country or wall rock lapilli which are brecciated schists and alkali silicates with a carbonatite matrix or veining.

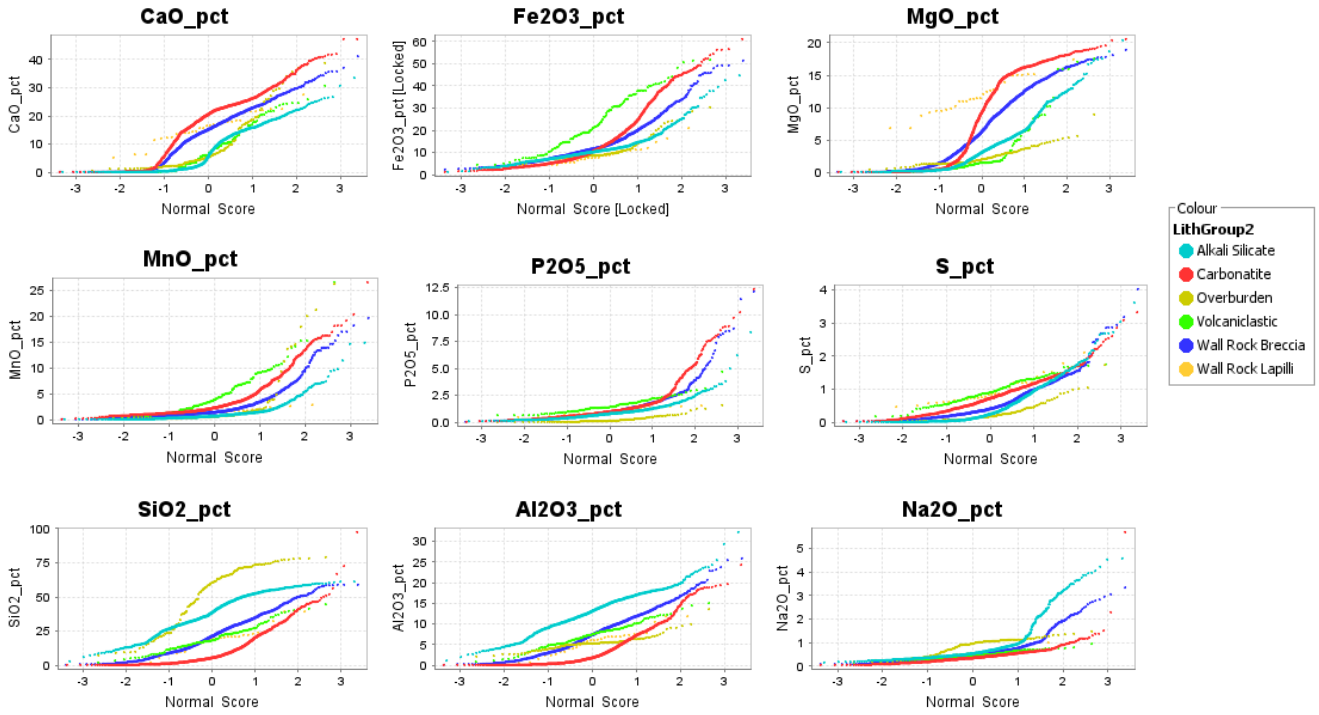

Figure 38: Geochemical Characterization using normalized score transformations of major oxides of the 6 main lithologies identified at Karingarab.

In Figure 38, carbonatite lithologies dominate with calcium, magnesium and phosphate content while alkali silicate group of rocks dominate with aluminium, the overburden which has significant sand components dominate with silica content. The volcaniclastic, wall rock breccia and wall rock lapilli also have unique signatures.

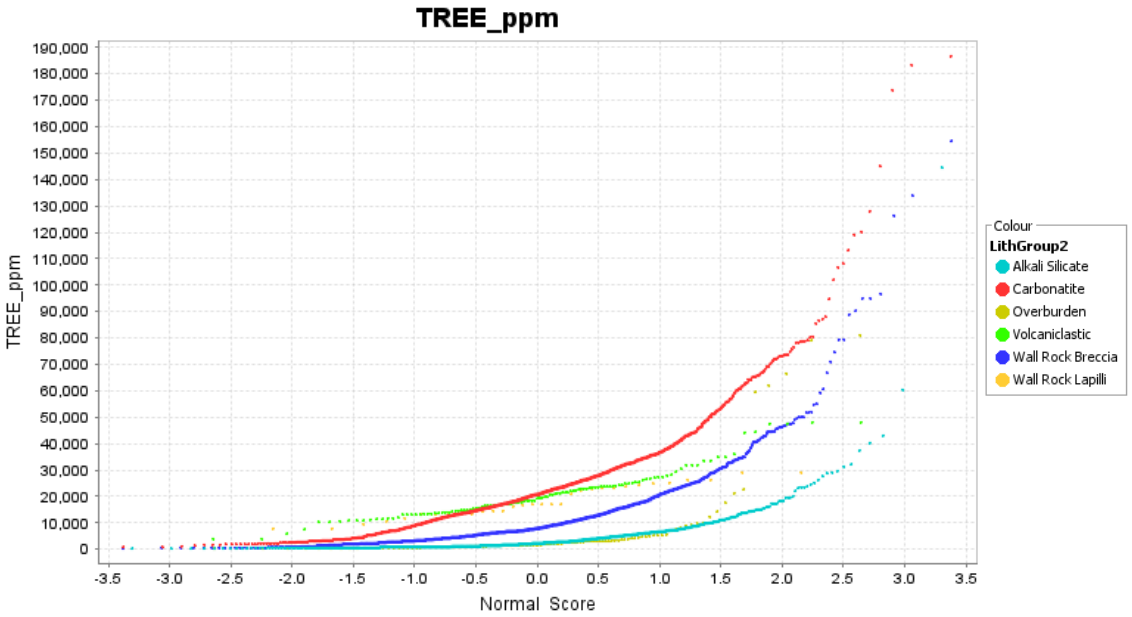

Figure 39: Split probability plots (normalized scores for TREE including Sc and Y) for the 6 main lithological types identified at Karingarab showing that enrichment is highest in the carbonatite and lower as dilution with country rock or alkali silicate rocks increases.

In a comparison of the REE content within the different lithology types, Figure 39 shows that the carbonatites (in red) are more enriched than any of the other lithological units and with the overburden (olive) and volcaniclastic material (lime green) form the bulk of the economic lithology units. The alkali silicates in light blue contain low to moderate amounts of TREE due to brecciation infill, crosscut veins and dykes of carbonatites. These lithological units can be identified in geochemistry from the high association with clay- or feldspar-associated elements such as aluminum and sodium.

The volcaniclastic unit shown in light green is the most variable unit for TREE and can be identified geochemically through high abundance of iron and manganese with very low calcium and are identified mostly towards the center of the complex in highly weathered zones, often with cavities and silica intergrowths. These units are also more likely to have cavities. Lastly, the overburden sands and regolith packages are the most barren units and are abundant in silica.

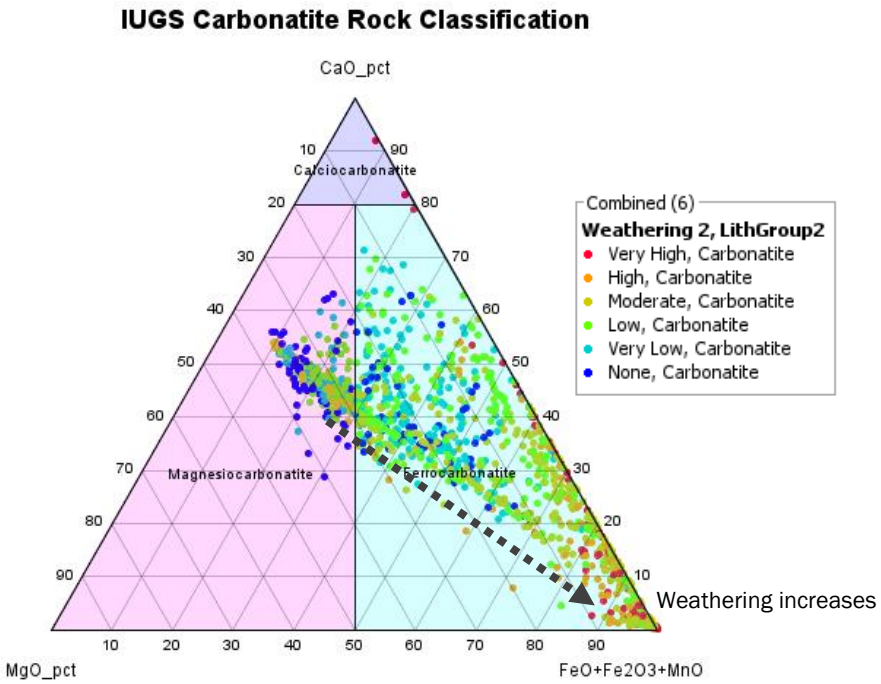

Figure 40: Karingarab data plotted into the IUGS rock classification of carbonatites indicating highly weathered carbonates in warm colours evolving to fresh carbonatites in cool colours. The highly weathered finer grained lithologies logged as carbonatites tend to be more enriched in iron and manganese while the fresh carbonatites have a higher composition of calcium and magnesium.

When grouping the carbonatite types according to the current globally accepted IUGS standard (Figure 40), which separates the carbonatite into 3 main types; calcium, magnesium and iron rich carbonatite types. The units logged as carbonatite at Karingarab plot in all 3 domains, however, if the carbonatite is grouped according to weathering as the legend shows, a clear trend is displayed indicating an elemental or compositional change in carbonatite as iron and manganese increases with weathering from a primarily calcium-, magnesium- or dolomite-rich carbonatite.

Observations show that fresh unweathered material is encountered at depth while weathered variants are closer to the surface of the deposit. The trend in Figure 40 combined with the observations can be either due to differentiation as the carbonatite magma moves upwards, immiscibility of the various carbonatite phases during intrusion or fractionation due to weathering at the surface as. Detailed petrographic studies will be useful to determine the petrogenesis of minerals and chemistry in the various phases to determine if magmatic or weathering related or a combination of both.

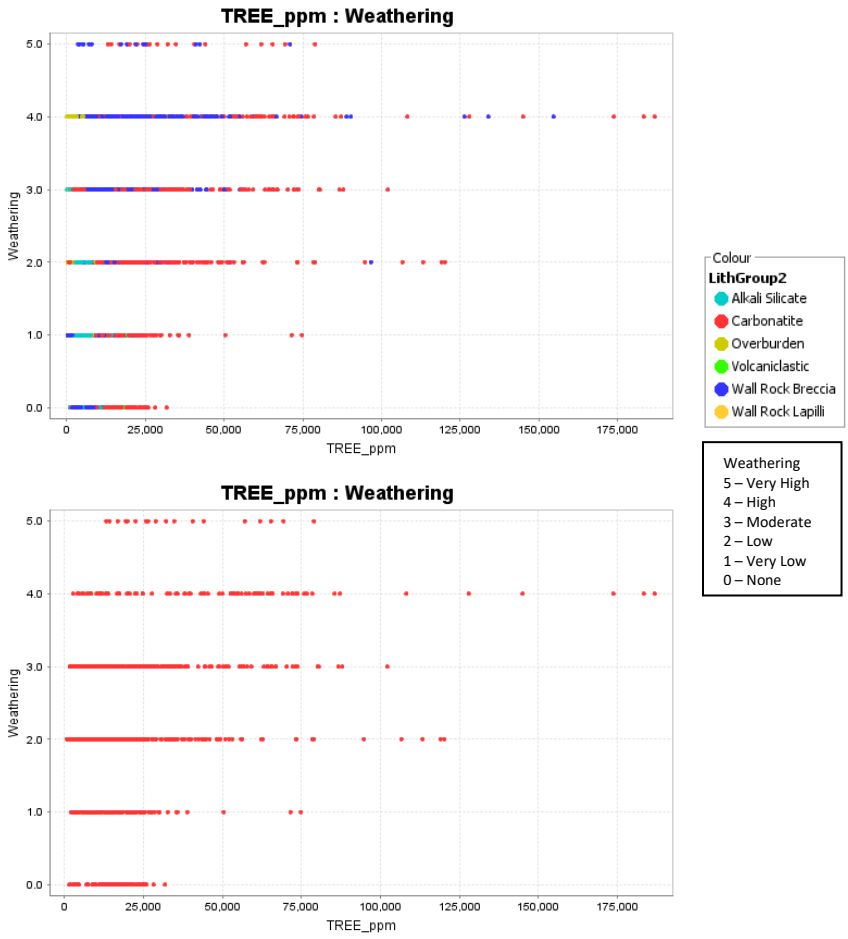

Figure 41: Comparison of TREE with Sc and Y content grouped by degrees of weathering for all the lithological units (top graph) and carbonatites only (bottom graph) for all drilling samples.

In Figure 41, the graph on the top shows all the lithological units with mineralization from TREE spread out across all lithological and weathering types, however a trend is observed that TREE content favours the carbonatite units coloured in red. Weathering of the carbonatite is logged in terms of colour, visible clays and textures of the carbonatite. It is evident in the upper graph, that carbonatites and rock types which have or did have carbonatite components such as the wall rock breccias or volcaniclastic rocks are more likely to weather. If we only view the carbonatite as shown in the lower graph, it is evident that although TREE is spread across all weathering types, the largest cluster is in the “High” weathered material. The carbonatite lithology with no weathering, still shows elevated TREE content, peaking with a maximum at 30,000 ppm or 3% while the slightly more weathered doubles in maximum TREE content.

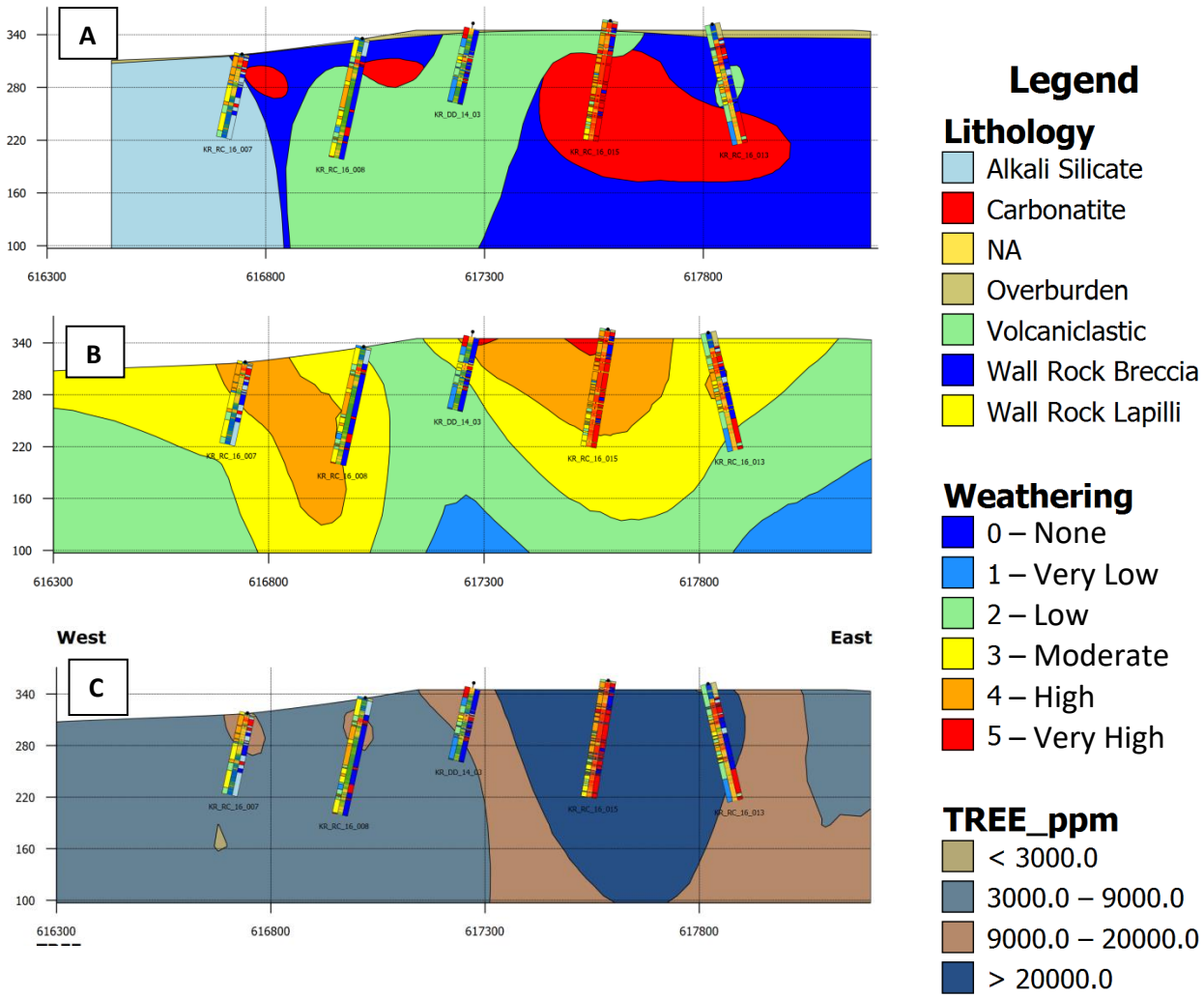

Figure 42: Cross Section of simplified models through the centre of the Karingarab Carbonatite from east to west showing interpreted A) Lithological model, B) weathering shells and c) grade shells. Borehole strips show weathering, TREE content and lithology from left to right with scale exaggerated (x2). Models were generated in Leapfrog Geo and Edge software using data from 31 drillholes from the 2014 and 2016 drilling campaigns.

Looking at the cross section from the west of the Karingarab Carbonatite towards the east (Figure 42), It is evident in Figure 42 A that the center hosts a thicker package of volcaniclastic units, flanked on either side with carbonatite. The carbonatite deepens and pinches off away from the volcaniclastic unit and although smoothed by interpretation will be diluted with country rock fragments such as schists or phyllites and with alkali silicate units either as breccias, dykes or veins. Traversing west, the carbonatite packages become smaller, and alkali silicate units become the dominant lithology. Breccias of alkali silicates, country rock and epiclastic units dominate the edges of the Karingarab Carbonatite and although

carbonatite units taper, there is still a presence of carbonatites within these breccias as younger crosscutting dykes and veins.

The weathering model, in Figure 42 B, shows a strong correlation of high weathering with the carbonatite and volcaniclastic units and decreases with depth. In the grade model, which used a radial basis function, it is evident that the highest TREE content is in zones that contain carbonatite and overlap with the most weathering in the centre and towards the east of the complex. The grade tapers off towards the edges as lithology becomes more brecciated or diluted with country rock and alkali silicate rocks particularly on the west. However, there are still patches of mineralization in moderately weathered zones close to surface.

6.7. Karingarab compared to other carbonatite hosted rare earth deposits.

A study of assay results of units logged as unweathered carbonatite compares Karingarab to CARDs described by Hou et al., (2015) as this will indicate whether enrichment of REEs is due to fluids or the actual melt or potentially both (**Error! Reference source not found.**). The legend shows carbonatites in red and alkali silicates or syenites in blue for Karingarab and the Dalucao, Lizhuang and Maoniupiung REE deposits. The Karingarab Carbonatite clusters in the group which shows a strong affinity towards fluid-related enrichment due to the high concentrations of barium, however a small population shows enrichment related to melts.

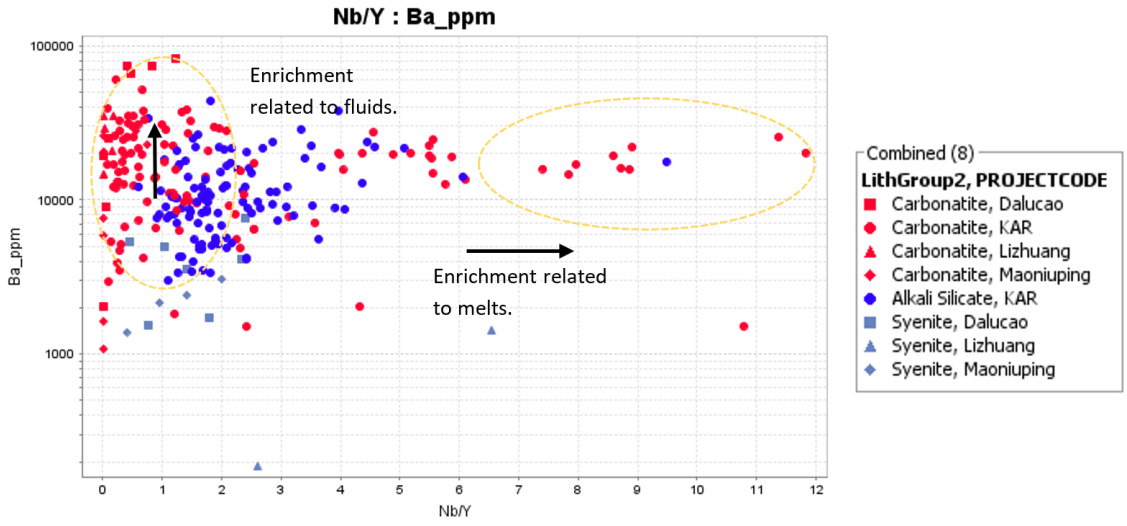

Figure 43: Comparison of Karingarab REE enrichment to global CARDs using data from Hou et al., (2015).

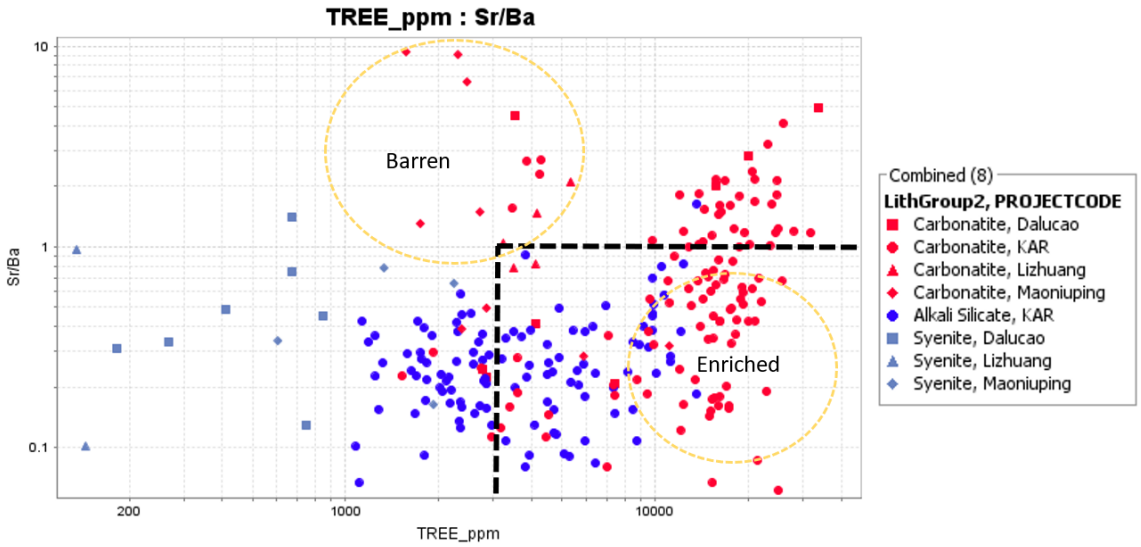

Figure 44: Comparison of Karingarab REE enrichment to global CARDs using data from Hou et al., (2015)

The relationship between Sr/Ba ratios and REE concentrations is weak and negatively correlated in CARDs (

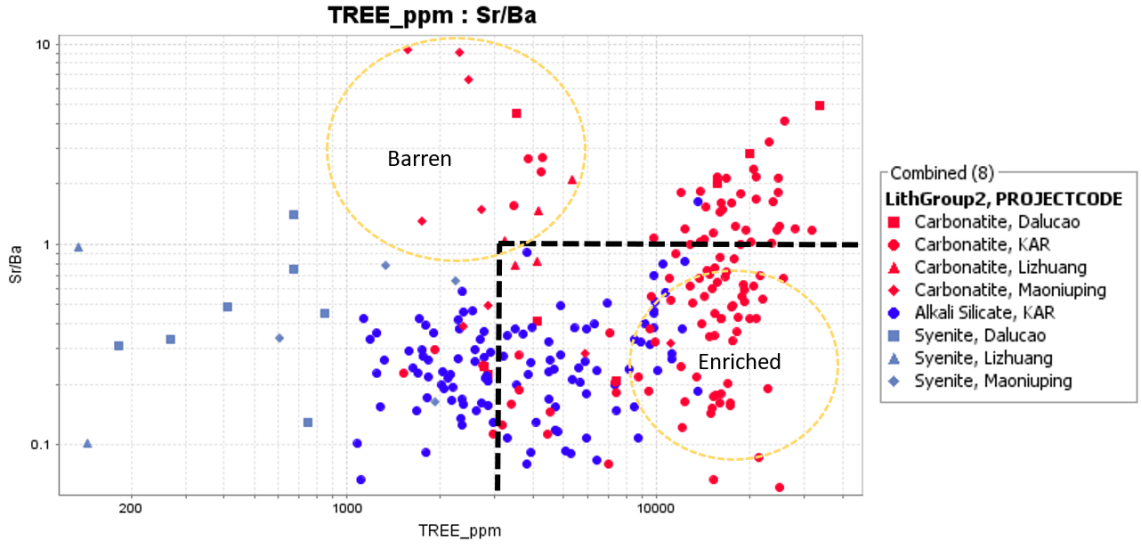

Figure 44). The graph shows that at the Karingarab carbonatite, enrichment related to melts is the primary source of REEs for unaltered and unweathered carbonatites, while the

decomposed and severely weathered carbonatites are enriched due to fluid metasomatism (

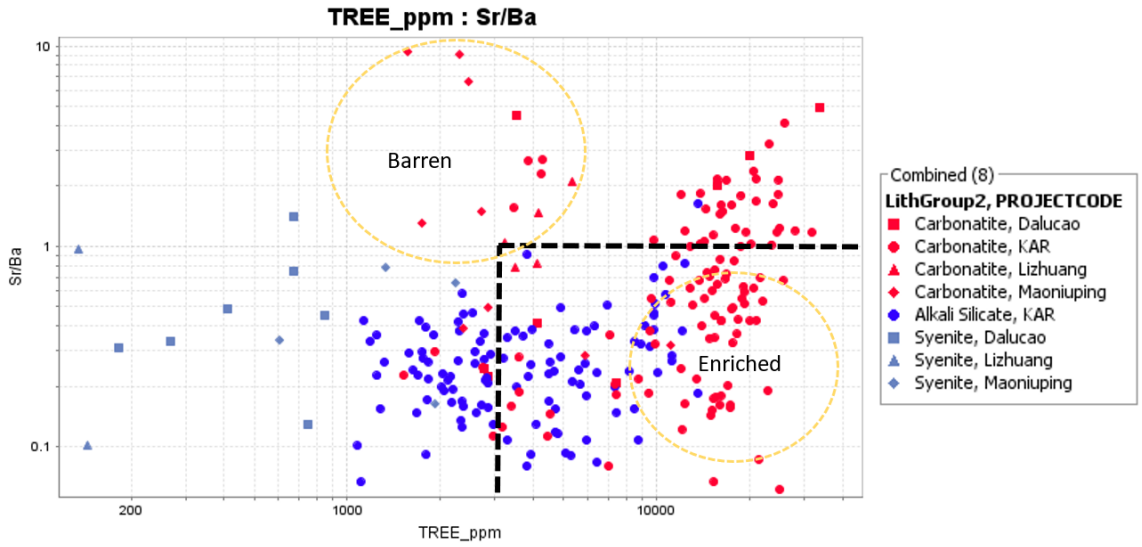

Figure 44). This indicates that the Karingarab deposit falls in the same category of CARDs as the Mianning-Dechang, Bayan-Obo and Mountain Pass deposits as in original Figure 14a and b.

Table 4 below summarizes the average chemistry content for the highlighted points which fall within the category for melt and fluid related enrichment in Figure 43 with the highest differences. The zones which signal fluid tend to have much higher Th, F and Ba with lower TREE grade, while the zones related to enriched melts tend to have higher Sr, Nb and TREE. All other chemical elements do not show major change in composition.

Table 4: Summary of element average concentrations showing the highest change between the fluids and melt enrichment clusters for units logged as fresh carbonatites at Karingarab.

	TREE_ppm	Ba_ppm	Sr_ppm	Nb_ppm	Th_ppm	Lu_ppm	Yb_ppm	F_ppm
Fluid	14,198.65	22,590.64	7,197.44	162.33	225.89	2.28	17.73	18,256.77
Melts	21,190.85	17,450.89	23,957.33	859.56	32.18	0.41	4.04	4,455.44

Table 5 below summarizes the average chemistry content for select points in Figure 44 with the highest differences noted as higher Ba, Th, W and F values for the enriched zones, while the barren zones had higher SiO2, Nb and Hf. All other chemical elements did not show major change during the comparison. Of importance to note and to monitor is the high association

of not only Ba, but Th and F particularly in zones of hydrothermal enrichment, while melt related enrichment is relatively low.

Table 5: Summary of elements showing the highest change in composition between the barren and enriched clusters for units logged as fresh carbonatites at Karingarab.

	TREE_ppm	Ba_ppm	SiO2_pct	Nb_ppm	Th_ppm	Hf_ppm	W_ppm	F_ppm
Enriched	16,676.40	29,175.39	5.19	275.80	320.13	1.35	6.96	11,082.36
Barren	3,958.70	1,715.78	13.79	627.90	45.98	3.33	1.33	3,171.00

7. Discussion on Potential of the Karingarab Carbonatite

The Karingarab Carbonatite has high potential to be a superior world-class rare-earth deposit due to the large size, high grades, relatively consistent lithology and proximity to market. In a local context it is comparable in size and lithology to Dicker Willem (49 Ma) and Gross Brukkaros (77 Ma) which all have a diameter close to 2.5 km and brecciated lithologies (Table 7). It is also comparable in terms of emplacement age to the Keishohe, Teufelskuppe and Kaukausib carbonatites which erupted in the upper Cretaceous (Verwoerd, 1993).

The lithology indicates that the Karingarab Carbonatite eruption event if similar to Gross Brukkaros may have been highly explosive but erupted under a different environment which upgraded the REE content, limited the erosion and allowed weathering under a calcrete overburden cap which is not present at Gross Brukkaros.

Through reviews of results of geochemical assays from the drilling at Karingarab, there is evidence to support that the deeper fresh and unaltered carbonatites carry relatively low grades in comparison to the shallower, more weathered or altered carbonatites. However, these grades less than 3,000 ppm at depth are still economic and show strong similarity to other CARDs. In support of Karingarab's comparison to CARDs, the dates obtained from the geochronology studies have returned results that indicate firstly, that the zircons were assimilated from host rocks of a pre-Gondwana age at an age prior to multiple tectonic events which created optimum crustal conditions for carbonatite emplacement and fluid metasomatism (Schneider, 2008) and secondly, the phlogopite from an intrusion contact event is dated prior to the events in the Northern Sperrgebiet (Tsau-//Khaeb) presented by Pickford et al, (2015) which preserved mineralization in Figure 16.

Combined, these sequences and mineralization events may place the Karingarab Carbonatite in the optimum setting for significant REE enrichment as with the carbonatites of south-west China. These carbonatites, like Karingarab, occur at cratonic edges, along divergent margins and form from the melting of sub-continental lithospheric mantle (SCLM), enriched by metasomatized REE and CO2 rich fluids derived from subducted marine sediments (Hou et al., 2015).

Although Gross Brukkaros does not have indicators for economic potential, the lithologies encountered at Karingarab have been described as mostly volcanic clastics and breccias potentially from an eruption The alkali silicate units such as the phonolites and syenites appear to be intrusive and crystalline. Decomposed carbonatite tuff, lapilli and clastic breccias dominate the center indicating a single potential crater setting or various smaller crater lakes. The Dicker Willem Carbonatite is comparable to Karingarab due to the banding of the carbonatites and the presence of fenitized country rock forming a rim around the complex.

The Dicker Willem Carbonatite has also been subject to the regional silicification event which may have trapped the mineralization and prevented erosion after eruption (Reid and Cooper, 1998). At the Karingarab Carbonatite, the various carbonatite units carry the highest grade which is explicitly high-graded in the weathered and shallow zones however, mineralization is present in diluted clastic and brecciated units too and confirmed by identified REE bearing minerals identified by XRD of various high-grade zones (Figure 28, Figure 29, Figure 30, Figure 31).

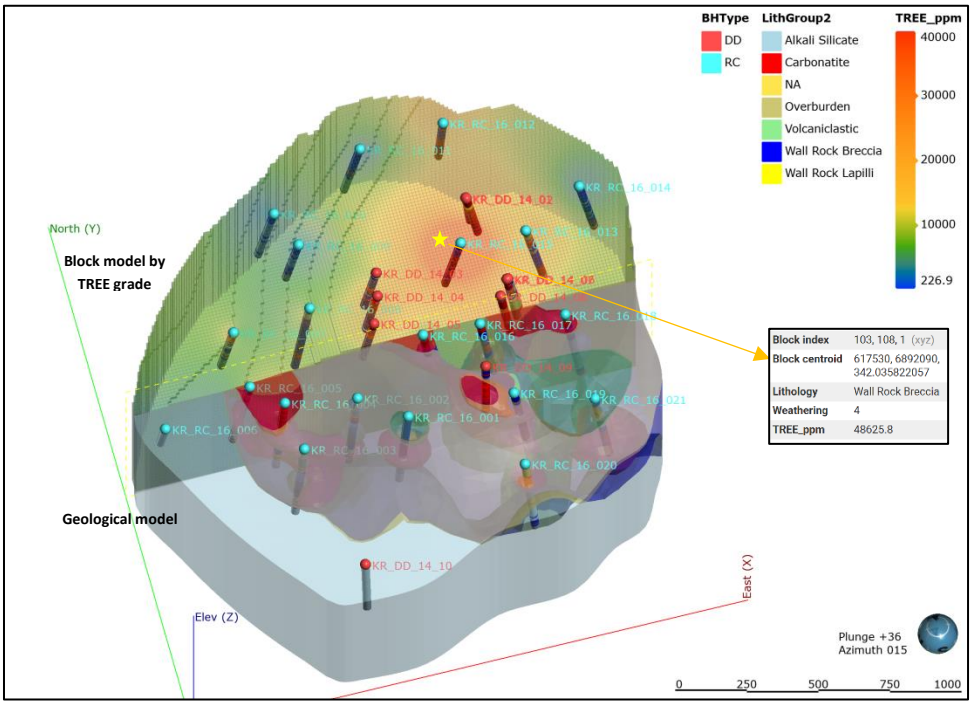

Figure 45: Overview of the geological model against the block model of the Karingarab Carbonatite, with yellow star indicating values TREE, lithology and weathering per block. Models and estimates produced using leapfrog geo and edge.

Exploration at the Karingarab target is still ongoing with preliminary estimates following the first two drilling campaigns (31 holes for a total of 3000 m) interpreted using Leapfrog geological modelling software (Figure 45) and results summarized in Table 6 below. The model estimate used a block size of 12x12x6 m, no ore cutoff grade, and an average density of 2.5 g/cm3. This rough estimate produced a total of 1.5 billion tonnes, and an average grade of 1% TREO which could potentially produce 15 million tonnes of TREE including Sc and Y. If only targeting the carbonatite that would produce 181 million tonnes with a grade of 1.9% producing 3.5 million tonnes of TREE. These tonnages will fluctuate as the deposit remains open at depth and the potential of the satellite intrusions is yet to be tested, these values may also be impacted by higher density drilling and selective ore targeting based on lithology, ore mineralogy and degree of weathering which will impact the processing methods.

Table 6: Report of block model estimates of the Karingarab Carbonatite grouped by lithology and degrees of weathering.

Report
Cut-off: TREE_ppm ≥ 0.00 ppm
Filter: None
Volume filter: Boundary (Entire block)
Density: 2.5 g/cm³

Weathering	Lithology	Volume m³	Mass t	*Average Value* TREE_ppm ppm	*Material Content* TREE_ppm t
0	Alkali Silicate	50,128,416.00	125,321,040.00	6,835.01	856,570.78
	Carbonatite	2,496,960.00	6,242,400.00	10,112.36	63,125.39
	Volcaniclastic	1,698,624.00	4,246,560.00	5,336.65	22,662.42
	Wall Rock Breccia	14,212,800.00	35,532,000.00	10,130.90	359,971.08
	Total	**68,536,800.00**	**171,342,000.00**	**7,600.76**	**1,302,329.67**
1	Alkali Silicate	111,861,216.00	279,653,040.00	5,955.77	1,665,549.29
	Carbonatite	26,424,576.00	66,061,440.00	14,959.71	988,260.03
	Volcaniclastic	27,326,592.00	68,316,480.00	7,223.36	493,474.65
	Wall Rock Breccia	137,242,080.00	343,105,200.00	11,036.19	3,786,572.82
	Total	**302,854,464.00**	**757,136,160.00**	**9,158.01**	**6,933,856.79**
2	Alkali Silicate	37,912,320.00	94,780,800.00	5,618.56	532,531.58
	Carbonatite	31,484,160.00	78,710,400.00	20,325.79	1,599,851.29
	Overburden	4,942,080.00	12,355,200.00	8,527.08	105,353.73
	Volcaniclastic	20,896,704.00	52,241,760.00	10,149.37	530,220.77
	Wall Rock Breccia	72,683,136.00	181,707,840.00	10,973.33	1,993,940.71
	Wall Rock Lapilli	28,512.00	71,280.00	25,446.62	1,813.84
	Total	**167,946,912.00**	**419,867,280.00**	**11,345.76**	**4,763,711.91**
3	Alkali Silicate	6,051,456.00	15,128,640.00	5,797.04	87,701.26
	Carbonatite	7,674,048.00	19,185,120.00	26,592.17	510,173.95
	Overburden	2,468,448.00	6,171,120.00	9,926.17	61,255.60
	Volcaniclastic	5,824,224.00	14,560,560.00	16,173.18	235,490.58
	Wall Rock Breccia	14,345,856.00	35,864,640.00	13,587.96	487,327.32
	Wall Rock Lapilli	19,008.00	47,520.00	26,558.87	1,262.08
	Total	**36,383,040.00**	**90,957,600.00**	**15,207.20**	**1,383,210.79**
4	Alkali Silicate	3,514,752.00	8,786,880.00	6,245.44	54,877.90
	Carbonatite	4,104,000.00	10,260,000.00	30,373.66	311,633.71
	Overburden	1,876,608.00	4,691,520.00	13,005.57	61,015.88
	Volcaniclastic	5,215,968.00	13,039,920.00	24,156.70	315,001.40
	Wall Rock Breccia	11,203,488.00	28,008,720.00	16,923.65	474,009.70
	Wall Rock Lapilli	30,240.00	75,600.00	21,934.88	1,658.28
	Total	**25,945,056.00**	**64,862,640.00**	**18,781.18**	**1,218,196.87**
5	Carbonatite	443,232.00	1,108,080.00	22,455.55	24,882.55
	Volcaniclastic	85,536.00	213,840.00	17,270.75	3,693.18
	Wall Rock Breccia	444,096.00	1,110,240.00	21,768.71	24,168.49
	Total	**972,864.00**	**2,432,160.00**	**21,686.16**	**52,744.22**
Total	**Alkali Silicate**	**209,468,160.00**	**523,670,400.00**	**6,105.43**	**3,197,230.81**
	Carbonatite	**72,626,976.00**	**181,567,440.00**	**19,265.17**	**3,497,926.92**
	Overburden	**9,287,136.00**	**23,217,840.00**	**9,803.89**	**227,625.21**
	Volcaniclastic	**61,047,648.00**	**152,619,120.00**	**10,487.17**	**1,600,543.00**
	Wall Rock Breccia	**250,131,456.00**	**625,328,640.00**	**11,395.59**	**7,125,990.11**
	Wall Rock Lapilli	**77,760.00**	**194,400.00**	**24,352.83**	**4,734.19**
	Total	**602,639,136.00**	**1,506,597,840.00**	**10,390.33**	**15,654,050.24**

Differences may occur in totals due to rounding.

The REEs are considered critical due to security of supply and prices often fluctuate in response to geopolitics, new deposit discoveries, technology substitution and recycling. However, if there is potential for the Karingarab Carbonatite to contain 15 million tonnes of REEs (converted to REO as per James Cook University (2022) conversion factors) and considering the average price per tonne per pure REO in Figure 46, it is possible to extrapolate

these values to the proportions of TREE shown in red dots in Figure 47. For which scandium and lutetium fetch the highest price per metric tonne of all the REOs while lanthanum and cerium have the lowest pricing.

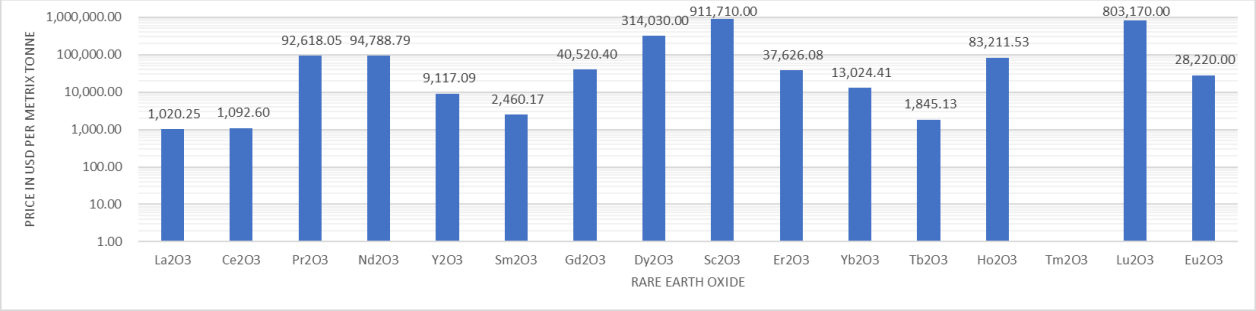

Figure 46: Market prices of rare earths per tonne in USD. Prices per kg have been converted to indicate per tonne values (Metal.com, 2022).

From these sums, the highest contribution of 80% to revenue based on current prices will be Nd, Pr, Dy and Sc which together represents only 30% of the total REO at the Karingarab Carbonatite. The 70% remaining material in the basket is dominated by La and Ce oxides which only contribute 2.5% of the total value.

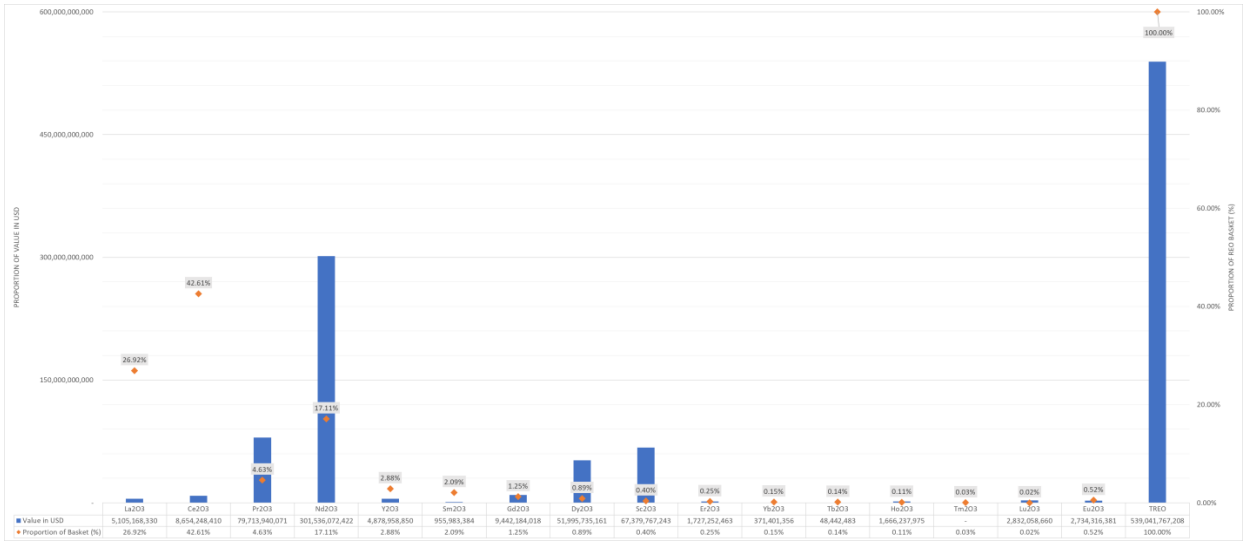

Figure 47: Estimate of potential value from the Karingarab Carbonatite using broad assumptions from resource estimate with no selective ore or cut-off applied. The deposit is potentially worth U$ 600 billion at current market prices (Metal.com, 2022).

Another factor that may affect the Karingarab Carbonatite is the scale of the deposit and the

potential to disrupt global supply. La and Ce are the dominant elements found in REE deposits, but Pr and Nd are the highest in demand means that most mines will therefore overproduce La and Ce which may lead consumers in the need for Nd, Pr, Dy or Sc to invest in methods to potentially recycle these elements from current end products at the end of their useful life. Recycling however, has its own challenges such as the varying content of REE in components from trace amounts to several kg, the separation of individual REE from alloys, permanent magnets and the long life-span of many REE products, these factors have led to only up to 1% of REEs used today being recycled, salvaged from permanent magnets, batteries, fluorescent lights and catalysts from chemical and petroleum refining industry (Jowitt, et al., 2018).

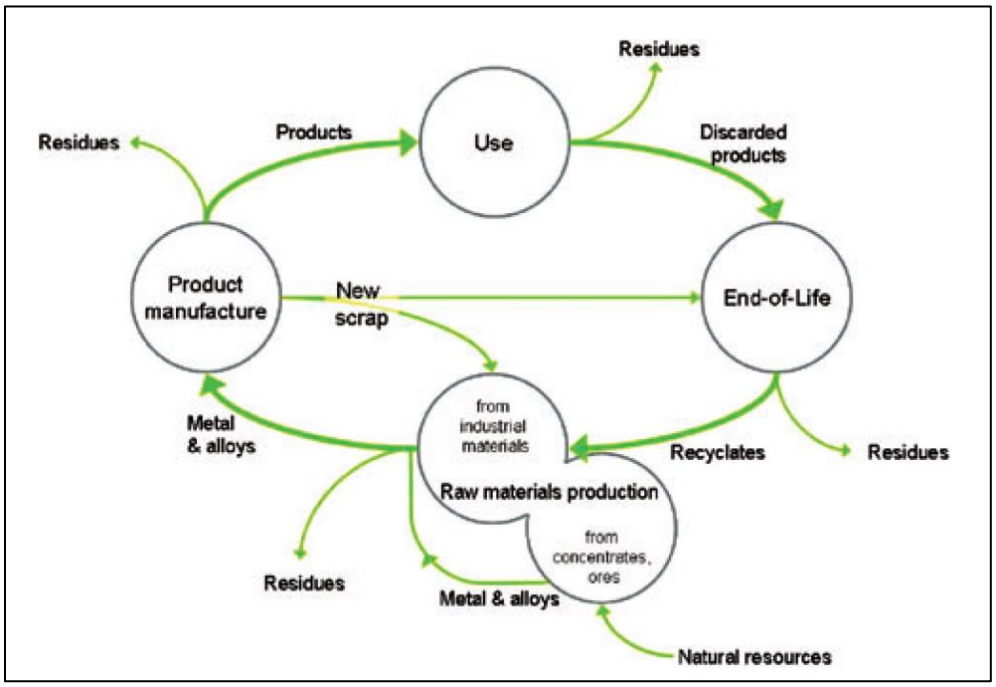

Figure 48: The life cycle of metals starting from natural resources, product manufacturing, and recycling from scrapping or end of life. At each stage material is lost to the environment indicated as residues (Graedel et al., 2011).

Figure 48, shows the life cycle of metals from Graedel et al., (2011) starting with raw material production from natural resources which are eventually turned into final products which can be scrapped or recycled at the of life. The recycling efficiency of metals is an important tracker to monitor during exploration for REEs, and can be calculated knowing firstly, at the end of life, how much of the metal reaches recycling centres instead of landfills, secondly it is important to know what the efficiency of the recycling process is, and lastly, when recycled,

does the material become pure or remain an alloy further limiting its use. Ciacci et al., (2015) studied the various material streams of 56 elements to determine losses by design and the subsequent material available for recycling and observed that the REE have the highest rates of un-recyclability higher than 10% particularly for La, Ce and the heavy REE in Figure 49 below.

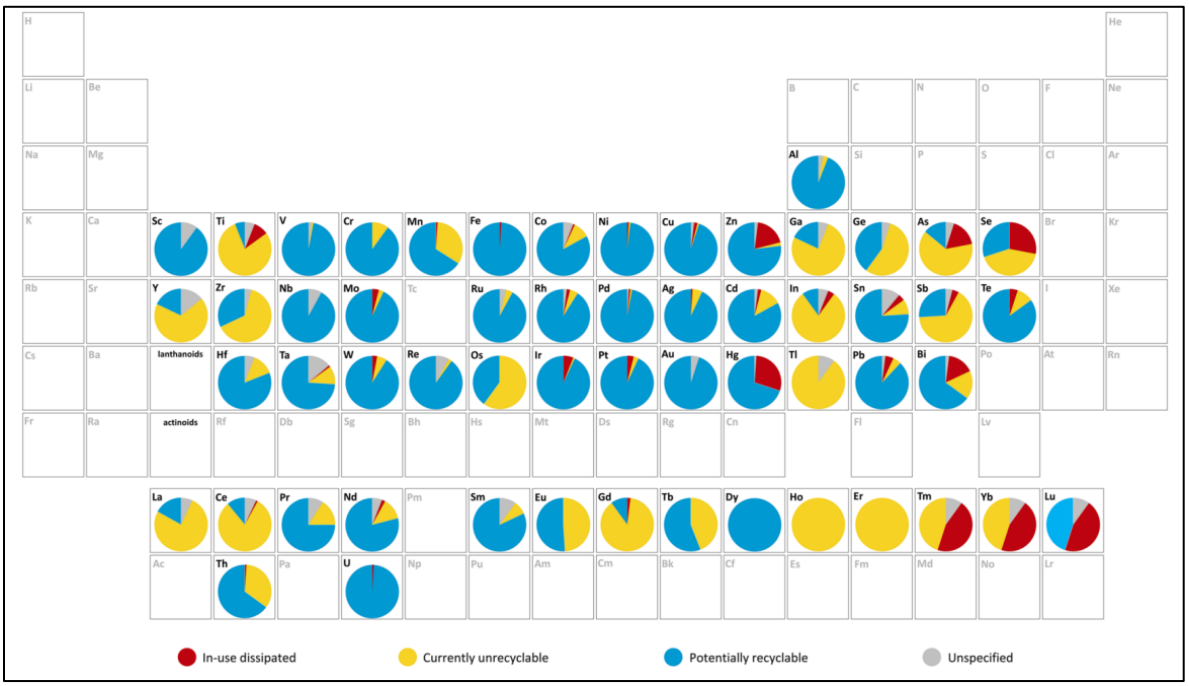

Figure 49: Distribution of elements within four material streams for intentional material loss caused by product design (Ciacci et al., 2015)

In Figure 49, Ciacci et al., (2015) explains that the red wedges indicate in use dissipation rates often associated with losses to the environment which are almost impossible to recover, these losses may be due to the nature or use of the product and examples of these are manganese in fertilizers or elements such as barium used in fireworks. The yellow wedges indicate elements that cannot currently be recycled such as REEs used in optical lenses and their polishing powders or aluminium and manganese used during steelmaking. In blue, potentially recyclable elements are ranked which indicates possible recovery as an alloy, this is particular to metals that are used in products specifically as alloys such as Nd, Pr and Dy which are used as permanent magnets in wind energy motors. Lastly, in grey, are the unspecified materials which require more information to be correctly categorized (Ciacci et al., 2015).

8. Conclusion and Recommendation

It is known that without substitution or improved recycling, demand for rare earth elements (REE) will continue to rise due to the many practical uses for medical, renewable energy, military and new technology applications (Jowitt, et al., 2018). There have been recent global commitments to green energy and sustainable development goals to fulfil climate change obligations by diversifying to alternative and renewable sources of energy, the biggest risk of prioritizing these green industries as narrated by Kalantzakos, (2019), will be focusing on how to extract, refine, transport and process REEs in a manner which satisfies environmental, social and governance requirements (ESG) responsible to the environment and to the people.

Responsible mining of this deposit will require stringent governance and for private partners to research and ensure compliance to the following list summarized by Wall et al., (2017); environmental plans, community relations, transparency in economic rents such as taxes and royalties as well as resource and reserve reporting, occupational health, and safety, monitoring of carbon footprint, energy and water usage and mining efficiencies.

The Karingarab Carbonatite has through its exploration shown great potential to be a large-scale REE mine in Namibia with potential to not only disrupt the market, but to place Namibia on the world stage as a producer of REEs warranted that ongoing exploration and subsequent studies on metallurgical processing are positive and ensuring the mineral value chain and potential industry spill-over is managed sustainably. It will be very important to monitor the market closely in terms of supply, pricing and developments in substitution and recycling.

These studies at Karingarab have shown that although mineralization is obvious in the weathered lithologies, in the fresher carbonatite it is related to both magmatic and fluid metasomatism events at depth, with the supergene process near to surface forming further upgrading. It will be very important to separate these ores as early XRD studies indicate that REE minerals tend to form larger interstitial grains closer to surface while the deeper material although more crystalline are finer and ingrained in the lithology. It would be recommended to model the ore in terms of weathering and again to separate fluid from magmatic signatures, it would also be beneficial to submit the multiple mineralized zones for liberation and metallurgical studies as mineralization is disseminated through all lithological types where

carbonatite is present as dykes, veins or matrix in clastic material. The presence of often clay-rich lithic autoclastic breccias (volcaniclastic rocks and wall rock breccia) and layered carbonatite lapilli being associated with mineralization and high-grade areas hints that mineralization is porosity controlled and requires further study to determine fluid and magma pathways and quantify a relationship between fractures and porosity with the REE mineralization and secondary clays. Additionally, a study of the events that occurred at the time of eruption will be useful to further characterize the potential of other carbonatites in Namibia. Lastly, in an area where much is covered by aeolian dunes, the Karingarab Carbonatite with its presence of calcrete and silcrete beds and transported country rock clasts may assist with stratigraphy in the Tsau-//Khaeb and provide insight to the missing pieces of the Gariep Belt and Oranjemund sub-terrane stratigraphy through positive fossil identification, geochronology and fluid inclusion or climate isotope studies.

The main target at the Karingarab Carbonatite is being explored due to positive returns and the concealed satellite intrusions at Karingarab remain to be tested as they show similar geophysical signatures. Regionally, further reconnaissance work is required to evaluate the potential of similar carbonatites in the Tsau-//Khaeb National Park such as the Keishohe, Teufelskuppe and Kaukausib that together with Karingarab can breathe renewed mineral economic life into the southwest coast of Namibia following a long romance with diamonds.

9. References

Anenburg, M., Broom-Fendley, S., & Chen, W. (2021). Formation of rare earth deposits in carbonatites. *Elements: An International Magazine of Mineralogy, Geochemistry, and Petrology*, *17*(5), 327-332.

Arribas, A., Broughton, D. & Mauk, J. (Eds.), 2018. *Metals, Minerals, and Society – A 2018 Update. Society of Economic Geologists Special Publication 21* (pp.25-38) Chapter: 2 Publisher: Society of Economic Geologists.

Basei, M.A.S, Frimmel, H.E., Nutman, A.P., Preciozzi, F. and Jacob, J. (2005). A connection between the Neoproterozoic Dom Feliciano (Brazil/Uruguay) and Gariep (Namibia/South Africa) orogenic belts - evidence from a reconnaissance provenance study. *Precambrian Research*, 195-221.

Bühn, B., Dörr, W., & Brauns, C. M. (2001). Petrology and age of the Otjisazu carbonatite complex, Namibia: implications for the pre-and synorogenic Damaran evolution. *Journal of African Earth Sciences*, 32(1), 1-17.

Burke, K., Ashwal, L. D., & Webb, S. J. (2003). New way to map old sutures using deformed alkaline rocks and carbonatites. *Geology,* 31(5), 391-394.

Carelse, C. (2017). Mineralogical analysis of four REE-bearing carbonatite samples originating from the Karingarab deposit in Namibia, prepared for Namdeb Mineral Resources: Exploration, Namibia Project No: MNC 50003034, Compact No : 2017-2.09 41 pp.

Coint, N. & Dahlgren, S. (2019). Rare earth elements (REE) in two long drill-cores from the Fen Carbonatite Complex, Telemark, Norway (preliminary version).

Ciacci, L., Reck, B. K., Nassar, N. T., & Graedel, T. E. (2015). Lost by design. *Environmental Science & Technology*, *49*(16), 9443-9451.

Dauteuil, O., Picart, C., Guillocheau, F., Pickford, M. & Senut, B. (2018). Cenozoic deformation and geomorphic evolution of the Sperrgebiet (Southern Namibia) *Communications of the Geological Survey of Namibia*, 18, 1-18.

Diehl, M. (1990). Geology, mineralogy, geochemistry and hydrothermal alteration of the Brandberg Alkaline Complex, Namibia. *Memoir-Geological survey. South West Africa, Namibia*, (10).

Dobrescu, E. M. (2015). Rare Earths Economy. New Branch of Economic Sciences. *Business & Leadership*, (1), 31-52.

Ewart, A., Milner, S. C., Armstrong, R. A., & Duncan, A. R. (1998). Etendeka volcanism of the Goboboseb Mountains and Messum Igneous Complex, Namibia. Part II: Voluminous quartz latite volcanism of the Awahab magma system. *Journal of Petrology*, 39(2), 227-253.

European Commission (EU), (2020). *Study on the EU's list of Critical Raw Materials – Final Report*. European Commission, B-1049, Brussels

Foster, D. A., & Goscombe, B. D. (2013). Continental growth and recycling in convergent orogens with large turbidite fans on oceanic crust. *Geosciences*, 3(3), 354-388.

Frimmel, H. E. (1995). Metamorphic evolution of the Gariep Belt. *South African Journal of Geology*, 98(2), 176-190.

Frimmel, H. E. (2000). The stratigraphy of the Chameis Sub-terrane in the Gariep Belt in southwestern Namibia. *Communications of the Geological Survey of Namibia: Special Issue*, *12*, 179-186.

Frimmel, H. E. (2008). Neoproterozoic Gariep Orogen. *Miller, R. McG., ed., The Geology of Namibia: Geological Survey of Namibia*, *2*, 14-1.

Gittins, J., & Harmer, R. E. (1997). What is ferrocarbonatite? A revised classification. *Journal of African Earth Sciences*, *25*(1), 159-168.

Graedel, T. E., Allwood, J., Birat, J. P., Buchert, M., Hagelüken, C., Reck, B. K., ... & Sonnemann, G. (2011). What do we know about metal recycling rates? *Journal of Industrial Ecology*, *15*(3), 355-366.

Grobbelaar, G.J., (2014) Karingarab 2014 Diamond Drilling plans on TMI geophysical data, *Internal comms, Not published.* Namdeb *1 pp.*

Grobbelaar, G.J., Itengula, J. & Siegfried, P.R. (2014) Karingarab 2014 Diamond Drilling Lithological logging codes. *Internal comms, Not published.* Namdeb *1 pp.*

Harmer, R. E., & Gittins, J. (1998). The case for primary, mantle-derived carbonatite magma. *Journal of Petrology*, *39*(11-12), 1895-1903.

Harmer, R. E., & Nex, P. A. M. (2016). Rare earth deposits of Africa. *Episodes*, *39*(2), 381-406.

Hou, Z., Liu, Y., Tian, S., Yang, Z., & Xie, Y. (2015). Formation of carbonatite-related giant rare-earth-element deposits by the recycling of marine sediments. *Scientific Reports,* 5(1), 1-10.

Hou, Z., Liu, Y., Tian, S., Yang, Z., & Xie, Y. (2015). Formation of carbonatite-related giant rare-earth-element deposits by the recycling of marine sediments – Supplementary Data. *Scientific Reports,* 5(1), 1-29.

James Cook University, Australia (2022). Element-to-stoichiometric oxide conversion factors. Available online: https://www.jcu.edu.au/advanced-analytical-centre/resources/element-to-stoichiometric-oxide-conversion-factors/ (accessed on 14 September 2022).

Jowitt, S. M., Mudd, G. M., Werner, T. T., Weng, Z., Barkoff, D. W., McCaffrey, D., & Mauk, J. L. (2018). The critical metals: an overview and opportunities and concerns for the future. *Metals, Minerals and Society: Economic Geology, Special Publication*, (21), 25-38.

Jowitt, S. M., Werner, T. T., Weng, Z., & Mudd, G. M. (2018). Recycling of the rare earth elements. *Current Opinion in Green and Sustainable Chemistry*, *13*, 1-7.

Jung, S., Hoffer, E., & Hoernes, S. (2007). Neo-Proterozoic rift-related syenites (Northern Damara Belt, Namibia): geochemical and Nd–Sr–Pb–O isotope constraints for mantle sources and petrogenesis*. Lithos,* 96(3-4), 415-435.

Kalantzakos, S. (2019). The Geopolitics of Critical Minerals. *Istituto Affari Internazionali (IAI).* 15 pp.

Kogut, A. I., Hagni, R. D., & Schneider, G. I. (1998). Geology, mineralogy, and paragenetic sequence of the Okorusu carbonatite-related fluorite ores, Namibia. *In Proceedings of the Quadrennial IAGOD Symposium* (Vol. 9, pp. 555-573).

Kramm, U., Körner, T., Kittel, M., Baier, H. & Sindern, S., (2017). Triassic emplacement age of the Kalkfeld complex, north-west Namibia: implications for carbonatite magmatism and its relationship to the Tristan Plume*. International Journal of Earth Sciences*. 106. 10.1007/s00531-017-1460-2.

Le Roex, A. P., Watkins, R. T., & Reid, A. M. (1996). Geochemical evolution of the Okenyenya sub-volcanic ring complex, northwestern Namibia*. Geological Magazine*, 133(6), 645-670.

Linning, K. (1968). Die Stollingskompleks Kaap Kruis, Suidwes-Afrika *MSc Thesis, Universiteit van Pretoria) 108 pp.*

Liu, Y., & Hou, Z. (2017). A synthesis of mineralization styles with an integrated genetic model of carbonatite-syenite-hosted REE deposits in the Cenozoic Mianning-Dechang REE metallogenic belt, the eastern Tibetan Plateau, southwestern China. *Journal of Asian Earth Sciences*, 137, 35-79.

Marsh, J.S. 1973. Alkaline Igneous Rocks of the Coastal Belt, South of Lüderitz, South West Africa: a Petrological Study. *Unpublished Ph.D. Thesis*, Cape Town, 285 pp

Marsh, J. S. (1976). The Lüderitz Alkaline Province, South West Africa, III: The Pomona and Drachenberg Syenite Complexes. *South African Journal of Geology,* 79(2), 168-176.

Menge, G. F. W. (1986). Sodalite carbonatite deposits of Swartbooisdrif, South West Africa/Namibia. *In Mineral deposits of Southern Africa* (pp. 2261-2268).

Menge, G. F. W. (1996). The eastern portion of the Kunene complex, its satellite intrusions and the alkaline suite between Epembe and Swartbooisdrif, Kaokoland, South West Africa. *Unpublished report for the Geological Survey of Namibia*, 122 pp.

Metal.com (2022). Mineral Prices. Rare Earth Metals. Available online: https://www.metal.com/Rare-Earth-Metals/ (accessed on 24 August 2022).

Miller, R. (2008). *The Geology of Namibia, 3 volumes.* Ministry of Mines and Energy Geological Survey, Windhoek, Namibia.

Miller, R. McG. & Corner, B. (2002). The Agate Mountain Carbonatite Complex: Post-Etendeka alkaline volcanism onshore of the Walvis Ridge in the Cape Fria area, Namibia. Extended Abstract, *11th IAGOD Quadrennial Symposium and GeoCongress*, Windhoek, Namibia. Geological Survey of Namibia.

Miller, R. McG. (1983). The Pan-African Damara Orogen of South West Africa/Namibia. *Special Publication of the Geological Society of South Africa*, *11*, 431-515.

Passchier, C. W., Trouw, R. A., Goscombe, B., Gray, D., & Kröner, A. (2007). Intrusion mechanisms in a turbidite sequence: the Voetspoor and Doros plutons in north-west Namibia. *Journal of Structural Geology*, 29(3), 481-496.

Pickford, M., Sawada, Y., Hyodo, H., & Senut, B. (2014). Radioisotopic age control for Palaeogene deposits of the Northern Sperrgebiet, Namibia. *Communications of the Geological Survey of Namibia*, 15, 3-15.

Pickford, M. (2015). Cenozoic geology of the northern Sperrgebiet, Namibia, accenting the Palaeogene. *Communications of the Geological Survey of Namibia*, 16, 10-104.

Reid, D. L. (1991). Alkaline rocks in the Kuboos-Bremen igneous province, southern Namibia: The Kanabeam multiple ring complex. *Communications Geological Survey Namibia*, 7, 3-13.

Reid, D. L., & Cooper, A. F. (1998, April). Carbonatite and silicate magmas at Dicker Willem, southern Namibia: their origin and source region characteristics. *In International Kimberlite Conference: Extended Abstracts* (Vol. 7, pp. 727-729).

Roesener, H. 1989. The pyroclastic sequences of the Paresis Igneous Complex, Namibia. *Unpublished BSc. (Hons) thesis, Rhodes University*, Grahamstown, 43 pp

Schaefer, M. (2005). Short presentation on Karingarab Carbonatite*, internal report prepared for Anglo American Prospecting Services (AAPS)*, Namdeb, Namibia. 6 pp.

Schaefer, M. (2010). Reconnaissance trip to the Karingarab Carbonatite on Exclusive Prospecting License 3729 in southwestern Namibia*, internal report prepared for Anglo American Prospecting Services (AAPS*), Namdeb, Namibia. 4 pp.

Schreuder, C.P. (1975). Carbonate-bearing eruptives between the Great Karas Mountains and the Bremen Igneous Complex, South West Africa. *M.Sc. thesis University of. Stellenbosch*, 86 pp.

Schneider, G. (2008), "*The Roadside Geology of Namibia" 2nd revised edition*, Gebrüder Borntraeger, Stuttgart 294 pp.

Seth, B., Armstrong, R. A., Brandt, S., Villa, I. M., & Kramers, J. D. (2003). Mesoproterozoic U–Pb and Pb–Pb ages of granulites in north-west Namibia: reconstructing a complete orogenic cycle. *Precambrian Research*, 126(1-2), 147-168.

Siegfried, P. (2014). Reconnaisance map of outcrop at Karingarab, *Internal report, not published.* Prepared for Namdeb Mineral Resources: Exploration, Namibia. 1 pp.

Siegfried, P.R., (2017) Karingarab Preliminary Age, *Internal communications, not published.* Namdeb 1 pp.

Simandl, G. J., & Paradis, S. (2018). Carbonatites: related ore deposits, resources, footprint and exploration methods. *Applied Earth Science,* 127(4), 123-152.

Skirrow, R. G., Huston, D. L., Mernagh, T. P., Thorne, J. P., Duffer, H., & Senior, A. (2013). *Critical commodities for a high-tech world: Australia's potential to supply global demand* (p. 126). Canberra: Geoscience Australia.

Smithies, R. H., & Marsh, J. S. (1998). The Marinkas Quellen Carbonatite Complex, southern Namibia; carbonatite magmatism with an uncontaminated depleted mantle signature in a continental setting. *Chemical Geology*, 148(3-4), 201-212.

Stachel, T., Lorenz, V., & Brey, G. (1995). Carbonatite magmatism and fenitization of the epiclastic caldera-fill at Gross Brukkaros (Namibia). *Bulletin of Volcanology*, 57(3), 185-196.

Stocken, C. G. (1978). A review of the later Mesozoic and Cenozoic deposits of the Sperrgebiet. *CDM Geological Department. Internal report, not published.* Namdeb Diamond Corporation (Pty) Ltd., Oranjemund, Namibia. 33 pp.

Stratfor (2019). Available online: https://worldview.stratfor.com/article/geopolitics-rare-earth-elements (accessed on 24 August 2022).

Swart, R. (1988). Notes on the geology of some of the guano islands off the coast of Namibia. *Communications of the Geological Survey of SWA/Namibia*, 4, 89-91.

Tappe, S., Romer, R. L., Stracke, A., Steenfelt, A., Smart, K. A., Muehlenbachs, K., & Torsvik, T. H. (2017). Sources and mobility of carbonate melts beneath cratons, with implications for deep carbon cycling, metasomatism and rift initiation. *Earth and Planetary Science Letters*, *466*, 152-167.

Trumbull, R. B., Emmermann, R., Bühn, B., Gerstenberger, H., Mingram, B., Schmitt, A., & Volker, F. (2000). Insights on the genesis of the Cretaceous Damaraland igneous complexes in Namibia from a Nd-and Sr-isotopic perspective. *Communications of the Geological Survey of Namibia*, 12, 313-324.

United States National Academy of Sciences (USNAS), 2008. Minerals, critical minerals and the U.S. economy. https://www.nap.edu/catalog/12034/minerals-critical-minerals-and-the-us-economy (Accessed: 18 May 2020).

Verwoerd, W. J. (1993). Update on carbonatites of South Africa and Namibia. *South African Journal of Geology*, 96(3), 75-95.

Verwoerd, W. J., Retief, E. A., & Prins, P. (2000). The Etanenoberg alkaline complex, Namibia. *Journal of African Earth Sciences*, 31(1), 86-86.

Wall, F., Rollat, A., & Pell, R. S. (2017). Responsible sourcing of critical metals. *Elements*, *13*(5), 313-318.

Wilson, P. A. (1978). The Bennett Carbonatite, SWA. *Internal report, not published*. Namdeb (CDM), Oranjemund. 21 pp.

Witley, J.C., Swinden, S., & Aghamrian, M., (2021). Namibia Critical Metals Inc. Lofdal Heavy Rare Earths Project Namibia. NI 43-101 Technical Report – 20 May 2021 Mineral Resource Estimate. *Khorixas District, Republic of Namibia, MSA Project No.: J4327*. *The MSA group*.

Woolley, A. R. (2001). Alkaline rocks and carbonatites of the world. Part 3: Africa. *Geol. Soc. Natural History Museum*, London, S, 56.

Yaxley, G. M., Anenburg, M., Tappe, S., Decree, S., & Guzmics, T. (2022). Carbonatites: Classification, Sources, Evolution, and Emplacement. *Annual Review of Earth and Planetary Sciences*, *50*.

10. Appendix

Table 7: Summary of Carbonatite and Alkaline Occurrence in Namibia, modified after Woolley (2001).

No	Name Type	Description	Age	Diameter (km)	Reference
1	Agate Mountain Carbonatite	The Agate Mountain Complex is the onshore satellite of a large offshore volcano emplaced within the marginal subsidence ring of the larger offshore volcano some 84-92 million years ago in north-west Namibia. This 2.4km in diameter complex lies between Khumib Formation basalts on the east and quartz latites of the Skeleton Coast Subgroup on the west. The quartz latites on the west are overlain by epiclastic, clast supported conglomerates which not only contain ferrugenized quartzite pebbles but also fenitized basement granite with a presence of carbonatite veining. Initially, yellow martite sövite intruded which was metasomatically altered to dark grey bastnaesite bearing beforsite, this was followed by a main explosive event which emplaced the main carbonatite along with 31 satellite diatremes, phonolite plugs and dykes. Later, deposition of pyrolusite and aragonites occurred followed by tertiary erosion, karsting of the carbonatite and infill of carbonatite karsts with aragonite. Lastly a silcrete duricrust formed over the carbonatite.	Upper Cretaceous (84 - 92)	2.4	Miller and Corner, (2002)
2	Epembe Carbonatite	The Epembe Carbonatite in northern Namibia is a sövite dyke which is 250m wide and 6.5km long. It was emplaced within and follows orientation of a north-west trending fault zone in a nepheline syenite. The carbonatite varies in grain size from very fine to coarse grained. Colours vary from grey to red with few varieties of brown and white. Towards the southeast, the dyke forks into shallower, thinner parallel dykes until pinching out. Xenoliths wrapped by flow banding consist of nepheline syenite, felsic and mafic gneiss. Common minerals observed include, magnetite, hematite, apatite, riebeckite, aegirine, epidote, cancrinite and titanite with minor and erratically distributed biotite, K-feldspar and plagioclase.	Mesoproterozoic (1216±2.4 or 1213±2.5)	6.5x0.25	Menge, (1996) Seth et al., (2003)
3	Kakumangua Nepheline Syenite	This syenite dyke was named after the proximal village of Kakumangua along the Kunene River in northwest Namibia. It is an elongate north-western trending plug intruded into anorthosite. It consists of strike parallel vertical layering of fine- and coarse-grained bands. Few carbonatite veins are present in the centre. Common constituents observed are microcline perthite with interstitial, euhedral nepheline. Brown biotite occurs interstitially in cracks of feldspar grains or associated with opaque ore in the matrix. Perthite phenocrysts up to 1cm occur with parallel orientation to layering. Considerable alteration is observed in thin section, with replacement of microcline by albite and albite by cancrinite or fine grained micaceous liebenerite. Some of the bands also contain sericite, carbonate and apatite with sodalite and cancrinite occurring mostly in the south-eastern part of the intrusion.	Mesoproterozoic (1216±2.4 or 1213±2.5)	NA	Menge, (1996) Seth et al., (2003)
4	Zebra Mountain Dykes Syenite	The Zebra Mountain dykes are a swarm of north-north-west trending dykes up to 15km long. The dykes consist mostly of calcite and biotite bearing syenite dykes with biotite-albite, carbonatite, lamprophyre and composites of syenite-lamprophyre-carbonatite also present. Where dykes are comprised of composites, contacts are sharp and gradational between syenite and lamprophyre. Thin, platy and large K-feldspar phenocrysts up to 2.5cm in length have been observed in the syenite dykes with sodalite-carbonatite dykes intruding into the syenite dykes. Other phenocrysts observed are in	Mesoproterozoic (1216±2.4 or 1213±2.5)	15	Menge, (1996) Seth et al., (2003)

No	Name Type	Description	Age	Diameter (km)	Reference
		lamprophyre dykes and include olivine, pyroxene in a matrix of biotite and feldspar with minor calcite, analcite and ore.			
5	Swartbooisdrif Syenite	The Swartbooisdrif subsuite consists of 2 syenites of which the first is a pear shaped, north-west trending syenite about 2.5km long and 1km wide and thickest on the north-western end. The second is a similar syenite 5km east and intruded into the Dwyka succession. It is composed of coarse-grained microcline, micro perthite with smaller interstitial grains of microcline, albite and quartz. Irregular patches of arfvedsonite, aegirine-augite and biotite occur along microfractures.	Mesoproterozoic (1216±2.4 or 1213±2.5)	2.5x0.1	Menge, (1986) Seth et al., (2003)
6	Okorusu Alkaline Complex	Okorusu is a large oval shaped complex that covers 32 km2. Some parts of the complex are not exposed except for the centre of the complex and the southern margin. The country rock through which the complex intruded during the early Cretaceous, consists of Damaran schistose greywackes, micaceous and calcareous quartzites, tillite-like conglomerate, calcitic marble and granite. Thermal alteration and fenitization is visible in the southern margin of the complex. Fenitization accompanied with carbonatite emplacement preceded the subsequent major events. The sequence of events in the complex started with 1) Intrusion of hortonolite monzonite, early syenites, white coarse-grained nepheline bearing syenite that grades inwards into urtite and dark fine-grained foyaite in that order. 2) Formation of pyroxene fenite. 3) Intrusion of a succession of four different carbonatites 4) formation of limonitic feldspar-carbonate metasomatic rocks and iron ore deposits. 5) Replacement of carbonates by fluorite to form the fluorite deposits. 6) Lastly, the intrusion of dykes and small plugs of lamprophyres and nephelinite.	Lower Cretaceous (126.6±7.3)	32km^2	Kogut et al., (1998)
7	Paresis Alkaline Complex	Paresis is an alkaline complex which is slightly oval ringed forming a fractured caldera with the longest diameter measuring 17km in a N-S direction. It is one of few complexes in the Damaraland Suite made up mainly of volcanic rocks. The evolution of the complex involved 3 cycles (RF1, RF2 and RF3) of volcanism followed by an entirely intrusive phase. The complexes topography is controlled by 3 hypothetical ring structures. The north-west margin comprises low hills of steeply dipping rhyolitic rocks invaded by cone sheets of bostonite. On the Paresis North Ridge which dips towards the central massif, the full volcanic sequence is exposed. The Paresis South and Schwarzenfels area is made up of two lower volcanic units and includes interbedded epiclastic rocks. The RF1 ring structure in the south is observed by intense brecciation of the oldest eruptive unit of feldspar rhyolite. The RF2 ring structure, which lies northwest of RF1, forms the central ring like massif of the complex marked by a series of volcanic domes of which 3 structural domes occur on the western margin. It is composed of inward dipping comendite flows which is the upper most volcanic unit. It is also marked with rim intrusions along the ring fractures of comendite and syenite. The youngest and largest RF3 ring structure, where final cauldron subsidence occurred is characterized by step dipping volcanic units on the margins intruded by syenite, bostonite and microgranite in the form of dipping cone sheets towards the centre. The surrounding Damara basement rocks do not show any evidence of deformation by the complex.	Lower Cretaceous (137)	NA	Roesener, (1989)

No	Name Type	Description	Age	Diameter (km)	Reference
8	Etaneno Alkaline Complex	The Etanenoberg complex is comprised of one visible and exposed main 300m high symmetrical hill and two more larger concentric zones which are not exposed but visible on high resolution aero-magnetic surveys. Rock types encountered in this complex in order of emplacement include a central plug of tephritic phonolite, pulaskite with xenoliths of sodalite syenite, foyaite and radial dykes of nepheline syenite. Country rock in this area consists of Damara supergroup schist, marble, quartzite and coarse grained, porphyritic, syntectonic Damaran biotite granite.	Lower Cretaceous (134±3)	NA	Verwoerd et al., (2000) Kramm et al., (2017)
9	Ondurakorume Carbonatite	The Ondurakorume Carbonatite Complex is a circular composite intrusion rising steeply above the surrounding plain to a height of 275 m and is 1.4 km in diameter, with related plugs of nepheline syenite and small bodies of lamprophyres. Except for a few patches of country rock breccia on the northern and western contacts, most of the structure has been stripped by erosion. Presence of early activities are preserved in syenite intrusions in outcrops and 5 carbonatite emplacement events of two sövites and 3 beforsites. Intricate exposures of carbonatite and country rock remain indicating that the carbonatite was emplaced as a series of ring dykes. The surrounding country rock is comprised of Damara Supergroup including marble, quartzite, greywacke, schist and granite. Blocks enclosed by carbonatites are present, with one forming a marble plateau. Although marble and sövite are in contact, the marble can be distinguished as pure white and fine grained while the sövite carbonatite is grey on fractured surfaces and carries metamorphic minerals such as diopside, tremolite, phlogopite, scapolite, titanite, prehnite and zoisite. The three main types of carbonatites at this complex are micaceous sövite, sövite and beforsite.	Lower Cretaceous (~132)	1.4	Verwoerd (1993) Trumbull et al., (2000)
10	Kalkfeld Carbonatite	The Kalkfeld Alkaline Complex is composed of an alkaline ring complex with carbonatite as a major component. Topographically it appears as a circular range of hills around the central hill, Eisenberg which rises 122 m above the surrounding plains. The crater like rim bears fenitized and intensely folded and metamorphosed country rock of Damara sediments and syntectonic granites. Main units of the complex are distributed concentrically and consist of syenite and feldspathic breccia, nepheline syenite, sövite with micaceous zones associated with iron ore. Additionally, late-stage minor intrusions form part of the complex. Carbonatite occurs in a near vertical flow structure observed at the Eisenberg hill in the centre of the complex with centre of the carbonatite hosting iron ore.	Lower Cretaceous (153.6-172.8)	5	Verwoerd et al., (2000) Verwoerd, (1993)
11	Osongombe Carbonatite	The Osongombe carbonatite diatreme is located at high altitude with an irregular outline. This carbonatite is not associated with any alkali intrusives and intrudes into Damara marble and marginal bodies of syntectonic granite. This diatreme consists mostly of breccia comprised of granite, quartzite, micaceous material and a highly altered basic rock with carbonatized phenocrysts. On the surface, a third of the diatreme is covered by carbonatite forming a central zone with no sharp contact between that and the breccia zones. Brown weathered beforsite dykes with well-rounded inclusions cut through the diatreme and the country rock with few dolerite dykes also present. The carbonatite is mainly apatite rich beforsite and sövite.	Lower Cretaceous (~130)	0.45	Verwoerd, (1993)
12	Okenyenya Alkaline Complex	The Okenyenya Igneous Complex, which is comprised of tholeiitic and alkaline suites, was intruded into the Kuiseb schist close to a contact with the massive Omangabo Pluton of Salem type porphyritic biotite granite. The tholeiitic rocks range from picritic gabbro, olivine gabbro to quartz monzodiorite to syenite, quartz syenite and minor microgranite. The alkaline suite is comprised of gabbro, nepheline syenite, essexite and minor foyaite, tinguaite, lamprophyre and bostonite. The Karoo sedimentary rocks at the margins of the intrusion dip outwards, while the oldest rocks form	Lower Cretaceous (123.4-128.6, Rb-Sr; 128-133, K-Ar)	5	Le Roex et al., (1996)

No	Name Type	Description	Age	Diameter (km)	Reference
		a shallow inward dipping saucer shaped body composed of olivine gabbro and quartz monzodiorite intrusions. Syenite forms a major ring dyke at the southern and western margins and a curved dyke in the southern part of quartz monzodiorite. The final and major intrusive phase of the complex formed a new vent named the Okenyenya Mountains at the north-eastern margin of the complex. This vent consists of an outer ring of nepheline syenite which cuts across the olivine and alkaline gabbros while enclosing an inner ring of andesine essexite. In the centre of the vent is a plug of oligoclase essexite. the end of the igneous activity was documented in the emplacement of two foyaite plugs, sodalite tinguaite dykes, numerous dykes and several plugs and diatremes of lamprophyre and the bostonite dykes.			
13	Kwaggaspan Carbonatite	The Kwaggaspan Carbonatite consists of 5 small plugs intruded into Kuiseb schist aligned along a 1.3 km gently curving E-W oriented breccia zone. The composition of these plugs consists of 2 carbonatite, 1 quartz-hematite-muscovite rock and 2 very fine-grained iron oxide and silica rich plugs. Most of the brecciated schist is intruded by thin veinlets of sövitic carbonatite. The largest plug is the western most and has a diameter of 150 m and is composed mainly of sövitic carbonatite with abundant disseminated hematite. In the centre of this plug, large xenoliths of sedimentary iron formation, dolomite and schist several meters in diameter are layered and potentially derived from Chuos and Karibib Formations which underlie the carbonatite at considerable depth. A body of high-grade hematite ore about 10 m in diameter is located on the north-western edge of this plug. Fenitization through the growth of green pyriboles is observed in small schist outcrop west of this plug.	Lower Cretaceous (~130)	1.3	Verwoerd, (1993)
14	Oas Syenite	The Oas syenite is a massive weather resistant elevated plateau, coarse grained and grey to bluish and black in colour with a brownish weathering tinge stock intrusion. It intrudes into the Nosib Group quartzites and Huab gneisses and at the southern edge has younger schist and marble of the Swakop Group thrust over the edge. A typical granitic texture becomes sericitic along the marginal chill zone. Main crystals are perthitic and anti-perthitic alkali feldspar up to 13mm in size with minor interstitial quartz, amphibole and accessory minerals such as green-brown biotite, apatite, titanite, epidote, muscovite, calcite and zircon.	Neoproterozoic (750)	NA	Verwoerd, (1993) Jung et al., (2007)
15	Lofdal Nepheline Syenite	The Lofdal Nepheline Syenite is a series of one large and four smaller plugs that intrude into Huab gneisses. Grain sizes vary between the various plugs but tend to be medium to coarse grained in the centre with finer grains at the margins. The southern edge of the large main plug is composed of breccia of gneiss fragments with a matrix of nepheline syenite. Unique and distinct to Lofdal is short, lenticular and irregular pegmatitic patches up to 1 m long containing octahedral up to 1cm in size brown zircon and rod-shaped biotite up to 5 mm in diameter and 2cm in length. The margins of the plugs although finer grained have porphyritic, tabular, weakly aligned K-feldspar crystals up to 1 cm long with small amounts of interstitial nepheline, cancrinite and calcite. Towards the centre of the plug, the composition and size of euhedral nepheline increases till it dominates 40% of the rock with red staining distinguishing the nepheline from the greyish white K-feldspar. In some parts cancrinite completely replaces nepheline. Highly variable amounts of blue Sodalite are also present in the eastern edges of the four small plugs and makes up 50% of the rock.	Neoproterozoic (764)	NA	Verwoerd, (1993)
16	Doros Syenite	The Doros North Syenite which intruded after the Damara Orogenic event, consists of two plutons (one formerly known as the Voetspoor Syenite and the other as the Doros pluton) which are	Lower Cretaceous (132±0.9)	NA	Passchier et al., (2007)

No	Name Type	Description	Age	Diameter (km)	Reference
		composed of sheets of early hornblende syenite containing large planar rafts of enclosing schists in which primary deformation fabrics are preserved. Both the plutons are marginally intruded by late phase biotite granite that contains xenoliths of schist and earlier syenite.			
17	Brandberg Alkaline Complex	The Brandberg Granitic Complex is a massive almost circular elongate mountain that rises 1800 m above the surrounding Namib plains. It is 25 x21 km in diameter and hosts the highest mountain in Namibia, Konigstein elevated at 2573 m above sea level. The base of the Brandberg is partially enclosed by Karoo sedimentary rocks and Etendeka volcanics. The Brandberg, which was formerly an active volcano, is characterized by a series of intrusive events of mostly alkali granites. Some of the granites observed have been altered by hot, post-magmatic, sub solidus, alkaline, metasomatic fluids. The Brandberg granites are medium to coarse grained even at the highest elevations indicate a slow cooling period into a thick cover potentially 2 km thick which has since eroded.	Lower Cretaceous (132±1)	2.1x2.5	Diehl, (1990)
18	Messum Nepheline Syenite	The Messum Complex is a deeply eroded circular complex 18 km in diameter with a central core and well-defined outer rings. The outer rings form a moat of ridges separated from the central core by a topographically low region covered with extensive sand in the west but hybrid granitoid gabbro cone sheets on the east. Country rocks are composed of the Etendeka Group basalts and quartz latites which steeply dip inwards. Early volcanic phases include basalts followed by chaotic volcanic breccias of rhyolite, forming domes. Goboboseb quartz latites and basalts from Copper Valley and Messum Mountain were followed by sheared quartz latites (Springbok) and quartz monzonite laccoliths and plugs. This was followed by a main intrusive phase of heterogenous sheeted granitoid rocks and gabbro cone sheets, thick in the west and thin in the east. The core consisted of syenite, quartz syenite and nepheline syenite while later stage intrusions consist of late-stage plugs, tinguaite rings and radial dykes associated with some minor intrusive rocks.	Lower Cretaceous (132±2.2 Ma, Rb-Sr; 149±1 Ma, Ar-Ar; 126.8±1.3 Ma, Rb-Sr)	18	Ewart et al., (1998)
19	Cape Cross Syenite	The Cape Cross foyaite plug with raised relief to surrounding plains, intrudes into the Cape Cross granites and a salt pan. The foyaite contains xenoliths of tinguaite and the tinguaite contains small, dark xenoliths of essexite. The foyaite ranges in colour due too presence of mafic tinguaite and has a granular texture consisting mostly of perthite, nepheline, albite, sodalite, aegirine-augite, barkevikite and biotite as well as accessory appetite, calcite and analcite. The nepheline forms discrete crystals as plagioclase is replaced and is associated with sodalite. The aegirine-augite is observed on the rims of primary, magmatic barkevikite. The tinguaite is darker than the foyaite and is fine grained and porphyritic in texture. Cutting across this plug are veins of nepheline and veins containing K-feldspar and orientated, acicular aggregates of aegirine-augite.	Lower Cretaceous (135±0.7)	1	Linning, (1968)
20	Eureka Carbonatite	The Eureka Carbonatite is a monazite rich igneous intrusion which has previously been classified as either a marble or a skarn. Several medium to coarse grained beforsite dykes up to 7m thick have been observed intruding into feldspathic quartzites interlayered with calc-silicate layers of the Nosib Group with a tourmaline-bearing pegmatite of late Pan-African age intersecting too. Fenitization is observed in the surrounding country rock.	Cambrian (450-500)	NA	Verwoerd, (1993)
21	Otjisazu Carbonatite	The Otjisazu Complex is a major carbonatite complex about 4 km at its widest and located next to the southern boundary of the highly deformed central zone of the Damara orogen. The complex is elongate and is composed of a core of sövite surrounded by alkali pyroxenite, ijolitic and gabbroic rocks all of which are intruded by leucocratic syenite and syenite pegmatite. The sövite has a	Cambrian (523-550)	12 km^2	Bühn et al., (2001) Verwoerd, (1993)

No	Name Type	Description	Age	Diameter (km)	Reference
		massive breccia structure and is rich in aegirine-augite, garnet, apatite and xenoliths of schistose garnet wollastonite rock. Large titanite and apatite crystals are present in sheet like mafic pegmatoids confined to the sövite and alkali pyroxenite. The pyroxenite is composed of aegirine-augite with minor K-feldspar, garnet, melanite, apatite, titanite, calcite and accessory monazite. The apatite is associated with Cu sulphides and occur in both pyroxenite and sövite along with titanite but devoid of magnetite indicating crystallization in iron poor reducing conditions. Although limited, fenitization is observed in surrounding pelites and semi-pelitic schists of the Swakop Group.			
22	Gross Brukkaros Carbonatite	The Brukkaros Mountain is a 3 km-wide crater formed by an explosive eruption event but is now partially eroded. No igneous material has been observed amongst the ejecta. Although initially described as a kimberlite due to textures indicating carbonatized lamprophyres, the classification leans towards carbonatite because of the presence of carbonatite lapilli, numerous narrow radiating dykes of beforsite carbonatite, breccia filled satellite vents with carbonatite matrix, evidence of fenitization in microbreccias and tuffs of the central crater, late veins of dolomite, calcite, quartz and barite in sediments and the updoming nature and rupture of surrounding strata indicating a volatile rich magma. At the elevated rim of the crater, which is filled with crater-lake sediments, rocks dip in towards the centre following a shallow, steep and then flat succession.	Upper Cretaceous (77)	3	Stachel et al., (1995) Verwoerd, (1993)
23	Dicker Willem Carbonatite	The Dicker Willem Carbonatite Complex is an almost circular intrusion with a maximum diameter of 2.8 km across and rising 600m above the surrounding plains where it intruded into the gneisses of the Namaqua Metamorphic Complex. Internal structure is steeply dipping, concentric and defined by flow banding. 5 main types of carbonatites have been identified which include sövite, alvikite, beforsite, ferro-alvikite and dykes of yellow carbonatite, microbreccias and tuffisite. Earliest rock types have been identified as xenoliths of ijolite grading into syenite with increasing K-feldspar content, these xenoliths are present in the next intrusions of nepheline sövite and biotite sövite. This was followed by trachytic rocks associated with phonolite. Alvikite is the most abundant rock type and it intrudes the sövite, both alvikite and sövite are intruded by various dykes of beforsite, ferro-alvikite, yellow calcitic carbonatite, microbreccias and tuffisite accompanied by steep sided carbonatite breccia bodies. The Namaqua gneisses included as fenitized xenoliths within the carbonatites and those surrounding the complex are faulted, brecciated, fenitized and intruded by peripheral plugs, concentric and radial dykes as well as concentric cone sheets of trachyte, various carbonatites and their brecciated equivalents.	Eocene (49)	2.8	Reid and Cooper, (1998)
24	Keishohe Carbonatite	The Keishohe Carbonatite is an outcrop of 1.3 km in length and 0.6 km wide and is comprised of several shallow dipping NE-SW striking 2 m thick sills of brown weathering, ferruginous beforsite with ironstone lenses containing alunite. The lenses are crosscut by narrow dykes of beforsite and microbreccias carrying clasts of Namaqua gneiss, schist and amphibolite.	Upper Cretaceous (NA)	1.3	Verwoerd, (1993)
25	Teufelskuppe Carbonatite	The Teufelskuppe Carbonatite is a circular intrusion about 1 km in diameter rising to 120 m above the surrounding plains. The carbonatite is formed by a series of cone sheets shallowly dipping inwards. A conical hill in the northern part of the intrusion is suggested to be a volcanic neck due to a band of black ferruginous lapilli at its base. The cone sheets are made up of dark brown, yellow calcitic and dolomitic carbonatites with fine grained alvikite being the dominant rock type. Flow banding is observed in some of the sheets enclosing xenoliths of biotite schist and amphibolites of the Namaqua Garub group. Some alvikites contain euhedral crystals of magnetite, apatite and dolomite. Country rocks in the area are fractured and altered potentially by fenitization.	Upper Cretaceous (NA)	1	Verwoerd, (1993)

No	Name Type	Description	Age	Diameter (km)	Reference
26	Kaukausib Carbonatite	The Kaukausib Carbonatite is located in the southern flank of a valley and is observed by raised relief above the surrounding plains and is 150 m in diameter. Outcrop of Kaukausib is of ferruginous silicified carbonatite and lateritic talus. The carbonatite dykes of beforsite intruded into schist, gneiss and migmatite.	Upper Cretaceous (NA)	0.15	Verwoerd, (1993)
27	Drachenberg Syenite	The Drachenberg Syenite Complex is 2.5 km in diameter and intrudes into Namaqua granitic gneisses and quartzite, quartz mica schist and pelitic schist of the Gariep supergroup. It is poorly exposed and the suggested sequence of intrusion started with quartz monzonite, porphyritic syenites, biotite-rich syenites, quartz and quartz free syenite, syenite porphyry plugs, bostonite dykes and quartz feldspar porphyry dykes.	Lower Cretaceous (NA)	2.5	Marsh, (1976)
28	Pomona Syenite	Formerly known as the Signalberg Syenite Complex, the Pomona Complex is a 5 km wide circular complex for which only half is visible onshore. Country rocks intruded include granitic and granodioritic gneisses of the Namaqua Metamorphic Complex. In order of emplacement, the complex consists of outer syenite rings and inner syenite rings with small outcrops of biotite-rich monzonite and quartz syenite at the centre of the complex. During the explosive eruption syenite porphyry and quartz-feldspar porphyry was emplaced with marginal brecciation of gneisses in the NE. A small intrusion of foyaite is at the centre of the complex with bostonite forming a partial ring dyke inside the northern part of the complex. There are many late-stage radial dyke swarms of bostonite, quartz bostonite, tinguaite and lamprophyre dykes that cut across all concentric rock types. The final igneous event is the emplacement of an outer ring dyke of nordmarkite in the Namaqua gneisses outside the outer syenite. The inner and central syenites do not have chilled margins indicating intrusion while the outer syenite was still hot. All subsequent intrusions show evidence of late-stage activity due to presence of chilled margins.	Lower Cretaceous (133 ± 2)	5	Marsh, (1976) Swart, (1988)
29	Granitberg Nepheline Syenite	The Granitberg Foyaite is an oval shaped ring complex 3 by 2.5 km in diameter. It intrudes into feldspathic quartzite, arkose and dolomite of the Gariep Supergroup near the contact of this group with the granitic gneisses of the Namaqua Metamorphic Complex. The Gariep rocks have open folds with axis trending north-north-west and the quartzite on the western margin of the complex dip steeply towards the contact. In order of emplacement age, the oldest rocks are marginal sheet-like intrusions of porphyritic syenite, a circular roof zone of chilled and layered xenolith rich nepheline syenites surrounded by an outer foyaite ring and an inner plug of foyaite with late stage tinguaite, breccia, quartz bostonite and grorudite dykes and sheets.	Lower Cretaceous (130 ± 2)	3x2.5	Marsh, (1973) Pickford et al., (2014)
30	Klinghardt Mountains Phonolite	The Klinghardt Phonolites consist of plugs, breccia pipes, extrusive bodies and dykes that form elevated domes at the Klinghardt Mountains. These phonolite lavas were viscous and experienced explosive emplacements forming steep sided hills and moat like structures at the base. These explosive events formed a tuff ring at the base of the crater composed of country rock fragments and agglomerate material. In the centre, a viscous lava dome formed which would expand and chill forming a talon apron or marginal crumble breccia. The Klinghardt domes present onion skin type of concentric flow banding and jointing, with chilled finer grained and darker marginal facies and coarser grained, lighter coloured facies towards the centre. Some spots of alteration are present locally.	Eocene (46)	NA	Verwoerd, (1993)
31	Chameis Carbonatite	The Chameis Carbonatite is a small carbonatite plug that is 100 m long and 50 m wide forming a spur on the eastern side of an escarpment 30 m high. The outline is irregular and with numerous dykes protruding into the chloritic Gariep Supergroup schists. Country rock xenoliths are present in	Upper Cretaceous (NA)	NA	Verwoerd, (1993)

No	Name Type	Description	Age	Diameter (km)	Reference
		the carbonatite and the carbonatite is a medium grained beforsite containing dolomite. Parankerite occurs as rims to dolomite and as replacement veins along fractures in the dolomite. Other minerals present include quartz and perthitic microcline and fine microlites with accessory minerals such as pyrite, zircon, rutile, greenish amphibole and biotite. Xenoliths are angular and unsorted and include Gariep schist and quartzites. Veins such as siliceous carbonatite and quartz are common along with miarolitic cavities in the carbonatite.			
32	Karingarab Carbonatite	The Karingarab Carbonatite is a circular hill feature elevated at 300 m from sea level. It has a diameter of 2.5 km and is comprised of a core of carbonatite expressed as interlayers of ferrous brown and dolomitic grey carbonatite with magnetic and manganese banding. The outer zone as a brecciated manganese rich and brown silicified carbonatite. His observations of outcrop noted that the area proximal to the main carbonatite hosts porphyritic phonolite plugs and dykes.	Upper Cretaceous (68)	2.5x2.5	Stocken, (1978)
33	Grootpenseiland Nepheline Syenite	The Grootpenseiland is a felsic complex for which the oldest rocks are nepheline bearing syenites which are the most intrusive phases into siliceous rocks in the southwest. In the northeast, the youngest and large granitic stocks intrude. These intrusions cut into granitoids of the Vioolsdrif Suite of the Richtersveld sub province with sharp contacts and very few chilled margins.	Cambrian (514-529)	NA	Smithies and Marsh, (1998)
34	Marinkas Quelle Carbonatite	The Marinkas Quelle carbonatite complex lies northwest of the Marinkas Quelle Felsic Complex. The complex covers 2.5 km^2 and is elongate in a north-easterly direction. It has two intrusive centres and the sequence of intrusive events as is typical with carbonatites starts with a nepheline syenite, sövite, beforsite, ferrocarbonatite and Mn-rich ferrocarbonatite. Fenitization is evident for up to 500m in the enclosing gneissic country rock of the Namaqua Metamorphic Complex. Younger granites of the Marinkas Quelle Felsic Complex cut across the fenite indicating younger activity.	Cambrian (514-529)	2.5 km^2	Smithies and Marsh, (1998)
35	Kanabeam Nepheline Syenite	The Kanabeam complex oldest intrusive phase is a series of concentric rings of nepheline syenite subsequently intruded by a plug of quartz syenite. Later intrusive events were of saturated micro syenites with a variety of granitic rock types which differed in texture and quartz content. Later, phonolitic breccia pipes intruded into the plutonic rocks along major contacts. Apart from these, several other alkali gabbroic types are present which may have been derived from deeper unexposed parts of the complex.	Cambrian (520)	3x2	Reid, (1991)
36	Bremen Syenite	The Bremen complex intrudes gneisses of the Namaqua Metamorphic Complex and of the Nama group along the north-western margin. The complex although large areas are covered with sand cover, is composed mostly of syenite and granitic intrusions with an associated swarm of dykes extending well into the country rock. The sequence of intrusion events are as follows: ferrosyenite, ferrobostonite dykes, granular syenite and concomitant intrusion of porphyritic microsyenite associated with a hornblende syenite ring dyke.	Cambrian (500-550)	NA	Verwoerd, (1993) Allsop et al., (1979)
37	Haruchas Nepheline Syenite	Haruchas is a pear shaped 2.25 km long northeast trending stock type pluton with its widest point 450m on its southwestern end. There exists a sharp contact between the pluton and the gneisses of the Namaqua Metamorphic Complex. The main intrusion is perthite syenite lacking nepheline and containing quartz. The central plug is composed of medium to coarse grained nepheline syenite within the perthite syenite. The nepheline syenite is composed of perthite, plagioclase, nepheline, biotite, aegirine and aegirine-augite. Sodalite and haüyne also occur locally with accessory minerals such as apatite, zircon and titanite present. Along the margins on the thick end of the stock, a ring dyke of fine grained and weather resistant foyaite intrudes with greenish grey bostonite dykes cutting the stock in a NS trend extending into the country rock.	Cambrian (NA)	2.25	Schreuder, (1975) Verwoerd, (1993)

No	Name Type	Description	Age	Diameter (km)	Reference
38	Mickberg Carbonatite	The Mickberg Diatreme pipe is a double crested intrusion that rises almost 100m above the surrounding plains and is elongate in an NNE direction. It is composed of gneiss brecciated in places and intruded by dark brown ankeritic beforsite. Nama quartzite intruded by Kainab type veins. Embedded in the carbonatite are inclusions of gneiss, grit and quartzite of the Kuibis Formation. Fenitization is evident in light blue coloured quartzite fragments and blue sodalite north of the hilltop. The carbonatite is composed of euhedral and anhedral ankerite, ferroan calcite, apatite, magnetite, biotite and chlorite, as well as zircon, quartz and feldspar derived from the surrounding gneiss with minor amounts of malachite and chrysocolla occur at the southern tip of the composite plug. A unique feature observed in the largest carbonatite body is spheroidal inclusions up to 15cm in diameter forming concentric shells of ankerite and fragments around lithic nuclei varying from 1 to 7cm in diameter. Between the concentric shells is matrix of medium grained silica with a mosaic texture of quartz, microcline and albite. These concentric shells are presence of accretionary events in a fluidized vent.	Cambrian (NA)	0.45	Schreuder, (1975) Verwoerd, (1993)
39	Weltevrede Carbonatite	The Weltevrede Carbonatite consists of two breccia plugs forming low round hills raising above a sandy flat. The northernmost plug is 1 km in diameter and has several smaller outcrops of gneissic country rock fragments in a matrix of variable brown carbonate material. Beforsite dykes full of clasts are present and cut across the breccia. The second plug is similar with less ankerite in the matrix, in this plug several blocks of quartzite and conglomerate (meters in diameter) are found in the breccia below the stratigraphic level where this formation used to be. Also present in this plug is beforsite veins and calcitic dykes up to 2 m wide following a zig zag course along strike of the country rock foliation. In the southern end, the carbonatite dyke contains galena, chalcopyrite, limonite, malachite, chrysocolla and quartz.	Cambrian (NA)	2	Schreuder, (1975) Verwoerd, (1993)
40	Garub Carbonatite?	The Garub intrusions are alnöitic tuffisite intrusions associated with a fluorite deposit in a region referred to as the Grunau Alkaline province. The Grunau Alkaline province has been renamed to the Kainab Alkaline province. This swarm consists of nearly 100 diatremes, dykes and sills of brown to dark brown carbonate-rich, basic, alkaline rock with numerous country rock fragments in a 150 km long and 30 km wide ENE trending swath. This carbonatite bearing rocks have so far been unsuccessfully grouped to carbonatite, kimberlite, lamprophyre, olivine melitite or peperite and grouped as an alnöitic tuffisite due to the geochemical composition.	Cambrian (491)	150x30	Schreuder, (1975) Allsop et al., (1979)
41	Bokiesbank Carbonatite?	Bokiesbank, initially identified as a "possible carbonatite of doubtful status" until Verwoerd likened the brown weathered veins as similar to those of ankeritic beforsite dykes of Brukkaros. The veins often cut across gneisses and amphibolites with veins often bent, folded, or broken by minor faulting. The veins are usually fine grained for the rusty brown material while coarse grained varieties remain grey with veins sometimes zoned and the central portion containing inclusions of angular feldspar, quartz, mica and galena fragments. Adding to the doubtful status that Bokiesbank is a carbonatite, the outcrop near the dykes are granite and gneiss impregnated with calcite with no geochemical affinity to carbonatite. Of specimens analysed, the composition was of 42% calcite, 33% albite, 25% orthoclase and no quartz with the origin of the calcite-feldspar rock being problematic.	Upper Cretaceous (NA)	NA	Verwoerd, (1993)

Table 8: Subset of Karingarab assay and lithology data

ID	from	to	PROJECTCODE	Weathering	Lith	Ba_ppm	CaO_pct	Fe2O3_pct	MgO_pct	SiO2_pct	Sr_ppm	TREE_ppm	Fe2O3/MgO	CaO/MgO	Sr/Ba	Nb/Y
Dalucao			Dalucao	None	Syenite	7,663.00	0.68	1.90	0.16		2,571.00	267.00	11.88	4.25	0.34	2.40
Dalucao			Dalucao	None	Syenite	1,719.00	0.49	1.41	0.10		780.00	846.00	14.10	4.90	0.45	1.79
Dalucao			Dalucao	None	Syenite	4,094.00	1.17	1.41	0.16		2,001.00	411.00	8.81	7.31	0.49	2.33
Dalucao			Dalucao	None	Syenite	4,999.00	3.19	1.41	0.06		3,752.00	672.00	23.50	53.17	0.75	1.03
Dalucao			Dalucao	None	Syenite	5,354.00	2.51	1.41	0.19		694.00	746.00	7.42	13.21	0.13	0.45
Dalucao			Dalucao	None	Syenite	1,541.00	1.55	1.41	0.70		483.00	182.00	2.01	2.21	0.31	0.76
Dalucao			Dalucao	None	Syenite	3,516.00	2.20	1.41	0.17		4,920.00	674.00	8.29	12.94	1.40	1.40
Dalucao			Dalucao	None	Carbonatite	19,220.00	23.36		0.01		54,590.00	20,062.00	-	2,336.00	2.84	0.01
Dalucao			Dalucao	None	Carbonatite	73,890.00	43.30		0.01		16,570.00	2,851.00	-	4,330.00	0.22	0.40
Dalucao			Dalucao	None	Carbonatite	81,880.00	36.45		0.01		17,030.00	7,411.00	-	3,645.00	0.21	1.22
Dalucao			Dalucao	None	Carbonatite	73,070.00	36.75		0.01		17,950.00	2,770.00	-	3,675.00	0.25	0.83
Dalucao			Dalucao	None	Carbonatite	24,960.00	33.40	0.45	0.05		50,520.00	15,808.00	9.00	668.00	2.02	0.09
Dalucao			Dalucao	None	Carbonatite	8,970.00	40.40	0.58	0.03		40,100.00	3,529.00	19.33	1,346.67	4.47	0.05
Dalucao			Dalucao	None	Carbonatite	65,780.00	42.90	0.16	0.02		27,380.00	4,123.00	8.00	2,145.00	0.42	0.47
Dalucao			Dalucao	None	Carbonatite	2,031.00	46.90	1.47	0.03		10,020.00	33,759.00	49.00	1,563.33	4.93	0.00
KR_DD_14_04	75.92	76.7	KAR	None	Carbonatite	6,456.90	40.52	8.90	5.97	0.87	2,730.60	16,173.20	1.49	6.79	0.42	2.55
KR_DD_14_04	76.7	76.92	KAR	None	Carbonatite	6,456.90	40.52	8.90	5.97	0.87	2,730.60	16,173.20	1.49	6.79	0.42	2.55
KR_DD_14_05	35.52	36.52	KAR	None	Carbonatite	15,531.30	40.69	8.17	7.50	0.84	8,000.20	19,273.40	1.09	5.43	0.52	0.37
KR_DD_14_05	36.52	36.6	KAR	None	Carbonatite	28,001.70	21.29	14.86	5.36	14.78	4,511.40	17,363.70	2.77	3.97	0.16	2.08
KR_RC_16_001	124	125	KAR	None	Alkali Silicate	3,379.30	19.15	8.83	2.19	27.31	1,662.10	4,907.60	4.03	8.74	0.49	1.26
KR_RC_16_001	125	126	KAR	None	Alkali Silicate	7,613.40	15.87	9.87	2.60	30.08	1,202.90	2,375.70	3.80	6.10	0.16	1.08
KR_RC_16_001	126	127	KAR	None	Alkali Silicate	7,054.40	17.86	10.00	3.15	26.59	1,677.30	4,666.80	3.17	5.67	0.24	1.24
KR_RC_16_001	129	130	KAR	None	Alkali Silicate	12,027.90	17.29	12.83	3.11	25.20	1,389.60	4,787.40	4.13	5.56	0.12	1.66

ID	from	to	PROJECTCODE	Weathering	Lith	Ba_ppm	CaO_pct	Fe2O3_pct	MgO_pct	SiO2_pct	Sr_ppm	TREE_ppm	Fe2O3/MgO	CaO/MgO	Sr/Ba	Nb/Y
KR_RC_16_001	130	131	KAR	None	Alkali Silicate	10,103.10	16.93	12.79	3.02	25.37	1,312.70	4,087.80	4.24	5.61	0.13	1.70
KR_RC_16_001	131	132	KAR	None	Alkali Silicate	18,105.80	19.16	11.52	3.09	21.24	1,682.30	5,072.40	3.73	6.20	0.09	1.03
KR_RC_16_001	132	133	KAR	None	Alkali Silicate	6,795.70	18.28	10.82	1.88	27.88	1,494.70	2,831.90	5.76	9.72	0.22	1.99
KR_RC_16_001	133	134	KAR	None	Alkali Silicate	4,270.60	15.83	11.44	3.30	29.95	1,253.60	1,582.30	3.47	4.80	0.29	1.33
KR_RC_16_001	134	135	KAR	None	Alkali Silicate	3,979.60	15.65	11.49	3.31	28.78	1,432.20	1,904.00	3.47	4.73	0.36	1.52
KR_RC_16_001	135	136	KAR	None	Alkali Silicate	2,983.10	15.66	12.73	3e.79	27.97	1,369.50	2,381.70	3.36	4.13	0.46	1.09
KR_RC_16_001	136	137	KAR	None	Alkali Silicate	5,141.00	16.02	9.66	3.75	28.69	1,985.60	3,963.30	2.58	4.27	0.39	1.66
KR_RC_16_001	137	138	KAR	None	Alkali Silicate	3,356.50	18.37	11.01	2.31	28.54	1,422.80	1,710.30	4.77	7.95	0.42	1.80
KR_RC_16_001	138	139	KAR	None	Alkali Silicate	4,130.10	15.98	10.82	2.25	31.98	1,224.20	1,751.80	4.81	7.10	0.30	2.41
KR_RC_16_001	139	140	KAR	None	Alkali Silicate	3,468.10	14.61	9.75	2.99	32.01	1,275.40	2,768.20	3.26	4.89	0.37	1.68
KR_RC_16_001	140	141	KAR	None	Alkali Silicate	3,419.80	16.12	9.54	2.82	31.24	1,344.60	1,788.20	3.38	5.72	0.39	1.49
KR_RC_16_001	141	142	KAR	None	Alkali Silicate	4,749.40	15.65	11.59	2.90	30.50	1,419.40	2,585.10	4.00	5.40	0.30	1.62
KR_RC_16_001	142	143	KAR	None	Alkali Silicate	5,456.50	15.98	11.77	2.27	31.19	1,264.90	2,038.10	5.19	7.04	0.23	1.88
KR_RC_16_001	143	144	KAR	None	Alkali Silicate	5,509.50	19.60	11.13	2.02	29.06	1,519.30	1,752.70	5.51	9.70	0.28	1.53
KR_RC_16_001	144	145	KAR	None	Alkali Silicate	5,126.60	17.69	11.82	2.54	32.73	1,353.70	1,318.90	4.65	6.96	0.26	1.95
KR_RC_16_001	145	146	KAR	None	Alkali Silicate	4,887.30	17.86	12.65	1.02	29.05	1,266.80	2,588.00	12.40	17.51	0.26	2.08
KR_RC_16_001	146	147	KAR	None	Alkali Silicate	5,044.80	18.47	11.50	1.46	27.81	1,394.40	3,188.00	7.88	12.65	0.28	1.83
KR_RC_16_001	147	148	KAR	None	Alkali Silicate	5,073.00	16.73	12.80	2.17	29.21	1,170.40	4,473.10	5.90	7.71	0.23	1.63
KR_RC_16_001	148	149	KAR	None	Alkali Silicate	4,804.60	15.12	11.92	2.60	31.28	1,237.60	3,930.40	4.58	5.82	0.26	1.67
KR_RC_16_001	149	150	KAR	None	Alkali Silicate	4,242.40	17.58	10.93	3.03	29.29	1,479.30	3,286.70	3.61	5.80	0.35	1.28
KR_RC_16_002	126	127	KAR	None	Carbonatite	14,113.80	15.91	5.80	13.36	21.75	4,568.50	9,877.30	0.43	1.19	0.32	1.73
KR_RC_16_002	127	128	KAR	None	Carbonatite	7,401.00	28.70	3.52	16.97	2.50	7,861.70	14,275.10	0.21	1.69	1.06	0.61
KR_RC_16_002	128	129	KAR	None	Carbonatite	6,537.90	28.83	3.71	17.53	1.75	7,418.40	15,220.90	0.21	1.64	1.13	0.89
KR_RC_16_002	129	130	KAR	None	Carbonatite	6,628.50	29.76	2.29	17.92	1.10	7,834.70	19,480.10	0.13	1.66	1.18	0.37

ID	from	to	PROJECTCODE	Weathering	Lith	Ba_ppm	CaO_pct	Fe2O3_pct	MgO_pct	SiO2_pct	Sr_ppm	TREE_ppm	Fe2O3/MgO	CaO/MgO	Sr/Ba	Nb/Y
KR_RC_16_002	130	131	KAR	None	Carbonatite	5,338.50	29.37	1.73	18.58	0.86	8,589.40	16,158.90	0.09	1.58	1.61	0.13
KR_RC_16_002	131	132	KAR	None	Carbonatite	3,909.70	30.64	2.24	18.93	0.69	8,356.20	16,798.60	0.12	1.62	2.14	0.25
KR_RC_16_002	132	133	KAR	None	Carbonatite	4,651.30	30.38	1.92	18.93	0.18	10,040.80	15,708.70	0.10	1.60	2.16	0.28
KR_RC_16_002	133	134	KAR	None	Carbonatite	5,115.70	28.31	2.35	18.54	1.96	9,310.00	12,011.10	0.13	1.53	1.82	0.30
KR_RC_16_002	134	135	KAR	None	Carbonatite	4,197.60	28.75	3.16	17.75	1.13	7,687.70	13,833.70	0.18	1.62	1.83	0.68
KR_RC_16_002	135	136	KAR	None	Carbonatite	6,275.50	24.00	4.02	18.82	7.08	6,270.50	12,903.80	0.21	1.28	1.00	1.28
KR_RC_16_002	136	137	KAR	None	Carbonatite	4,835.60	26.75	4.09	20.56	6.06	6,974.80	16,083.60	0.20	1.30	1.44	2.31
KR_RC_16_002	137	138	KAR	None	Carbonatite	5,540.70	23.73	5.42	17.91	7.94	5,669.30	13,818.50	0.30	1.32	1.02	2.25
KR_RC_16_002	138	139	KAR	None	Alkali Silicate	5,569.90	24.07	8.15	17.50	7.32	3,907.40	9,824.00	0.47	1.38	0.70	3.63
KR_RC_16_002	139	140	KAR	None	Alkali Silicate	8,684.00	11.87	7.30	18.67	24.07	3,505.40	9,183.70	0.39	0.64	0.40	4.07
KR_RC_16_002	140	141	KAR	None	Alkali Silicate	8,800.30	10.19	6.66	20.41	26.23	2,774.40	9,529.10	0.33	0.50	0.32	2.65
KR_RC_16_002	141	142	KAR	None	Carbonatite	7,809.50	19.62	4.76	19.32	13.02	5,280.60	11,012.00	0.25	1.02	0.68	3.14
KR_RC_16_002	142	143	KAR	None	Carbonatite	8,094.60	26.06	3.35	19.07	4.56	7,222.60	11,517.90	0.18	1.37	0.89	2.23
KR_RC_16_002	143	144	KAR	None	Carbonatite	7,123.90	12.67	6.69	17.88	24.06	3,907.20	9,639.60	0.37	0.71	0.55	3.57
KR_RC_16_002	144	145	KAR	None	Carbonatite	9,086.70	16.48	6.16	20.38	21.15	4,787.30	11,173.40	0.30	0.81	0.53	2.12
KR_RC_16_002	145	146	KAR	None	Carbonatite	9,762.70	22.68	3.71	18.17	9.32	6,935.60	14,877.00	0.20	1.25	0.71	0.75
KR_RC_16_002	146	147	KAR	None	Alkali Silicate	9,686.80	14.56	6.27	17.57	20.90	4,482.00	9,815.10	0.36	0.83	0.46	2.36
KR_RC_16_002	147	148	KAR	None	Alkali Silicate	8,174.40	15.32	6.31	16.76	20.68	4,228.60	9,897.90	0.38	0.91	0.52	2.51
KR_RC_16_002	148	149	KAR	None	Alkali Silicate	11,273.40	14.07	6.86	17.31	22.49	3,644.60	8,909.30	0.40	0.81	0.32	2.81
KR_RC_16_002	149	150	KAR	None	Alkali Silicate	8,946.00	15.81	6.50	16.94	19.73	4,063.30	9,827.00	0.38	0.93	0.45	3.09
KR_RC_16_003	110	111	KAR	None	Alkali Silicate	5,265.70	9.32	9.57	4.18	41.42	2,447.90	2,551.60	2.29	2.23	0.46	2.17
KR_RC_16_003	111	112	KAR	None	Alkali Silicate	17,415.90	9.29	12.75	7.85	32.13	3,444.80	7,325.60	1.62	1.18	0.20	2.16
KR_RC_16_003	112	113	KAR	None	Alkali Silicate	13,489.60	10.68	9.49	7.58	30.35	3,254.30	5,599.20	1.25	1.41	0.24	1.72
KR_RC_16_003	113	114	KAR	None	Alkali Silicate	12,463.80	8.82	9.63	6.21	36.91	2,781.50	3,854.20	1.55	1.42	0.22	2.07

ID	from	to	PROJECTCODE	Weathering	Lith	Ba_ppm	CaO_pct	Fe2O3_pct	MgO_pct	SiO2_pct	Sr_ppm	TREE_ppm	Fe2O3/MgO	CaO/MgO	Sr/Ba	Nb/Y
KR_RC_16_003	114	115	KAR	None	Alkali Silicate	9,363.80	8.26	9.08	4.52	41.44	2,563.20	2,777.40	2.01	1.83	0.27	2.85
KR_RC_16_003	115	116	KAR	None	Alkali Silicate	11,227.30	9.27	8.96	5.16	35.74	2,972.30	4,516.00	1.74	1.80	0.26	2.91
KR_RC_16_003	116	117	KAR	None	Alkali Silicate	18,566.60	7.24	9.57	4.58	36.94	2,315.80	2,350.10	2.09	1.58	0.12	3.40
KR_RC_16_003	117	118	KAR	None	Carbonatite	20,653.40	10.52	9.31	5.28	32.98	2,583.90	3,178.60	1.76	1.99	0.13	1.78
KR_RC_16_003	118	119	KAR	None	Carbonatite	22,418.50	15.62	9.10	6.91	26.51	3,267.10	4,518.20	1.32	2.26	0.15	1.17
KR_RC_16_003	119	120	KAR	None	Carbonatite	12,691.70	19.26	8.47	10.60	10.92	4,807.50	9,505.70	0.80	1.82	0.38	0.36
KR_RC_16_003	120	121	KAR	None	Carbonatite	25,506.00	20.74	7.33	9.00	12.00	4,728.30	9,460.50	0.81	2.30	0.19	0.40
KR_RC_16_003	121	122	KAR	None	Alkali Silicate	16,324.10	8.08	9.18	4.25	37.55	2,559.70	2,861.30	2.16	1.90	0.16	3.68
KR_RC_16_003	122	123	KAR	None	Alkali Silicate	20,311.30	10.50	10.28	8.39	29.99	3,015.20	7,431.30	1.23	1.25	0.15	2.43
KR_RC_16_003	123	124	KAR	None	Alkali Silicate	21,963.70	11.74	8.86	6.62	28.15	3,376.80	4,719.90	1.34	1.77	0.15	1.56
KR_RC_16_003	124	125	KAR	None	Alkali Silicate	24,876.80	13.35	8.09	9.27	24.69	3,854.20	8,463.10	0.87	1.44	0.15	1.51
KR_RC_16_003	125	126	KAR	None	Alkali Silicate	17,883.80	17.84	7.10	11.43	17.49	6,791.30	12,099.00	0.62	1.56	0.38	1.38
KR_RC_16_003	126	127	KAR	None	Carbonatite	25,877.20	24.36	3.56	15.73	2.33	9,419.00	18,227.70	0.23	1.55	0.36	0.21
KR_RC_16_003	127	128	KAR	None	Carbonatite	2,943.20	26.47	3.65	17.14	1.51	9,512.60	23,133.20	0.21	1.54	3.23	0.09
KR_RC_16_003	128	129	KAR	None	Carbonatite	20,740.00	23.92	3.76	15.70	4.86	8,772.20	20,066.60	0.24	1.52	0.42	0.32
KR_RC_16_003	129	130	KAR	None	Carbonatite	3,495.70	23.73	4.36	15.96	6.16	8,269.00	20,605.40	0.27	1.49	2.37	0.28
KR_RC_16_003	130	131	KAR	None	Carbonatite	16,854.40	23.07	5.98	15.40	3.07	7,571.10	15,444.90	0.39	1.50	0.45	0.19
KR_RC_16_003	131	132	KAR	None	Carbonatite	13,994.50	21.23	6.02	15.05	9.19	7,696.90	14,337.50	0.40	1.41	0.55	0.62
KR_RC_16_003	132	133	KAR	None	Carbonatite	9,836.40	17.59	8.12	12.71	14.86	5,917.70	15,177.30	0.64	1.38	0.60	1.45
KR_RC_16_003	133	134	KAR	None	Carbonatite	9,492.80	15.48	8.52	12.38	17.77	5,854.00	12,824.00	0.69	1.25	0.62	1.58
KR_RC_16_003	134	135	KAR	None	Carbonatite	17,737.30	18.12	8.16	14.49	10.81	6,169.00	14,834.70	0.56	1.25	0.35	1.04
KR_RC_16_003	135	136	KAR	None	Alkali Silicate	11,944.80	12.90	8.98	11.57	25.04	4,549.20	9,791.40	0.78	1.11	0.38	1.54
KR_RC_16_003	136	137	KAR	None	Alkali Silicate	9,629.90	11.02	8.43	6.56	36.30	3,154.30	4,476.50	1.29	1.68	0.33	1.76
KR_RC_16_003	137	138	KAR	None	Alkali Silicate	8,431.80	12.41	8.67	8.41	30.66	3,185.60	5,956.40	1.03	1.48	0.38	1.76

ID	from	to	PROJECTCODE	Weathering	Lith	Ba_ppm	CaO_pct	Fe2O3_pct	MgO_pct	SiO2_pct	Sr_ppm	TREE_ppm	Fe2O3/MgO	CaO/MgO	Sr/Ba	Nb/Y
KR_RC_16_003	138	139	KAR	None	Alkali Silicate	6,526.90	8.46	8.38	5.18	39.41	2,331.60	3,717.40	1.62	1.63	0.36	1.79
KR_RC_16_003	139	140	KAR	None	Alkali Silicate	17,077.70	15.74	8.76	9.42	20.99	4,853.70	11,184.20	0.93	1.67	0.28	1.29
KR_RC_16_003	140	141	KAR	None	Alkali Silicate	8,233.00	13.84	8.37	7.31	31.72	3,279.60	6,318.40	1.15	1.89	0.40	1.94
KR_RC_16_003	141	142	KAR	None	Alkali Silicate	8,662.30	17.28	8.11	8.56	22.91	4,379.80	6,944.00	0.95	2.02	0.51	1.47
KR_RC_16_003	142	143	KAR	None	Alkali Silicate	11,426.70	9.67	8.18	6.50	32.50	2,954.70	5,868.70	1.26	1.49	0.26	2.35
KR_RC_16_003	143	144	KAR	None	Alkali Silicate	11,154.40	10.89	8.84	6.82	32.77	3,133.20	4,907.20	1.30	1.60	0.28	1.76
KR_RC_16_003	144	145	KAR	None	Alkali Silicate	8,241.60	12.04	8.82	5.31	35.06	2,387.00	2,909.50	1.66	2.27	0.29	1.67
KR_RC_16_003	145	146	KAR	None	Alkali Silicate	5,637.30	10.63	9.36	4.99	35.69	2,379.10	2,287.30	1.88	2.13	0.42	1.90
KR_RC_16_003	146	147	KAR	None	Alkali Silicate	4,157.30	16.54	10.85	4.31	31.43	2,405.70	2,360.40	2.52	3.84	0.58	2.41
KR_RC_16_003	147	148	KAR	None	Alkali Silicate	5,702.30	10.74	9.73	4.86	35.34	1,910.20	2,689.60	2.00	2.21	0.33	2.07
KR_RC_16_003	148	149	KAR	None	Alkali Silicate	7,725.80	13.57	9.83	7.30	27.15	2,943.40	5,419.80	1.35	1.86	0.38	1.45
KR_RC_16_003	149	150	KAR	None	Alkali Silicate	10,651.50	12.45	7.44	10.09	26.25	3,558.50	8,510.80	0.74	1.23	0.33	1.67
KR_RC_16_004	85	86	KAR	None	Carbonatite	11,015.90	21.18	12.40	13.22	4.73	4,704.10	21,099.90	0.94	1.60	0.43	1.18
KR_RC_16_004	86	87	KAR	None	Carbonatite	51,384.00	19.40	11.69	12.07	5.19	3,132.50	25,065.40	0.97	1.61	0.06	0.67
KR_RC_16_004	87	88	KAR	None	Carbonatite	32,964.40	20.80	10.96	12.78	3.85	2,836.40	21,445.30	0.86	1.63	0.09	0.69
KR_RC_16_004	121	122	KAR	None	Alkali Silicate	15,041.70	9.62	9.48	4.90	34.88	2,861.50	2,061.30	1.93	1.96	0.19	1.99
KR_RC_16_004	122	123	KAR	None	Alkali Silicate	12,382.30	9.37	9.12	4.20	35.93	11,230.90	3,826.20	2.17	2.23	0.91	2.06
KR_RC_16_004	127	128	KAR	None	Alkali Silicate	22,062.00	6.00	8.36	4.68	40.29	2,620.30	4,710.20	1.79	1.28	0.12	4.58
KR_RC_16_004	128	129	KAR	None	Carbonatite	37,193.30	16.31	8.52	11.19	13.91	4,538.50	12,078.80	0.76	1.46	0.12	1.33
KR_RC_16_004	129	130	KAR	None	Carbonatite	37,587.90	19.04	9.69	12.16	6.88	5,371.50	14,978.90	0.80	1.57	0.14	0.69
KR_RC_16_004	130	131	KAR	None	Alkali Silicate	43,782.40	10.99	9.34	8.65	25.46	4,736.90	8,720.80	1.08	1.27	0.11	1.81
KR_RC_16_004	131	132	KAR	None	Alkali Silicate	21,210.00	10.53	9.42	6.31	32.75	4,322.20	5,680.40	1.49	1.67	0.20	2.04
KR_RC_16_004	132	133	KAR	None	Alkali Silicate	21,462.60	11.90	10.26	7.93	28.04	4,543.00	5,354.10	1.29	1.50	0.21	2.16
KR_RC_16_004	133	134	KAR	None	Alkali Silicate	21,663.10	11.02	10.11	5.97	32.36	4,283.90	3,538.60	1.69	1.85	0.20	2.70

ID	from	to	PROJECTCODE	Weathering	Lith	Ba_ppm	CaO_pct	Fe2O3_pct	MgO_pct	SiO2_pct	Sr_ppm	TREE_ppm	Fe2O3/MgO	CaO/MgO	Sr/Ba	Nb/Y
KR_RC_16_004	134	135	KAR	None	Alkali Silicate	20,797.00	18.12	8.54	11.37	15.64	4,864.50	10,061.00	0.75	1.59	0.23	1.25
KR_RC_16_004	136	137	KAR	None	Alkali Silicate	15,951.00	10.16	8.94	6.81	33.97	2,868.60	5,924.80	1.31	1.49	0.18	2.46
KR_RC_16_004	137	138	KAR	None	Alkali Silicate	16,290.90	16.77	9.40	10.36	18.22	4,338.00	11,186.20	0.91	1.62	0.27	1.26
KR_RC_16_004	138	139	KAR	None	Carbonatite	30,905.80	18.03	9.26	11.84	10.11	4,828.70	17,313.90	0.78	1.52	0.16	0.59
KR_RC_16_004	139	140	KAR	None	Carbonatite	17,208.40	10.09	9.61	7.18	30.96	3,116.40	7,405.80	1.34	1.41	0.18	2.55
KR_RC_16_004	140	141	KAR	None	Alkali Silicate	33,734.20	17.86	9.52	12.58	8.63	6,231.70	13,592.00	0.76	1.42	0.18	0.77
KR_RC_16_004	141	142	KAR	None	Alkali Silicate	15,639.90	9.01	8.82	7.02	32.65	3,713.40	8,138.80	1.26	1.28	0.24	2.27
KR_RC_16_004	142	143	KAR	None	Alkali Silicate	12,151.30	9.45	9.60	5.88	36.77	2,833.20	6,424.50	1.63	1.61	0.23	2.39
KR_RC_16_004	143	144	KAR	None	Alkali Silicate	28,706.30	10.98	9.06	7.77	29.14	3,086.40	5,947.10	1.17	1.41	0.11	3.33
KR_RC_16_004	144	145	KAR	None	Carbonatite	24,554.10	24.41	6.21	15.08	1.63	4,947.70	17,066.40	0.41	1.62	0.20	0.34
KR_RC_16_004	145	146	KAR	None	Carbonatite	12,391.30	22.85	9.90	15.59	0.89	6,101.80	17,639.50	0.64	1.47	0.49	0.52
KR_RC_16_004	146	147	KAR	None	Carbonatite	28,363.10	17.85	9.64	12.17	11.90	4,565.50	16,010.60	0.79	1.47	0.16	1.06
KR_RC_16_004	148	149	KAR	None	Alkali Silicate	21,684.40	7.07	11.16	4.90	39.41	1,967.20	5,282.90	2.28	1.44	0.09	5.07
KR_RC_16_004	149	150	KAR	None	Alkali Silicate	22,373.40	6.36	11.70	6.20	35.77	1,863.30	6,421.00	1.89	1.03	0.08	3.51
KR_RC_16_005	6	7	KAR	None	Carbonatite	10,762.50	23.65	6.81	16.15	5.99	3,863.50	7,068.40	0.42	1.46	0.36	2.37
KR_RC_16_009	101	102	KAR	None	Alkali Silicate	21,821.30	12.42	10.23	2.60	32.69	1,987.10	3,934.00	3.93	4.78	0.09	1.95
KR_RC_16_009	102	103	KAR	None	Alkali Silicate	9,758.30	10.02	9.63	2.61	34.85	1,636.50	2,343.80	3.69	3.84	0.17	2.61
KR_RC_16_009	103	104	KAR	None	Carbonatite	11,011.00	15.87	8.16	2.92	31.20	2,062.50	3,606.70	2.79	5.43	0.19	1.11
KR_RC_16_009	104	105	KAR	None	Carbonatite	22,930.90	13.50	9.59	4.76	28.37	2,577.00	4,433.30	2.01	2.84	0.11	1.04
KR_RC_16_009	105	106	KAR	None	Carbonatite	15,615.20	12.55	9.02	3.66	33.11	2,499.10	3,391.50	2.46	3.43	0.16	1.22
KR_RC_16_009	106	107	KAR	None	Carbonatite	13,958.40	6.98	8.77	3.89	41.59	1,584.80	2,963.00	2.25	1.79	0.11	0.89
KR_RC_16_009	107	108	KAR	None	Alkali Silicate	10,563.80	14.31	9.23	2.97	30.31	2,180.70	2,850.50	3.11	4.82	0.21	1.16
KR_RC_16_009	108	109	KAR	None	Alkali Silicate	12,106.20	8.44	9.77	4.55	39.83	1,308.30	3,285.70	2.15	1.85	0.11	0.61
KR_RC_16_009	109	110	KAR	None	Alkali Silicate	11,363.40	6.78	8.90	3.93	41.66	1,466.00	2,973.50	2.26	1.73	0.13	0.97

ID	from	to	PROJECTCODE	Weathering	Lith	Ba_ppm	CaO_pct	Fe2O3_pct	MgO_pct	SiO2_pct	Sr_ppm	TREE_ppm	Fe2O3/MgO	CaO/MgO	Sr/Ba	Nb/Y
KR_RC_16_009	110	111	KAR	None	Alkali Silicate	7,631.40	10.53	7.73	3.29	39.81	1,735.70	1,687.90	2.35	3.20	0.23	0.90
KR_RC_16_009	111	112	KAR	None	Alkali Silicate	16,522.50	10.86	8.74	1.85	38.86	1,502.30	1,801.90	4.72	5.87	0.09	2.09
KR_RC_16_009	112	113	KAR	None	Alkali Silicate	12,215.10	12.61	10.77	4.15	34.85	2,759.10	1,249.40	2.60	3.04	0.23	3.10
KR_RC_16_009	113	114	KAR	None	Alkali Silicate	7,869.50	13.79	11.19	4.59	32.88	2,823.30	1,246.80	2.44	3.00	0.36	3.20
KR_RC_16_009	114	115	KAR	None	Alkali Silicate	7,308.30	13.79	11.35	4.59	33.46	3,110.30	1,132.20	2.47	3.00	0.43	2.94
KR_RC_16_009	115	116	KAR	None	Alkali Silicate	9,131.90	13.47	11.97	4.77	32.47	3,066.20	1,184.60	2.51	2.82	0.34	3.53
KR_RC_16_009	116	117	KAR	None	Alkali Silicate	14,982.70	16.19	12.24	4.12	26.75	3,348.80	2,163.30	2.97	3.93	0.22	2.50
KR_RC_16_009	117	118	KAR	None	Carbonatite	74,257.00	19.49	14.89	8.98	3.14	4,950.90	15,360.20	1.66	2.17	0.07	0.83
KR_RC_16_009	118	119	KAR	None	Carbonatite	38,230.10	8.73	11.12	6.19	27.84	3,047.50	7,012.60	1.80	1.41	0.08	1.41
KR_RC_16_009	119	120	KAR	None	Alkali Silicate	26,353.80	7.55	11.51	5.32	31.33	2,107.00	3,801.30	2.16	1.42	0.08	1.59
KR_RC_16_009	120	121	KAR	None	Alkali Silicate	10,704.80	6.28	9.27	3.80	41.24	1,576.60	1,672.30	2.44	1.65	0.15	1.81
KR_RC_16_009	121	122	KAR	None	Alkali Silicate	8,847.10	4.78	8.59	3.34	47.88	1,370.60	1,275.80	2.57	1.43	0.15	2.43
KR_RC_16_011	73	74	KAR	None	Carbonatite	34,858.70	14.57	22.63	7.98	12.69	7,592.70	8,776.80	2.84	1.83	0.22	0.42
KR_RC_16_011	74	75	KAR	None	Carbonatite	21,619.50	18.12	11.12	11.20	16.99	4,421.20	7,358.60	0.99	1.62	0.20	0.60
KR_RC_16_011	75	76	KAR	None	Carbonatite	17,706.20	23.60	12.04	13.05	4.69	4,330.70	11,993.60	0.92	1.81	0.24	0.33
KR_RC_16_011	76	77	KAR	None	Carbonatite	25,551.60	22.33	13.44	12.28	4.04	5,562.80	13,492.90	1.09	1.82	0.22	0.52
KR_RC_16_011	77	78	KAR	None	Carbonatite	32,695.70	23.85	14.39	10.90	1.66	5,871.50	16,142.70	1.32	2.19	0.18	0.28
KR_RC_16_011	78	79	KAR	None	Carbonatite	31,373.70	22.12	12.79	11.79	6.53	5,120.10	12,330.90	1.08	1.88	0.16	0.42
KR_RC_16_011	79	80	KAR	None	Carbonatite	27,916.70	18.12	24.42	9.38	5.03	4,245.00	15,141.50	2.60	1.93	0.15	0.29
KR_RC_16_011	80	81	KAR	None	Carbonatite	34,755.80	22.62	13.88	12.07	3.85	6,169.40	15,543.80	1.15	1.87	0.18	0.51
KR_RC_16_011	81	82	KAR	None	Carbonatite	20,192.80	23.00	10.92	13.19	3.33	6,629.30	17,595.70	0.83	1.74	0.33	0.48
KR_RC_16_011	82	83	KAR	None	Carbonatite	29,904.40	20.44	15.67	12.27	4.10	5,173.60	15,335.90	1.28	1.67	0.17	0.50
KR_RC_16_012	111	112	KAR	None	Carbonatite	19,660.60	22.67	8.78	14.88	3.06	14,984.40	15,454.80	0.59	1.52	0.76	0.65
KR_RC_16_012	112	113	KAR	None	Carbonatite	26,878.10	23.04	9.20	14.78	2.56	19,903.00	14,613.40	0.62	1.56	0.74	1.43

ID	from	to	PROJECTCODE	Weathering	Lith	Ba_ppm	CaO_pct	Fe2O3_pct	MgO_pct	SiO2_pct	Sr_ppm	TREE_ppm	Fe2O3/MgO	CaO/MgO	Sr/Ba	Nb/Y
KR_RC_16_012	113	114	KAR	None	Carbonatite	28,938.20	22.25	7.18	15.89	1.67	15,859.70	18,881.10	0.45	1.40	0.55	1.96
KR_RC_16_012	114	115	KAR	None	Carbonatite	32,317.20	16.96	7.50	15.07	9.06	22,534.10	21,722.40	0.50	1.13	0.70	1.48
KR_RC_16_012	115	116	KAR	None	Carbonatite	30,839.20	16.31	7.48	15.46	9.65	19,853.30	15,728.40	0.48	1.05	0.64	0.99
KR_RC_16_012	116	117	KAR	None	Carbonatite	27,267.10	19.91	5.81	15.76	5.92	18,371.60	25,657.80	0.37	1.26	0.67	4.55
KR_RC_16_012	117	118	KAR	None	Carbonatite	29,832.20	17.95	6.17	15.04	12.60	12,802.30	18,368.50	0.41	1.19	0.43	1.87
KR_RC_16_012	118	119	KAR	None	Carbonatite	25,493.60	23.05	4.68	17.11	4.17	15,763.00	20,631.90	0.27	1.35	0.62	11.36
KR_RC_16_012	119	120	KAR	None	Carbonatite	21,861.30	24.42	3.86	17.41	4.18	11,601.60	22,088.90	0.22	1.40	0.53	8.91
KR_RC_16_012	121	122	KAR	None	Carbonatite	19,691.60	21.92	4.13	17.76	8.79	16,629.50	17,815.10	0.23	1.23	0.84	3.98
KR_RC_16_012	122	123	KAR	None	Carbonatite	20,179.10	24.04	2.72	18.11	3.30	30,097.30	16,409.30	0.15	1.33	1.49	3.96
KR_RC_16_012	123	124	KAR	None	Carbonatite	20,064.80	19.59	4.19	17.75	8.79	30,745.30	14,491.10	0.24	1.10	1.53	5.18
KR_RC_16_012	125	126	KAR	None	Carbonatite	19,376.50	22.58	3.91	17.99	5.77	19,897.70	13,896.10	0.22	1.26	1.03	5.49
KR_RC_16_012	126	127	KAR	None	Carbonatite	19,994.80	21.57	3.15	16.37	5.78	23,856.10	12,369.20	0.19	1.32	1.19	4.37
KR_RC_16_012	127	128	KAR	None	Carbonatite	15,876.90	23.24	3.55	16.37	2.50	26,650.20	20,938.30	0.22	1.42	1.68	7.40
KR_RC_16_012	128	129	KAR	None	Carbonatite	15,946.40	25.00	3.33	17.19	1.15	25,931.70	23,886.60	0.19	1.45	1.63	8.72
KR_RC_16_012	129	130	KAR	None	Carbonatite	14,831.70	24.28	3.59	17.28	1.58	32,288.50	20,979.70	0.21	1.41	2.18	5.55
KR_RC_16_012	130	131	KAR	None	Carbonatite	14,534.80	25.73	3.82	17.85	1.95	17,129.90	24,512.70	0.21	1.44	1.18	7.84
KR_RC_16_012	131	132	KAR	None	Carbonatite	19,054.00	25.27	3.33	17.18	1.19	22,884.50	28,115.50	0.19	1.47	1.20	5.88
KR_RC_16_012	132	133	KAR	None	Carbonatite	16,919.70	24.87	3.34	17.10	1.52	19,814.20	31,801.00	0.20	1.45	1.17	7.96
KR_RC_16_012	133	134	KAR	None	Carbonatite	13,448.70	25.61	3.59	18.09	2.06	21,603.90	17,498.80	0.20	1.42	1.61	6.10
KR_RC_16_012	134	135	KAR	None	Carbonatite	15,614.50	22.67	4.28	17.51	4.91	28,056.60	18,770.20	0.24	1.29	1.80	4.04
KR_RC_16_012	136	137	KAR	None	Carbonatite	12,669.30	21.64	4.28	16.96	1.16	52,384.70	25,922.30	0.25	1.28	4.13	5.76
KR_RC_16_012	137	138	KAR	None	Carbonatite	18,544.80	22.62	4.70	17.18	2.25	33,822.60	24,723.30	0.27	1.32	1.82	5.53
KR_RC_16_012	138	139	KAR	None	Carbonatite	15,726.00	16.61	6.49	16.03	9.93	33,780.50	24,845.80	0.40	1.04	2.15	8.86
KR_RC_16_012	139	140	KAR	None	Carbonatite	19,244.00	20.18	5.94	16.91	6.15	23,777.00	25,010.10	0.35	1.19	1.24	8.59

ID	from	to	PROJECTCODE	Weathering	Lith	Ba_ppm	CaO_pct	Fe2O3_pct	MgO_pct	SiO2_pct	Sr_ppm	TREE_ppm	Fe2O3/MgO	CaO/MgO	Sr/Ba	Nb/Y
KR_RC_16_012	140	141	KAR	None	Carbonatite	20,217.80	16.68	7.52	16.29	11.22	20,605.20	23,529.70	0.46	1.02	1.02	11.82
KR_RC_16_012	141	142	KAR	None	Carbonatite	19,750.10	22.43	5.55	17.68	3.86	20,197.60	20,179.60	0.31	1.27	1.02	4.88
KR_RC_16_012	143	144	KAR	None	Carbonatite	15,327.30	23.59	4.79	17.34	2.50	18,866.10	17,963.60	0.28	1.36	1.23	2.32
KR_RC_16_012	144	145	KAR	None	Carbonatite	22,541.80	16.13	4.88	13.96	7.23	15,200.90	13,791.70	0.35	1.16	0.67	5.48
KR_RC_16_012	145	146	KAR	None	Alkali Silicate	23,717.40	16.34	7.86	14.16	15.33	18,910.90	10,508.70	0.56	1.15	0.80	2.86
KR_RC_16_012	146	147	KAR	None	Alkali Silicate	23,835.40	15.31	8.32	14.45	15.37	19,559.40	12,324.30	0.58	1.06	0.82	4.45
KR_RC_16_012	147	148	KAR	None	Alkali Silicate	37,679.20	16.67	7.54	14.22	13.06	21,712.80	10,729.90	0.53	1.17	0.58	3.96
KR_RC_16_012	148	149	KAR	None	Alkali Silicate	17,659.10	12.67	7.50	12.61	22.81	28,890.60	13,669.80	0.59	1.00	1.64	9.48
KR_RC_16_012	149	150	KAR	None	Carbonatite	24,581.90	20.73	5.60	16.34	6.38	24,642.70	18,709.90	0.34	1.27	1.00	5.56
KR_RC_16_014	140	141	KAR	None	Alkali Silicate	14,056.50	9.08	5.54	6.23	41.65	1,906.60	2,332.90	0.89	1.46	0.14	6.06
KR_RC_16_014	143	144	KAR	None	Alkali Silicate	12,860.80	2.40	7.36	5.09	50.35	855.30	1,103.40	1.45	0.47	0.07	4.37
KR_RC_16_014	144	145	KAR	None	Alkali Silicate	8,906.20	1.99	7.04	5.67	52.19	899.00	1,081.20	1.24	0.35	0.10	3.91
KR_RC_16_014	145	146	KAR	None	Carbonatite	1,817.40	29.46	3.06	11.29	11.63	4,166.40	4,243.10	0.27	2.61	2.29	1.21
KR_RC_16_014	146	147	KAR	None	Carbonatite	1,501.90	30.28	3.24	11.25	12.04	4,058.50	4,286.10	0.29	2.69	2.70	2.41
KR_RC_16_014	147	148	KAR	None	Carbonatite	2,025.90	24.49	4.18	9.12	22.64	3,143.40	3,451.10	0.46	2.69	1.55	4.32
KR_RC_16_014	148	149	KAR	None	Carbonatite	1,517.90	31.85	3.48	11.04	8.84	4,068.70	3,854.50	0.32	2.88	2.68	10.78
KR_RC_16_014	149	150	KAR	None	Carbonatite	10,600.30	24.77	6.76	10.36	11.35	11,370.90	9,773.30	0.65	2.39	1.07	1.41
KR_RC_16_016	107	108	KAR	None	Carbonatite	8,566.70	20.15	10.36	3.07	25.44	2,565.00	1,917.80	3.37	6.56	0.30	1.24
KR_RC_16_016	108	109	KAR	None	Carbonatite	10,575.40	19.15	10.97	4.89	26.02	2,400.00	1,517.80	2.24	3.92	0.23	1.20
KR_RC_16_016	109	110	KAR	None	Carbonatite	13,842.30	32.02	9.77	3.86	11.59	3,417.80	2,750.20	2.53	8.30	0.25	0.87
KR_RC_16_016	110	111	KAR	None	Carbonatite	9,696.00	19.59	11.20	5.41	24.04	2,699.00	3,579.50	2.07	3.62	0.28	1.37
KR_RC_16_016	114	115	KAR	None	Alkali Silicate	10,310.50	20.13	12.58	4.66	21.34	2,222.40	2,790.10	2.70	4.32	0.22	1.22
KR_RC_16_016	115	116	KAR	None	Alkali Silicate	8,354.70	22.35	11.05	3.29	22.66	2,011.70	1,636.70	3.36	6.79	0.24	1.48
KR_RC_16_016	116	117	KAR	None	Alkali Silicate	8,085.10	25.10	10.57	3.46	20.63	3,058.50	2,296.30	3.05	7.25	0.38	1.20

ID	from	to	PROJECTCODE	Weathering	Lith	Ba_ppm	CaO_pct	Fe2O3_pct	MgO_pct	SiO2_pct	Sr_ppm	TREE_ppm	Fe2O3/MgO	CaO/MgO	Sr/Ba	Nb/Y
KR_RC_16_016	117	118	KAR	None	Alkali Silicate	7,999.60	33.51	10.04	2.23	12.33	3,023.50	3,491.60	4.50	15.03	0.38	0.94
KR_RC_16_016	128	129	KAR	None	Alkali Silicate	9,048.20	16.46	11.77	5.03	27.29	1,973.90	1,825.80	2.34	3.27	0.22	1.06
KR_RC_16_016	129	130	KAR	None	Alkali Silicate	7,920.50	17.00	12.49	5.57	25.81	2,131.80	2,280.10	2.24	3.05	0.27	1.12
KR_RC_16_016	130	131	KAR	None	Alkali Silicate	10,211.10	19.35	11.72	4.28	24.28	2,197.70	2,121.30	2.74	4.52	0.22	1.25
KR_RC_16_016	131	132	KAR	None	Alkali Silicate	10,508.60	18.65	11.90	3.93	25.33	2,038.30	2,192.20	3.03	4.75	0.19	1.16
KR_RC_16_016	132	133	KAR	None	Alkali Silicate	11,937.10	14.87	10.95	4.60	27.87	2,362.40	2,024.60	2.38	3.23	0.20	2.02
KR_RC_16_016	133	134	KAR	None	Alkali Silicate	13,965.90	15.99	12.72	7.67	21.13	2,346.70	4,496.30	1.66	2.08	0.17	1.43
KR_RC_16_016	142	143	KAR	None	Alkali Silicate	9,646.80	17.03	14.75	4.68	24.54	1,427.70	2,610.00	3.15	3.64	0.15	1.59
KR_RC_16_016	143	144	KAR	None	Alkali Silicate	8,599.10	16.10	12.78	4.86	26.15	1,429.40	2,172.80	2.63	3.31	0.17	1.74
KR_RC_16_016	144	145	KAR	None	Alkali Silicate	7,020.20	13.98	12.59	6.00	27.03	1,864.00	1,823.80	2.10	2.33	0.27	1.60
KR_RC_16_016	145	146	KAR	None	Alkali Silicate	8,782.50	15.95	13.14	4.33	25.98	1,508.60	1,817.30	3.03	3.68	0.17	1.32
KR_RC_16_016	146	147	KAR	None	Alkali Silicate	10,727.30	17.42	12.97	4.72	25.11	1,728.90	2,716.10	2.75	3.69	0.16	1.70
KR_RC_16_021	120	121	KAR	None	Carbonatite	39,311.10	31.57	5.49	12.23	0.17	13,692.20	15,398.90	0.45	2.58	0.35	0.08
KR_RC_16_021	121	122	KAR	None	Carbonatite	15,118.30	31.75	5.37	16.16	0.17	13,049.80	16,096.60	0.33	1.96	0.86	0.27
KR_RC_16_021	122	123	KAR	None	Carbonatite	16,373.70	30.62	4.94	14.39	0.22	8,310.20	13,082.40	0.34	2.13	0.51	0.60
KR_RC_16_021	123	124	KAR	None	Carbonatite	16,821.90	25.24	7.05	14.16	0.12	6,732.40	13,985.90	0.50	1.78	0.40	0.08
KR_RC_16_021	124	125	KAR	None	Carbonatite	11,981.80	26.30	6.79	13.95	0.13	8,276.50	16,737.20	0.49	1.89	0.69	0.22
KR_RC_16_021	125	126	KAR	None	Carbonatite	12,189.80	26.14	6.97	12.36	0.09	7,229.70	19,235.70	0.56	2.11	0.59	0.18
KR_RC_16_021	126	127	KAR	None	Carbonatite	19,598.30	28.29	6.93	12.86	0.12	9,493.10	17,523.70	0.54	2.20	0.48	0.38
KR_RC_16_021	127	128	KAR	None	Carbonatite	12,983.20	25.44	6.58	12.51	0.11	8,196.20	19,154.70	0.53	2.03	0.63	0.27
KR_RC_16_021	128	129	KAR	None	Carbonatite	12,952.50	28.19	7.77	11.55	0.11	9,379.00	16,836.10	0.67	2.44	0.72	0.24
KR_RC_16_021	129	130	KAR	None	Carbonatite	60,499.00	31.05	5.83	10.99	0.19	11,515.80	22,905.40	0.53	2.83	0.19	0.22
Lizhuang			Lizhuang	None	Syenite	1,436.00	0.34	1.06	0.11		146.00	144.00	9.64	3.09	0.10	6.54
Lizhuang			Lizhuang	None	Syenite	186.00	0.51	0.66	0.16		181.00	135.00	4.13	3.19	0.97	2.60

ID	from	to	PROJECTCODE	Weathering	Lith	Ba_ppm	CaO_pct	Fe2O3_pct	MgO_pct	SiO2_pct	Sr_ppm	TREE_ppm	Fe2O3/MgO	CaO/MgO	Sr/Ba	Nb/Y
Lizhuang			Lizhuang	None	Carbonatite	20,740.00	26.17		0.05		30,480.00	4,151.00	-	523.40	1.47	0.15
Lizhuang			Lizhuang	None	Carbonatite	28,910.00	29.69		0.01		29,990.00	3,221.00	-	2,969.00	1.04	0.03
Lizhuang			Lizhuang	None	Carbonatite	35,100.00	33.27		0.14		27,430.00	3,488.00	-	237.64	0.78	0.18
Lizhuang			Lizhuang	None	Carbonatite	14,730.00	21.41		0.21		31,060.00	5,330.00	-	101.95	2.11	0.02
Lizhuang			Lizhuang	None	Carbonatite	34,740.00	33.46		0.18		28,390.00	4,101.00	-	185.89	0.82	0.02
Maoniuping			Maoniuping	None	Syenite	2,418.00	1.86		0.39		1,885.00	1,331.00	-	4.77	0.78	1.41
Maoniuping			Maoniuping	None	Syenite	2,145.00	1.47		0.45		728.00	606.00	-	3.27	0.34	0.95
Maoniuping			Maoniuping	None	Syenite	3,044.00	1.17		0.30		2,004.00	2,234.00	-	3.90	0.66	2.00
Maoniuping			Maoniuping	None	Syenite	1,384.00	0.15	0.93	0.35		225.00	1,926.00	2.66	0.43	0.16	0.40
Maoniuping			Maoniuping	None	Carbonatite	5,864.00	52.25		0.01		8,706.00	2,714.00	-	5,225.00	1.48	0.01
Maoniuping			Maoniuping	None	Carbonatite	25,900.00	48.23	0.45	0.17		8,302.00	11,104.00	2.65	283.71	0.32	0.02
Maoniuping			Maoniuping	None	Carbonatite	27,870.00	46.75	0.70	1.95		7,987.00	5,871.00	0.36	23.97	0.29	0.55
Maoniuping			Maoniuping	None	Carbonatite	20,580.00	50.04	0.16	0.41		10,230.00	2,856.00	0.39	122.05	0.50	0.02
Maoniuping			Maoniuping	None	Carbonatite	1,071.00	50.88	0.22	0.67		10,010.00	1,571.00	0.33	75.94	9.35	0.01
Maoniuping			Maoniuping	None	Carbonatite	7,547.00	51.33	0.57	0.32		9,843.00	1,744.00	1.78	160.41	1.30	0.01
Maoniuping			Maoniuping	None	Carbonatite	22,630.00	39.60	2.74	1.50		8,846.00	2,368.00	1.83	26.40	0.39	0.75
Maoniuping			Maoniuping	None	Carbonatite	1,629.00	55.40	0.36	0.10		10,781.00	2,470.00	3.60	554.00	6.62	0.00
Maoniuping			Maoniuping	None	Carbonatite	1,295.00	54.20	0.20	0.10		11,677.00	2,309.00	2.00	542.00	9.02	-